Doctoral Dissertation
Doctoral Program in Energy Engineering (36th Cycle)

The auto-ignition characteristics of ammonia turbulent flames in high temperature co-flow

Meng Ji

* * * * * *

Supervisors
Prof. Alessandro Ferrari,Supervisor
Prof. Zhijun Wu, Co-Supervisor

Doctoral Examination Committee:

Prof. Zhe Kang, Referee, Chongqing University

Prof. Michele Manno, Referee, Università degli Studi di Roma Tor Vergata

Prof. Ming Zheng, Referee, University of Windsor

Politecnico di Torino
April 6, 2024

I hereby declare that, the contents and organisation of this dissertation constitute my own original work and does not compromise in any way the rights of third parties, including those relating to the security of personal data.

…….....

Meng Ji

Turin, April 6, 2024

Abstract

In order to cope with the emission regulations and meet with the zero carbon policy requirements, ammonia (NH_3), as a carbon-free fuel, has a widely potential application for internal combustion engines. Due to the physical and chemical properties of ammonia, which lead to the issues of combustion instability and high emissions, the lower combustion efficiency and higher emission are the main challenges for ammonia as a fuel in application. The fundamental combustion experiment is an indispensable method to investigate combustion characteristics of ammonia. In this work, based on the Controllable Active Thermo-Atmosphere experimental platform, the experimental researches of ammonia and ammonia blending fuels have been explored in different addition ratios, co-flow temperatures, co-flow velocities, equivalence ratios and injection pressures. Furthermore, a pollutant generation simulation prediction has been used to reveal the emissions production mechanism at a high-temperature and high-background pressure condition, using the detailed chemical reaction kinetic mechanism.

Firstly, auto-ignition characteristics of turbulence jet flame of pure ammonia at a high temperature, based on Controllable Active Thermo-Atmosphere burner, have been investigated. The overall color of ammonia jet diffusion flames is orange. With jet pressure increases from 1.3 bar to 2.5 bar, lowest auto-ignition temperature increases from 1128 K to 1218 K. The ammonia jet flow cannot reach min auto-ignition temperature because a higher jet velocity reduces the mixing time between the jet flow and the co-flow. Flame morphology parameters including length, area and perimeter increase with co-flow temperature increases, while first increase then decrease when the injection pressure increases. If injection pressure beyond 2.2 bar, ammonia combustion is incomplete, which lead to a decline of flame morphology parameters. Once the co-flow temperature beyond the critical temperature (1198 K), slope of ignition delay and lifted height

decrease because the effect of co-flow temperature on ignition delay and lifted height dramatically reduces. Lifted height data are satisfactorily fitted by a modified mixing-strain model, showing that ammonia auto-ignition is controlled by the large-scale mixing. With increasing in co-flow temperature from 1148 K to 1223 K, standard deviation of lifted height shows a 90% decline which means combustion stability of ammonia increases significantly. A standard deviation of lifted height below 2 indicates a stable flame.

Second, three different flame enhancement methods (ammonia-hydrogen, ammonia-methane and ammonia-oxygen) have been investigated. Compared to pure ammonia, both ammonia-hydrogen and ammonia-methane flames have a higher flame brightness and a large flame area. Flame morphology parameters of ammonia-hydrogen increase tendency become slowly when hydrogen ratio beyond 10%. The 20% hydrogen is an optimal ratio for combustion stability of ammonia-hydrogen blending fuels because standard deviation declines tendency decreases. With co-flow temperature increases, ignition delay and lifted height of two blending fuels show a downward trend, and both are lower than that of pure ammonia combustion. Hydrogen has a stronger flame enhancement ability than methane which shows a max 46% decreases to ignition delay. Adding 20% hydrogen or 8% methane into ammonia can decrease 175 K or 50 K of minimum auto-ignition temperature compared to pure ammonia respectively. The brightness of ammonia-oxygen flame is brighter than that of pure ammonia, which represents that chemical reaction of combustion is more violent. With excess oxygen coefficient (R_o) increases, the ignition delay first decreases then increases. The ignition delay of ammonia-oxygen has a 30% to 39% decline than the pure ammonia at same co-flow temperatures.

Finally, the auto-ignition and emission characteristics of ammonia, ammonia-hydrogen, ammonia-methane and ammonia-oxygen blending fuels at different temperatures have been investigated by CHEMKIN simulation. As the temperature increases, the NO, NO_2 and N_2O, all increase. NO is the main combustion pollutant under high temperature conditions. For ammonia-hydrogen blending fuels, with the increase of temperature and hydrogen ratio, NOx increases. The N_2O has an obvious increment at the auto-ignition boundary. Compared to the pure ammonia, ammonia disassociation blending fuel has a lower N_2O emission at auto-ignition boundary. The NOx of ammonia/10% methane blending fuel is higher than that of pure ammonia. The NO and CO_2 show a competition under higher temperatures. When temperature beyond 1400 K, the NO will be main pollutant.

Key words: Ammonia, Auto-ignition, Turbulent flame, NOx pollutant.

Acknowledgment

This thesis was carried out at DENERG of Politecnico di Torino, in Turin, from 2020 to 2024.

I wish to express my sincere appreciation to my two supervisors, Prof. Alessandro Ferrari and Prof. Zhijun Wu, for all their talented guidance. Without their persistent help, the goal of those projects would not have been realized.

I want to express my gratitude to Assistant Professor. Oscar Vento, who have always given me a hand from experimental tests to draft reviewed, and have provided me ideas to optimize the solutions.

I want to express my gratitude to my PhD colleagues, Quanbo Shang, Guanyu Zhang and Chaoqun Hu, who have shared sincerely suggestions for my experimental test and simulation.

I want to express my gratitude to my PhD colleagues, Jiale Cai, Yihan Guo, Hanqing Zhao and Qian Gao, who give precious company, especially under the Covid-19 emergency.

I would like to acknowledge the support and great love of my parents.

Thank the fund support from Natural Science Foundation of China (No. T2241003) and Chinese Ministry of Science and Technology (grant numbers G2023133001L).

I would like to dedicate this thesis to my loving parents

In the grand theatre of my academic quest,
my kin have been the brightest stars;
It's their love, a constant northern light,
guiding through many toilsome nights.

Contents

List of Tables

List of Figures

Nomenclature

Main Gas Symbols

NH_3	ammonia
CH_4	methane
H_2	hydrogen
O_2	oxygen
N_2	nitrogen
Ar	argon
NO	nitric oxide
NO_2	nitrogen dioxide
N_2O	nitrous oxide
OH	hydroxyl
CO	carbon monoxide
CO_2	carbon dioxide

Physical Parameter

U_{cf}	co-flow velocity
P_{inj}	injection pressure
u_{inj}	injection velocity
T_{cf}	co-flow temperature

L	flame length
S	flame perimeter
C	flame area
S/C	flame perimeter-to-area ratio
d_{cf}	diameter of burner disk
L_p	core length
$\tau_{ign,ad}$	ignition delay at adiabatic stoichiometric conditions
k_{st}	strain rate
τ'_{mix}	mixing time
R_o	excess oxygen coefficient
X_d	disassociation ratio
X_H	hydrogen ratio
X_{CH4}	methane ratio
T_f	flame temperature
φ	chemical equivalent
g	local gravitational acceleration
T_∞	ambient temperature
ρ_n	jet flow density
ρ_{CO}	co-flow atmosphere gas density

Abbreviation

RCMs	rapid compression machines
ICEs	internal combustion engines
LNG	liquefied natural gas
CI	compression ignition
SI	spark ignition

Chapter 1

Introduction

1.1 Global carbon policy

In September 2020, China government proposed peaking CO_2 emissions before 2030 and achieving "carbon neutrality" by 2060 at the 75th session of the United Nations General Assembly [1]. In December 2020, China further announced that CO_2 emissions would be reduced by 65% by 2030 [2]. On July 16, 2021, China launched national carbon market, which included the transportation industry in China's carbon trading scheme [3]. These political and economic policies demonstrate the Chinese government's determination to achieve "carbon neutrality" and provide a strong foundation for developing zero-carbon technologies in China. The main driver behind these radical policies is China's heavy fossil fuel dependence and severe carbon emissions. By the end of 2020, crude oil import dependence had reached 73% and natural gas import dependence was over 40% in China. This high external dependence has become an important challenge for China's energy transition. Developing carbon-neutral alternative fuels is an important way to reduce energy dependence, which can help promote a decline in national gasoline and diesel consumption. In order to address energy challenges, using carbon-neutral alternative fuels has great potential to reduce CO_2 emissions and conserve fossil fuels.

Meanwhile, Europe is striving to be the first climate-neutral continent in the world. A priority objective for the EU is to drastically reduce CO_2 emissions from passenger cars and vans by imposing reductions of 55% for passenger cars and 50% for vans by 2030 [4,5]. The EU also plans that from 2035 all new vehicles will have net-zero emissions to achieve neutrality in carbon emissions as already set for 2050 [6-8]. To this end, among other measures, the aim is to promote growth in the market for vehicles with zero or very low emissions. Strict emission standards are also an important driver to develop zero-carbon fuels. On November 10, 2022, the European Commission put forward a new road vehicle emission standard framework proposal, EU7 (COM_202/586). This proposal aims to ensure

that EU7 regulations are ahead of major global markets such as the US and China to maintain a competitive advantage. On December 18, 2023, the European Parliament and the Council of the European Union reached a provisional agreement on the EU7 emission regulation, determining important technical requirements and implementation dates. As the European Union has basically established its carbon emission reduction regulatory path (EU2023/851), it will completely phase out vehicles powered by fossil fuels by 2035, so the period for the actual implementation of EU7 will be extremely limited. This also shows major challenges for car manufacturers worldwide in terms of planning, designing, developing and producing with low carbon emission. New zero-carbon vehicles need to be developed.

Electric vehicles are an important technology for reducing carbon emissions. However, electric vehicles also face many challenges. Issues like high prices, lithium mineral extraction and recycle, and distributing electricity to fuel cell vehicles limit the widespread adoption of batteries and fuel cells [9-11]. The lack of hydrogen fuel infrastructure for fuel cell vehicles also poses barriers. Given the infrastructure gaps, immature market, high battery costs, and urgent need to meet emission regulations, transitioning entirely to electric vehicles within a short timeframe will be difficult. Thus, developing alternative zero-carbon fuels for internal combustion engines is potential to help reduce CO_2 emissions in transportation industry.

1.2 Global ammonia fuel policy and application

Hydrogen (H_2) energy is one of the most promising clean energy sources due to hydrogen's excellent properties like its high heating value, non-carbon emissions, and abundant resources. However, hydrogen's low liquefaction temperature and high storage cost have hindered its widespread application. As a result, many researchers are focusing on hydrogen storage and transformation technologies. In fact, liquefaction temperature of ammonia (NH_3) is much higher than hydrogen, offering the potential for lower storage pressures. Lower storage pressures can significantly reduce storage and transportation costs, which are about 10 times lower than for hydrogen [12].

From the perspective of ammonia preparation, the Haber-Bosch method is currently the only large-scale ammonia synthesis method, which consumes about 1% to 2% of the world's energy, and 5% of natural gas, accounting for 1.6% of global CO_2 emissions [13]. According to the source of hydrogen, ammonia can be divided into brown ammonia, blue ammonia and green ammonia. Brown ammonia refers to ammonia products that obtain raw hydrogen from methane reforming (SMR), heavy fuel oil hydrogen production, coal hydrogen production and other processes [14]. Blue ammonia refers to ammonia products that obtain ammonia from by-product hydrogen, SMR with carbon capture, electrified SMR. Green ammonia refers to electrolytic hydrogen production, biomass hydrogen production with carbon capture and other processes to obtain hydrogen or ammonia products, green ammonia is classified as basically zero carbon

emissions of ammonia [15]. Moreover, the industrial production and application of ammonia had a history of more than 100 years, and it has matured application infrastructure such as storage and transportation. Based on the energy properties of liquid ammonia and the existing application infrastructure, liquid ammonia has great potential as a hydrogen carrier. In terms of energy consumption, the energy consumption of synthetic ammonia is equal to that of hydrogen liquefaction. From the perspective of storage and transportation, liquid ammonia storage and transportation is more convenient. On the one hand, the transportation regulations of ammonia are systemic. On the other hand, the cost of ammonia storage and transportation is lower compared to liquid hydrogen.

In recent years, China has paid increasing attention to ammonia development and application. Storage capability of ammonia, as a new energy source, have led to a further exploration. Ammonia has transitioned from a fertilizer and chemical raw material into a novel "zero carbon" energy carrier. Many companies are now focusing on ammonia's application, as shown in table 1.1 highlighting main ammonia power and engine projects in China.

Table 1.1: The application project of ammonia in China

Date	Organization or Enterprise	Project
Jan 2022	CHN Energy Investment Group	Combustion technology of ammonia-coal
April 2022	State Power Investment Corporation Limited	Research on ammonia energy gas turbine technology
Dec 2021	Foshan Xianhu laboratory	Research on ammonia- natural gas mixed combustion, ammonia-hydrogen zero carbon and zero carbon pure combustion
Dec 2019	China State Shipbuilding	Design of tons class ammonia fuel ship
Dec 2021	Jiangnan Shipyard	Green ammonia ship
Aug 2022	Fuzhou university	Ammonia-hydrogen station

In order to cope with the increasingly stringent emission regulations of the internal combustion engines and meet with the zero carbon policy requirements, the traditional internal combustion engine industry has an urgency to develop new clean energies. The ammonia-hydrogen combustion technology that using hydrogen to ignite the ammonia has been proposed. Tongji university, cooperated with Tsinghua university, proposed ammonia-hydrogen fused fuel can be used to reduce the carbon emission. Furthermore, Tongji university establish the ammonia-hydrogen engine test platform and begin to investigate the ammonia emission control strategy in cylinder. In Asia, Japan is the first country to realize

the ammonia potential as a hydrogen carrier. A ‘green ammonia’ strategy has been designed by Japan Science and Technology Agency (JST) to improve the leading position in chemicals production and energy application [16]. IHI (Ishikawajima-Harima Heavy Industries) has developed a low NOx burner for ammonia-methane mixture combustion in medium power generators. The company has successfully developed a 2 MW class gas turbine with an ammonia mixture combustion ratio of 20% [17]. Mitsubishi Heavy Industries Engineering and Mitsubishi Hitachi Electric Power Systems aim to develop an ammonia supply system for gas turbines [18]. The Japan Institute of Industrial Technology (AIST) has successfully realized the ammonia/air combustion using a 50 KW micro-gas turbine system [19]. In this system gaseous ammonia fuel and diffusive combustion had been used in the combustion chamber to enhance flame stability. The ammonia/air gas turbine had a combustion efficiency of 89%-96% at 80,000 rpm. The emissions of NO and unburned NH_3 depend on the burner inlet temperature. Selective non-catalytic reduction (SNCR) can be used between unburned NH_3 with NO to reduce emissions [19]. The results of the NH_3/CH_4/air combustion test showed that an increase in the NH_3 fuel proportion significantly increases NO emission [19]. South Korea Energy Research Institute predicted: between 2030 and 2050, the total demand for ammonia in South Korea will increase from 21 million tons to 75 million tons. 80% will be used as a carrier of hydrogen energy, and 20% ammonia will be used as a zero-carbon fuel in power generation and transportation [20]. Korean researchers successfully tested a passenger car with 70% ammonia/30% gasoline. This fuel substitution ratio reduces carbon emissions by about 70% compared to pure gasoline. Because ammonia is corrosive to materials including copper, zinc and their alloys, the team also conducted a series of tests to determine which components needed to be upgraded during the fuel conversion process [21].

America has been pioneering ammonia energy application. In the 1960s, America began developing long-distance pipeline transportation of liquid ammonia, with two lines still in operation today-the longest stretches over 1900 miles [22]. Based on the advanced ammonia transportation, companies pay attachment to use ammonia into heavy-duty car. Moreover, A 2008 US patent proposed a 90% ammonia engine system [23]. Recently, Amogy has invested $46 million to accelerate the commercialization of its ammonia-powered technology in heavy transportation. Amogy's scalable ammonia-powered zero-emission energy systems have already been successful in heavy-duty tractors. Due to the high requirement of agricultural machinery in America, a diesel-ammonia dual fuel heavy-duty farm tractor had been designed [24]. An ammonia recycles in farm is a potential energy cycle method to enhance the energy efficiency.

Europe leads the research and development of ammonia fuel Marine engines. Man and Wartsila are both involved in the development of ammonia fuel engines [25,26]. Since 2019, Man has been working on developing a two-stroke ammonia engine by using diesel principles. These dual-fuel system is scheduled to be available until 2024. Compared to automobile, the advantage is that no space limitation to assemble an after-treatment system to reduce NOx emission in a ship.

Wartsila [27] mainly conducts research in the field of medium and high-speed machines, and expects to launch ammonia hybrid fuel engines with a ratio of up to 70% ammonia, and to launch pure ammonia fuel engines. The International Maritime Organization (IMO) has set ambitious targets for reducing greenhouse gas emissions. Overall greenhouse gas emissions should fall by at least 50% and CO_2 emissions by at least 70% by 2050, so at least 15% of long-haul ships should be powered by ammonia or hydrogen by 2050 [28]. Deutsche Rail and Fortescue Future Industries partnered to modify diesel locomotives to use ammonia and hydrogen fuels. A small onboard ammonia dissociation unit produces the hydrogen needed for combustion [29]. The Netherlands envisages a transnational market for ammonia and hydrogen and a renewable energy supply network, with storage of excess hydrogen produced by wind power. Ammonia is an important storage and transport carrier, and the network will include Belgium and Germany [30].

1.3 Introduction of ammonia fuel internal combustion engines

The investigation into ammonia combustion's application potential has a lengthy history dating back to 1809, when the first officially documented flammability testing of NH_3 limits in oxygen was published [31]. Thirteen years later, a design was proposed for using ammonia as fuel to power small vehicles, which led to limited application of this fuel in internal combustion engine vehicles in Europe from 1905 to 1942 [32]. The main purpose at that time was utilizing ammonia as a civilian alternative fuel to address the problem of diesel shortages during wartime.

Following the end of the war, due to the limitations of ammonia fuel application technology at the time as well as advances in gasoline and diesel vehicle technology, ammonia fuel vehicles gradually faded from focus. It was not until the 1960s that the United States undertook extensive research into the feasibility of NH_3 combustion within military equipment such as gas turbines, compression ignition engines, and spark ignition engines. Considering its high-octane number of over 130 [33], ammonia was considered a potential alternative fuel option for spark ignition engines [34]. Both laboratory tests and engine tests showed that compared to hydrocarbon fuels, utilizing NH_3 in combustion systems had disadvantages including lower mass calorific value, lower combustion speed, higher ignition energy, a narrow flammable range, higher autoignition temperature, lower adiabatic flame temperature, longer ignition delay and slower chemical reaction kinetics. Ultimately these factors resulted in inferior performance in terms of power and efficiency when used under similar conditions as hydrocarbon fuels.

In addition, the toxicity of NH_3 poses non-negligible impacts on human health. The corrosive nature of ammonia can also corrode materials like copper, brass, bronze, zinc alloys and plastics. Due to ammonia contains nitrogen, its

combustion also significantly increases the potential for nitric oxide production. Therefore, conventional combustion systems require retrofitting or redesigning to enable the reliable, safe and clean application of pure NH_3. Given the characteristics of ammonia as a fuel, in order to utilize it within internal combustion engines, many researchers have explored mixing ammonia gas with other fuels to investigate the application of ammonia.

1.3.1 Pure ammonia spark internal combustion engines

The stoichiometric air-fuel ratio of ammonia is approximately 6, compared to 14.3 for diesel and 14.7 for gasoline. This means more ammonia is required in the same amount of air. As a result, injecting a larger quantity of ammonia is needed to attain a similar energy density to gasoline and diesel [35]. However, the lower combustion performance of pure ammonia means engine performance may decrease due to the increased ammonia injection.

Starkman investigated pure ammonia as a fuel in spark internal combustion (SI) engines [36]. The power output is reduced by 12-14% compared to the power output using iso-octane and the fuel consumption of ammonia is high. Loullier [37] determined that SI engines using pure ammonia show a higher indicated mean effective pressure (IMEP) than SI engines using methane. But the max NOx emission reach to 8000 ppmv, far surpassing gasoline levels. An amount of NH_3 emissions (8000 ppmv) was measured in the exhaust gas [37], which indicates that ammonia escape is another potential risk for ammonia engines due to its corrosive and toxic. Given ammonia's high octane and antiknock potential, Mounaim [38] studied the performance of spark-assisted compression ignition single-cylinder engines with a higher compression ratio (CR=14-17). The results show that pure ammonia can be used over a wide operating range and showed a good potential compared with a current single cylinder SI engine.

In summary, pure ammonia engines still face challenges in internal combustion engines directly: lower power, higher emissions and narrow combustion conditions. Pure ammonia engines need much more modifications to match hydrocarbon fuelled engine performance. The available method is that ammonia need a pilot flame to ignite ammonia or dual-fuel combustion. So, liquid hydrocarbon fuels (gasoline/diesel), recycle fuels (methanol/ethanol/dimethyl ether), gas fuels (methane/natural gas) or zero carbon fuels (hydrogen).

1.3.2 Ammonia-hydrogen spark internal combustion engines

Injecting ammonia or hydrogen separately from the intake manifold is a reasonable strategy for SI engines. As early as 2013, Frigo [39] design an electric fuel injection system which inject the gaseous ammonia and hydrogen using two injectors. The experimental results show that the engine performance is lower than initial 4-stroke gasoline engine and the max nitric oxide (NOx) reach to 1700 ppm. The ammonia-hydrogen mixture ratio and injection reliability need to solve. After further ammonia-hydrogen engines research by Mørch [40], the experiment

results showed that mixing ammonia with 5% hydrogen still has a good power performance. Increasing the hydrogen content to 10vol%, the engine thermal efficiency increased by 0.5% compared with the pure gasoline engine. However, when the hydrogen content was increased to 20%, NOx emissions of 750 ppm were generated, indicating the need for SCR on the exhaust under these conditions. Rousselle tested a GDI PSA engine (compression ratio 10.5:1) in 2021 [41] and the engine operated stably under majority conditions with 10% hydrogen and 90% ammonia. Thus, adding proper amount of hydrogen into ammonia can reduce the shortages of ammonia and enhance the combustion performance. But due to the hydrogen increases, the emission has an obvious change. With the hydrogen ratio increases, the thermal NOx production increases due to flame temperature increases. Dinesh [42] found when the hydrogen is close to 20%, the engine has a balance power and emission performance.

A non-negligible problem with using ammonia mixed with hydrogen as fuel in vehicles is the need to install ammonia storage tanks and hydrogen storage tanks, which increase a lot of space and cost in fuel system. In order to solve the lower combustion performance of ammonia and the high storage cost of hydrogen, the ammonia dissociation technology is a potential method in ammonia engine. The ammonia dissociation means the ammonia can be dissociated to hydrogen and nitrogen in high temperature w/wo catalyst. The chemical function is: $2NH_3 => 3H_2+N_2$. Therefore, some scholars considered partial cracking of ammonia to obtain hydrogen, and the combustion enhancement effects of partial dissociation gas ($NH_3/H_2/N_2$) were basically the same as hydrogen addition [43]. Gill [44] injected ammonia cracked gas into the intake port of a direct injection single-cylinder diesel engine, and studied its combustion and emission characteristics. The experimental results showed that the mixed gas after ammonia dissociation can be used as an alternative fuel for diesel engine. A Hydrogen Generation System (HGS) of ammonia was successfully developed and coupled to an ICE fuelled with ammonia by Comotti [45]. The main component of the HGS is a cracking reactor housing a ruthenium-based catalyst. This system can use the combusted gases exhausted by the engines as a thermal source. Beside the cracking reactor, an integrated system was designed and realized, in order to allow system cold-start and increase overall efficiency during steady state operations. Ryu [46] developed an ammonia cracking device in the engine exhaust manifold. The cracking device is heated according to the exhaust gas temperature. The experimental results showed that the hydrogen produced by partial ammonia cracking can improve engine performance and reduce exhaust emissions. The ammonia cracking dissociation rate is affected by the ammonia flow rate, and the effect is better when the ammonia flow rate is low, which can increase the engine output power and reduce the fuel consumption to a certain extent. Furthermore, only 5% dissociation ratio can improve the combustion stability and efficiency by a single cylinder spark-ignited engines experimental test and about 1% of unburned NH_3 was found in the exhaust [47]. Adding hydrogen can reduce NH_3 emissions and enhance combustion, while worsen NOx emissions. Mercier [48]

studied the effects of ammonia-hydrogen blending fuel with different cracking rates on the performance and emission characteristics of a single-cylinder spark ignition engine. Experiments were carried out under different equivalence ratio, cracking rate and loading conditions. The results showed that: even with a small amount of nitrogen in the mixture, ammonia dissociation technology can improve combustion stability and extend the engine's operating range at low loads. When the ammonia cracking rate reaches 10%, the stability of fuel combustion can be significantly improved; however, in terms of emissions, when the cracking rate reaches 15%, the N_2O produced by combustion will increase exponentially. As dissociation increases combustion efficiency, it reduces unburned ammonia emissions, but the hydrogen emissions increase with disassociation ratio increases. Although the hydrogen content in the exhaust emissions is still less than 2%, the potential impact of hydrogen on global greenhouse effect is not be ignored. The N_2O emission must be considered because when the dissociation ratio is 15%, it reaches to the double value (60 ppm), which is equal to 1.5% of CO_2. The best equivalent ratio to run the engine is rich fuel condition, because NOx emission decline, but unburned ammonia can be captured by the after-treatment system. The hydrogen produced by dissociation contains a large amount of nitrogen, which hinder flame propagation. In addition, the ammonia dissociation device needs to operate at about 700℃ [49], so the temperature of the hydrogen produced is usually high and needs to be cooled to allow the injector to function properly. The pressure of the decomposing gas decreases after cooling, which may negatively affect the mixed gas injection system. Therefore, the combustion characteristics of ammonia cracking gas need to be further investigated.

In summary, utilizing ammonia as the primary fuel in internal combustion engines presents several challenges. These include the difficulty in igniting pure ammonia, and a slow combustion speed. To overcome these obstacles, many researchers are investigating advanced methods such as mixing ammonia with hydrogen and partially cracking ammonia to enhance its potential use in internal combustion engines. Controlling in-cylinder combustion is indispensable and significant for the efficient operation of these engines.

1.3.3 Ammonia compression ignition internal combustion engines

The researches on compression ignition (CI) engines are less extensive than spark ignition (SI) engines. A successful compression ignition of CI engine has been obtained in high CR (35:1). Auxiliary devices such as glow plugs, glow coils, and heating jackets can be used to achieve stable combustion with a lower CR (<30) [50]. Consequently, dual-fuel engines play a critical role in the advancement of ammonia-fuelled CI engines. Diesel remains the preferred fuel for ammonia CI engines, serving either as a pilot flame or the primary fuel in diesel-ammonia dual-fuel engines. Based on ammonia-diesel high-pressure injection dual-fuel (HPDF) mode, the ammonia high-pressure spray model was established. The results showed that the maximum ammonia ratio is close to 80%,

based on low pressure injection dual fuel (LPDF) mode, further increasing the diesel substitution rate will increase the misfire probability. While the diesel substitution rate may achieve 97% under the high-pressure injection dual fuel (HPDF) mode. Compared with pure diesel mode, HPDF mode has similar thermal efficiency, cooling and exhaust losses, while it can significantly reduce equivalent CO with little increase in ammonia emissions. A CI diesel engine had been used to investigate diesel-ammonia combustion and emission performance [52]. In order to ignite ammonia, ammonia was injected into the intake manifold and diesel or bio-diesel was injected into the cylinder directly. The advantage of this solution is that it does not need to redesign the intake system. The experimental results showed that under certain load conditions, adding more ammonia, can exceed the rated power [52]. When the percentage of ammonia gas does not exceed 60%, NOx emissions will not increase significantly. Zehra [53] investigated emission characteristics using ammonia and diesel on a small diesel engine. The experiment found that injecting ammonia into the intake manifold will improve the effective efficiency of the engine at 2200, 2600 and 3000 rpm. But the emissions of NOx, CO and HC also increased with the addition of ammonia. Adding 11% of ammonia lead to an increase of 23% in NOx emissions. At the 2600 rpm, although the growth rate of CO_2 decreased, the emissions of CO, HC and NOx all increased. Ebrahim Nadimi [54] explored the combustion and emissions performance of pure ammonia and ammonia/diesel dual-fuel CI engines. Ammonia can provide 84.2% of the input energy, while improving thermal efficiency (ITE) by increasing diesel substitution. Increasing the ammonia energy share shifted the combustion mode from pure diesel diffusion combustion to combustion in dual-fuel mode. While ammonia significantly reduced CO_2 and particulate matter emissions, it also increased NO emissions and unburned ammonia (14,800 ppm). Ammonia can be used instead of diesel to reduce greenhouse gas emissions. The critical ammonia ratio is 35.9% to make a balance to NO and CO_2 emission.

Solubility of ammonia in ethanol and methanol offers new dual-fuel possibilities, with dimethyl ether (DME) being another potential for ignition in CI engines [55-59]. Christopher [60] studied combustion and emission characteristics of ammonia and dimethyl ether on a CI engine, which dimethyl ether was used for ignition. Studies indicate that high auto-ignition temperature and low flame speed extend ignition delay of ammonia, limiting engine load. The addition of ammonia to the fuel also reduces combustion temperature, resulting in higher CO and HC emissions. However, raising the injection pressure above 30 bar can mitigate these effects.

In summary, utilizing ammonia as a primary fuel in internal combustion engines presents several practical challenges, including higher ignition temperatures, slower flame speed, unstable combustion, and higher combustion pollutants. Therefore, enhancing the combustion efficiency with lower emission of ammonia or ammonia blending fuel is a critical issue. Due to the difficulty of observing and recording combustion in internal combustion engines, researchers

have proposed various methods to improve the combustion activity of ammonia or mixture fuels, using fundamental combustion devices. Understanding the fundamental combustion characteristics of ammonia and ammonia blending fuels are essential for guiding fuel design, combustion control, and engine development specific to ammonia.

1.4 Introduction of ammonia fundamental combustion researches

Based on the preceding discussion, two primary challenges need to be addressed for the effective use of ammonia in engines: enhancing the combustion performance of ammonia fuel, and achieving cleaner combustion with ammonia. These challenges are intrinsically linked to physical and chemical properties of ammonia. The first issue is largely influenced by lower flame speed and higher ignition temperature of ammonia, while the second is associated with the presence of nitrogen in the ammonia fuel. Figure 1.4.1 provides a comprehensive summary of methods to enhance ammonia combustion. However, only "fuel blending" and "process intensification" show potential for application in internal combustion engines.

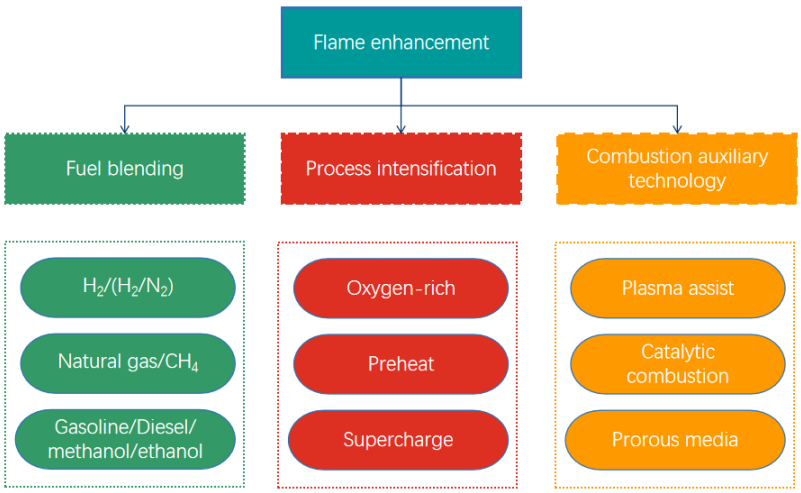

Figure 1.4.1: The main flame enhancement methods

1.4.1 Flame enhancement researches based on fuel blending

Hydrogen is the optimal additive for design ammonia blending fuels, not only because of its high flame speed, extensive flammable range and higher combustion stability, but also due to hydrogen is an advanced zero-carbon fuel. To understand the impact of hydrogen on ammonia combustion, many researches have been conducted using rapid compression machines (RCMs) [61-67] and shock tubes [68-75]. These experiments have explored the basic combustion properties of ammonia-hydrogen blends under a variety of conditions.

The hydrogen addition into ammonia has been verified to have an enhancement ability for the mixture chemical reactions, with experiments

demonstrating that a mere 5% addition of hydrogen can reduce the ignition delay of ammonia in RCMs tests [61]. Through experiments in a constant volume combustion chamber, Hayakawa [76] determined the laminar flame velocity and Markstein length of ammonia/air premixed flames at 0.5 MPa. The results indicate that the maximum laminar burning velocity is below 7 cm/s, substantially slower than that of traditional hydrocarbon flames. The ammonia/air premixed flame is orange, and Hayakawa [77] found that the source of the orange light is the spectral band of NH_2 and the superheated water vapor spectral band [78].

In 2020, Lhuillier [79] acquired experimental data on the laminar flame speed of ammonia with hydrogen mixtures ranging from 0% to 60%, using the spherical explosion method. It was observed that the reaction rate increases with both the addition of hydrogen and rising temperatures. The combustion performance of ammonia is notably improved with hydrogen content between 20% and 40%, even the enhancement effect decreases when the proportion of hydrogen falls below 20% or rises above 60%. Kumar [80] evaluated the accuracy of different mechanisms (GRI-Mech3.0, Tian and Konnov) for simulating hydrogen/air combustion. The Tian and Konnov mechanism were able to predict the downward trend in flame speed when NH_3 was added, with maximum flame speeds dropping by 90-95%. Rocha [81] investigated the flame speed and NO emissions of premixed ammonia-hydrogen blending fuel. The findings confirmed that a pure NH_3 flame experiences a longer ignition delay and a slower flame speed, but with the addition of H_2, the flame speed increases exponentially. Concurrently, there is a significant rise in NOx emissions, underscoring the balance involved in optimizing ammonia-hydrogen fuel blends for internal combustion engines.

Methane (CH_4), the primary component of Liquefied Natural Gas (LNG), is a widely used fuel in ships [82-84] and heavy-duty vehicles [85-89]. In recent years, nearly 11 million vehicles using LNG as it main fuels [90]. Italy ranks as the sixth largest owner of natural gas vehicles with close to 600,000 units, while China is the seventh with nearly 500,000 natural gas vehicles [91]. Consequently, methane has also been considered as a potential flame enhancement additive for ammonia combustion. Extensive researches have been conducted to evaluate the combustion performance of ammonia-methane mixtures, focusing on aspects such as reaction mechanisms, laminar flame properties, and emission characteristics. Wang [92] introduced a new NH_3/syngas/air reaction mechanism derived from an experimental study of laminar flame propagation using the heat flux method at 298 K. The simulation results from mechanism showed a good match with experimental data for NH_3/CH_4 mixtures. Due to a higher combustion performance of methane, the methane addition can increase the adiabatic flame temperature of ammonia-methane mixtures fuel [93]. As the proportion of methane in the mixture rises, both the flame temperature and the heat release rate continue to increase [94]. Concurrently, the flame speed increases, indicating an elevation in the mole fractions of H, O, and OH radicals [95]. The variation in flame brightness can serve as an indicator of the ammonia concentration within the mixture. In a study [96], the chemiluminescence of premixed ammonia-

methane-air flames was analyzed. The intensity of chemiluminescence from excited radicals such as NO*, OH*, NH*, CN*, CH*, and CO_2* was examined, revealing that the fraction of ammonia in the mixture could be deduced from the presence of these free radicals.

Furthermore, the addition of methane is known to reduce the ignition delay [97] and expand the combustion limits [98]. However, the relationship between ignition delay and methane ratio is not linear, particularly when the ammonia fraction exceeds 50% [99]. This non-linear relationship underscores the complexity of optimizing ammonia-methane blending fuel for combustion applications and indicates that there are multiple factors that have effect on combustion behavior.

1.4.2 Other main ammonia flame enhancement methods

Combustion performance of ammonia can be improved in oxygen-enriched condition [100]. The experimental in constant volume combustion chamber showed that the max laminar flame speed can increase to 113 cm/s when the oxygen volume is 40%, and the ignition delay has been decreased at 21%-35% oxygen ratio. In oxygen-enriched condition, on the one hand, the increment of oxygen intense the ammonia propagate due to the flame temperature increases; on the other hand, increased rates of ammonia oxidation reactions lead to higher laminar flame speeds and shorter ignition delays of the ammonia/air mixture. However, the NOx production also increases due to the oxygen reaction and mechanism booster. The optimal oxygen ratio is not clear to make a balance between high combustion performance and low emission. Using oxygen-enriched combustion technology into ammonia has a wilder application potentiality.

According to the increase of jet fuel temperature, the pure ammonia combustion stability and flammable limit can be enhanced [101]. With the initial temperature of ammonia gas increases, the flame structure and color have an obvious change. The reason is that chemical reactions and heat transfer increase due to flame temperature increases. The chemical free radical of OH, H and N has an important function on preheat combustion. However, the preheat temperature need to reach 600 K and the higher preheat requirement temperature hinders its application in combustion engines.

1.4.3 Ammonia emission researches

The management of NOx emissions can be summarized two primary strategies: one consists of reducing NOx formation within the combustion chamber through various combustion methods; the other involves mitigating NOx post-combustion, typically through Selective Catalytic Reduction (SCR) technology. Ammonia combustion, however, presents unique challenges due to inherently higher levels of fuel NOx emissions compared to traditional fuel like gasoline or diesel. It is a huge challenge to use the general SCR device into pure ammonia or ammonia blending fuel engines because of a higher fuel NOx

emission from ammonia compared to gasoline or diesel engines. So, the combustion control of emission production in cylinder is indispensable for ammonia and ammonia blending fuels engines.

The strategy for controlling NOx emissions from ammonia combustion is intrinsically linked to the chemical mechanisms of NOx formation. The conventional mechanism for NOx generation from nitrogen is the Zeldovich mechanism [102]. For ammonia combustion, two pathways for NOx formation are identified: thermal NOx and fuel NOx. The thermal NOx is from N_2 oxidation reaction at 1800 K; and the fuel NOx is form ammonia fuel. The main limiting reactions of Zeldovich mechanism is $N_2+O=NO+N$ which happen above 1800 K usually. Conversely, for ammonia, fuel NOx constitutes the primary source of emissions [103], producing directly from the nitrogen content within the ammonia fuel itself. Historically, researches on chemical reaction kinetics of ammonia were not directed towards validating and simulating its combustion but was instead focused on its role in the formation of nitrogen oxides within the broader context of hydrocarbon fuel combustion at high temperatures. Thus, a series of investigations needs to be developed to delineate the specific combustion characteristics of ammonia and its implications for NOx production.

Miller [104] proposed the first complete ammonia combustion mechanism based on the experimental data of NH_3/O_2 and $NH_3/H_2/O_2$ flame in shock tube. This mechanism can accurately predict the production compared with experiment results, but the lack of ammonia disassociation mechanism has a worse effect on ammonia production especial in poor-oxygen condition. HNO is produced by the reaction of NH_2+O, $NH+OH$, or $NH+O_2$, and then HNO produces NO. In rich-ammonia condition, NH_2 and NH are rapidly converted to N atoms, facilitating the formation of NO and the conversion of NO to N_2. In order to improve Miller 's mechanism, the study of ammonia combustion was extended to more pressure and temperature conditions [105,106]. The effect of ammonia addition on soot production in n-heptane flames has been systematically investigated [107]. The results indicated a significant reduction in the soot volume fraction upon the introduction of ammonia, signifying that ammonia inhibited the formation of soot. Moreover, a marked decrease in OH free radical concentrations is observed with ammonia addition, showing that ammonia contributes to the chemical suppression of soot oxidation mediated by OH radicals. Recently, A lot of mechanism for ammonia combustion has been proposed in different experimental devices. The popular mechanisms had been selected in table 1.2.

Enhancing background pressure has been identified as an approach to mitigate emissions. Studies on NH_3/air swirl flames within a gas turbine framework had shown that an increase in pressure leads to a reduction in both NOx and residual NH_3 emissions [108]. The observed shortening of flame length with rising pressures points to an increased rate of chemical reactions. Further investigations revealed that elevated pressures can promote the generation of N_2 and lower the threshold temperatures for N_2 conversion [109]. The effects of high pressure on

combustion dynamics and NOx reduction are currently the focus of continued research efforts [110-113].

Fuel preheating is a potential strategy to improve combustion efficiency and reduce NOx emissions, and it has been extensively utilized in the combustion of hydrocarbon fuels [114-116]. Experiments on laminar non-premixed flames using pure ammonia [117] had demonstrated that preheating the ammonia fuel extends the flammability limits due to the enhancement of chemical reaction kinetics, as well as heat and mass transfer processes, at elevated fuel injection temperatures. Moreover, a pronounced decrease in NOx emissions was observed alongside a reduction in unburned ammonia residues, indicating a more complete combustion.

Water injection technology is an innovative attempt for ammonia gas turbine or ICEs. The water addition serves a dual purpose: it not only elevates the thermal efficiency of the engine and mitigates knocking tendencies but also effectively mitigates NOx emissions associated with ammonia combustion. Studies involving the steam injection into the combustion chamber of ammonia or ammonia-hydrogen gas turbines had consistently reported a substantial decrease in NOx emissions. However, these studies also noted an increase in the steam content of the exhaust [118-120]. Subsequently, the influence of water on ammonia combustion was investigated using fundamental combustion devices. Investigations on the combustion characteristics of NH_3/H_2 flames with steam in a premixed vortex burner revealed that the introduction of water vapor led to a reduction in NOx concentrations within the flame zone [121].

Ariemma [122] investigated the effects of water on the emissions from pure ammonia gas combustion. The results indicated that ammonia itself could promote the DeNOx chemical reaction, and the presence of water further enhanced this DeNOx reaction. The kinetic principle of the chemical reaction is that steam can consume the O radical $H_2O+O=OH+OH$ through the reaction decomposition, so it inhibits the reaction $NH_2+O=NO+H_2$ and reduces the generation of NO. Experimental evidence confirmed that water can reduce NOx emissions without compromising the stability of premixed and non-premixed combustion. Javed [123] studied the impact of water vapor on the catalytic reduction of nitrogen oxides in soot, finding that water exerted a slight inhibitory effect on NO reduction. The addition of 2.75% water vapor did not alter the optimal temperature for reduction but expanded the temperature range conducive to reduction and increased the amount of NO reduced.

Due to the lower combustion stability, the plasma assisted method has been used to enhance ammonia combustion. Relevant studies have provided evidences that the combustion stability of ammonia, along with reduced NOx emissions, can be effectively improved by non-equilibrium plasma [124, 125]. While plasma and electrochemical reactions are known to increase flame speed [126], the cooperative mechanisms between these processes require further experimental investigations to be fully understood.

Table 1.2: The main ammonia mechanisms

Mechanism	Species /Reactions	Experiment	Mixtures	T (K)	P (bar)	Φ
Glarborg [137-139]	151/1395	FR spec [138]	$NH_3/CH_4/O_2$	900-1800	1.06	0.13, 1.07,1.55
		RCM IDT [62]	$NH_3/CH_4/O_2/Ar/N_2$	900-1100	20, 40	0.5, 1.0, 2.0
Stagni [140-142]	31/203	JSR/FR spec [140]	$NH_3/O_2/He$	500-2000	1	0.01-0.375
	156/2437	ST IDT [141]	$NH_3/O_2/N_2$	1100-1600	20-40	0.5-2.0
		RCM IDT [61]	$NH_3/O_2/Ar$	1000-1130	40-60	0.5-2.0
		JSR/FR spec [142]	$NH_3/CH_4/O_2/He$	500-2000	1	0.5, 1.0, 2.0
CEU [143-145]	91/445	ST IDT [146]	$NH_3/CH_4/air$	1400-1800	2, 5	0.5,1.0,2.0
		FR spec [145]	$NH_3/CH_4/O2$	900-1800	1.06	0.13, 1.07,1.55
USD [147]	68/311	RCM IDT	$NH_3/CH_4/O_2/Ar/N_2$	900-1100	20, 40	0.5, 1.0, 2.0
Okafor [148,149]	59/356	Flame spec [40]	$NH_3/CH_4/O_2$	900-1800	1.06	1.07
Dagaut [150]	41/250	Flame spec	$NH_3/CH_4/O_2$	900-1800	1.06	1.07
Otomo [151]	32/204	Flame spec [152]	$NH_3/H_2/air$	450-925	30, 100	1
Mei [153,154]	38/265	Flame spec [153]	$NH_3/O_2/N_2$	298	1	0.6-1.5
		Flame spec [154]	$NH_3/H_2/N_2/air$	298	10	0.7–1.4

1.4.4 Ammonia auto-ignition researches

Auto-ignition is a critical combustion mode, particularly relevant for compression ignition (CI) engines, and understanding its characteristics is essential for engine design and operation. However, the experimental data on the auto-ignition characteristics of ammonia in turbulent conditions are currently limited. Chen [127] investigated on a non-premixed laminar ammonia flame in an air co-flow at temperatures ranging from 723 K to 923 K, and observed that ammonia jet flame stability was significantly inferior to that of hydrogen. The experimental results indicated that ammonia requires a higher jet or co-flow temperature to maintain combustion stability, showing the necessity for a specialized ammonia burner designed for higher temperature co-flows to further investigate ammonia combustion. A study on ammonia-methane non-premixed flames [128] revealed that at an ammonia mole ratio of 50%, the fuel mixture was unable to sustain a stable flame. This is attributed to the combined effects of ammonia and the co-flow velocity, leading to increase lifted height and reduce combustion stability. The exploration of suitable auto-ignition evaluation methods for ammonia is also crucial. Since ammonia behaves as a gas in air,

methodologies used for analysing the auto-ignition characteristics of hydrocarbon gas fuels could be adapted for ammonia. A lifted height model based on a modified large-scale mixing model has shown good match with experimental behaviours of acetylene auto-ignition [129], showing a strong dependence of flame auto-ignition stability on ignition delay and chemical kinetics. Liu [130] investigated the auto-ignition in different oxygen content and found that: with the oxygen ratio decreases, the lifted height increases. A lifted height model considering the mixed effects of small-scale strain and large scale is established, based on Li's model. In [131], dimensionless number model Ka_{mix}/Da_{ign} had been used to describe the lifted height behaviours and found the lifted height were positively correlated with Ka_{mix}/Da_{ign}. It also found the lifted height model need to consider both Kolmogorov time scale and the chemical time scale. Due to the high flame speed and low ignition delay of hydrogen, the model from hydrocarbon fuel data do not have a good match with pure hydrogen auto-ignition. Thus, a modified hydrogen auto-ignition stability model has been proposed in [132], considering flame propagation and stability. A new model considering contribution of the Ka and Da had been proposed in [133], and found the flame propagation had a higher contribution to hydrogen combustion but the auto-ignition had a stronger contribution to hydrocarbon fuel.

In summary, recently, ammonia researches focus on laminar premixed flame to establish the mechanism of ammonia. Compared with laminar flame fundamental researches, there are few reports on ammonia turbulent diffusion flame which is widely used in CI engines [134,135]. Turbulent flames not only enhance flame speed but also impact flame extinction limits through diffusion thermal instability [136]. Additionally, the combustion characteristics of ammonia become increasingly complex under turbulent conditions. Therefore, it is of great significance to study the combustion of ammonia fuel under turbulent conditions to reveal the combustion characteristics of ammonia. As for the insufficient experimental data of ammonia turbulent diffusion combustion, the turbulent auto-ignition combustion characteristics of ammonia fuel at high temperature are not clear, which is not enough to reveal the combustion characteristics of ammonia fuel under turbulent conditions and is not enough to guide the design of ammonia engine. Thus, the study of ammonia and ammonia blending fuels (hydrogen, methane and oxygen) turbulent auto-ignition characteristics should be clarified based on an advanced combustion burner.

1.4.5 Researches on Controllable Active Thermo-Atmosphere burner

The Controllable Active Thermo-Atmosphere burner often referred to as the Dibble burner, is an experimental device that has been extensively utilized for the investigation of auto-ignition phenomena within high-temperature and turbulent flow fields. Different with the burners with cold co-flow and closed pressure, the Controllable Active Thermo-Atmosphere burner can separate the combustion process from the complex fluid circulation in the engine cylinder. The chemical

reaction in the jet diffusion combustion process and the auto-ignition combustion stability mechanism of the lifted flame can be studied. A center jet of fuel is injected into the high temperature co-flow which supplies thermal field to the jet fuel auto-ignition. The large diameter of the co-flow is produced by hydrogen combustion and isolates the jet flow from the environment, so that the fluid domain may be simplified as a two-stream flow. Due to a clear physical boundary and a simple geometry structure, the burner is potential and popular to use in the experiment test and simulation. In 2002, Professor Robert Dibble studied the experiment of H_2/N_2 jet flames. Through series of studies, a turbulence model was proposed to predict the lifted height of the jet flames, which is a critical parameter in assessing flame stability and auto-ignition behavior. The lifted height is influenced by both the turbulent mixing of the fuel with oxidizer and the kinetics of the combustion reaction [155, 156]. Subsequent researches expanded on Dibble's work by examining the auto-ignition characteristics of CH_4 jet flames within a high-temperature co-flow, shown in figure 1.4.2 [157]. These experimental investigations yielded insights into the sensitivity of the lifted height to various parameters, such as jet and co-flow velocities, as well as co-flow temperature.

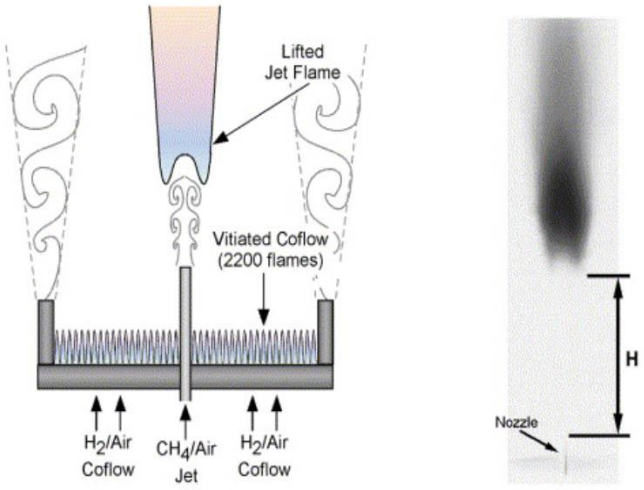

(a) Burner schematic (b) Lifted CH_4 flame

Figure 1.4.2: Burner schematic (left) and luminosity image of a lifted CH_4/air jet flame in vitiated co-flow(right).

Further studies on the flame stability of the lifted flame were finished by University of Sydney [158-160]. The stability of H_2/N_2 flame is controlled by fuel auto-ignition and flame propagation at different temperatures, while that of CH_4/air flame is different. Then, the OH and CH_2O had been used to characterize the flame structure, and found the fluctuation of heat release rate with OH, which was used as a sign of auto-ignition combustion [161,162]. Delft University of Technology [163-166] modified the burner and studied the burner parameters, velocity, temperature, and OH production of a variety of fuel jet flames (Reynolds number from 3000 to 9500). It is found that the formation of fire core is the main

factor for the stability of the lifted flame, and the increase of turbulence intensity will inhibit the auto-ignition once the chemical reaction proceeds slowly.

A series of researches had been implemented in Tongji University based on Dibble burner. Tongji University [167,168] studied auto-ignition combustion mechanism and flame stability mechanism of different liquid fuels. The concepts of critical temperature and stability mechanism of liquid fuel had been proposed. The conclusion was that auto-ignition of liquid fuel had been controlled by physical mixing process and chemical reaction at different temperature regions. The liquid fuels like diesel-propane, ethanol and dimethyl ether had been investigated [169,170]. The experimental result of diesel-propane found that: both chemical factor and physics factor control the flame lifted height in different temperatures, and lower ignition delay fuel can improve the mixture combustion performance. The experimental results of ethanol and DME found that: the lifted height is controlled by ignition delay, and fluctuation of lifted height is affected by the sensitivity of co-flow temperature. The higher sensitivity of co-flow temperature, the more dramatic fluctuation of lifted height occurs. The lifted flame phenomenon at a high co-flow temperature is mainly controlled by ignition delay and reaction path before auto-ignition.

Besides the liquid fuels, the gas fuels like H_2/N_2 [171], H_2/CO_2 [172], $H_2/Ar/O_2$ [173] and CH_4 [174] has been tested based on Dibble burner. Xie [172] investigated the H_2 auto-ignition performance in a series of co-flow gas (N_2, Ar and CO), and found that different co-flow lead to a different flame brightness, lifted height and auto-ignition temperature. Yu [173] investigated the hydrogen/oxygen co-axis auto-ignition performance in Ar co-flow, and found that: increasing the oxygen ratio can improve the flame performance and the flame lifted height is different based on different oxygen injection method. Qin [174] investigated the methane auto-ignition characteristics at a high background pressure based on a modified dibble burner. The results were that: with the background pressures increases, the lifted height and flame fluctuation decline which represent the flame stability has an obvious improvement in a higher background pressure. But the flame color transform to a luminous yellow at a higher background pressure, which means soot production.

Previous researches, based on Controllable Active Thermo-Atmosphere burner (CATA), had mostly focused on high calorific value gaseous or liquid fuels such as hydrogen, methane, propane, ethanol and diesel. It is still unclear about low calorific value fuels such as ammonia and ammonia blending fuels. Due to the physical and chemical properties of ammonia (extremely high auto-ignition temperature and combustion instability), a higher temperature is required to achieve stable auto-ignition. Using Controllable Active Thermo-Atmosphere burner to study auto-ignition of ammonia fuel has obvious advantages: on the one hand, the Controllable Active Thermo-Atmosphere burner can provide a stable homogeneous high temperature auto-ignition conditions for ammonia fuel; on the other hand, a large of researches fundamental flames provides a research guideline for the combustion of ammonia and ammonia blending fuels.

Prior studies utilizing the Controllable Active Thermo-Atmosphere burner have predominantly focused on fuels with high calorific values, such as hydrogen, methane, propane, ethanol, and diesel. The combustion properties of low calorific value fuels, notably ammonia and ammonia blending fuels, remain less report. Because of high auto-ignition temperature and combustion instability of ammonia, a higher temperature environment is necessary for a stable auto-ignition. Using the Controllable Active Thermo-Atmosphere burner to investigate auto-ignition characteristics of ammonia presents distinct advantages: it can generate stable, homogeneous high-temperature conditions suitable for ammonia auto-ignition, and reveal fundamental flame behaviors to guide studies on ammonia. The ammonia fuel combustion experiment, based on the Controllable Active Thermo-Atmosphere burner, can explore the combustion characteristics of turbulent jet flame, reveal the auto-ignition flame stability mechanism of ammonia fuel at high temperature, supply the ammonia fuel turbulent combustion database, and guide the fuel control strategies of ammonia CI engines.

1.5 The contributions and outline

In this thesis, the auto-ignition characteristics of ammonia have been investigated at a high homogeneous temperature co-flow, based on the Controllable Active Thermo-Atmosphere burner firstly. In order to evaluate the different flame enhancement methods, which include the fuel blending (hydrogen and methane) and oxygen-enriched combustion, have been tested under various conditions. The auto-ignition boundary, flame morphology parameters, flame ignition delay, lifted height and combustion stability have been investigated. The main research route has shown in figure 1.5.1 and the outline has summarized in figure 1.5.2.

In chapter 2, the experimental platform has been introduced, including controlled thermal atmosphere burner, co-flow control system, jet control system, cooling system and data acquisition system. The experimental parameters and boundary conditions of combustion characteristics have been defined. The simulation method has been introduced with validation.

In chapter 3, the turbulent jet flame characteristics of pure ammonia in a high-temperature co-flow have been investigated. The jet flame morphology of ammonia, auto-ignition boundary, ignition delay, combustion stability mechanism and flame fluctuation have been explored and summarized.

In chapter 4, combustion characteristics of ammonia-hydrogen and ammonia-methane blending fuels have been investigated. The jet flame morphology, lifted height, ignition delay, combustion stability mechanism and flame enhancement ability have been explored and summarized.

In chapter 5, combustion characteristics of ammonia-oxygen mixture at a high temperature have been investigated. The jet flame morphology of ammonia, auto-ignition boundary, ignition delay, combustion stability mechanism and combustion diluent effect have been explored in oxygen-enriched condition.

In chapter 6, emission characteristics of ammonia, ammonia-hydrogen, ammonia dissociation fuel, ammonia-methane and ammonia-oxygen blending fuels have been predicted and investigated by CHEMKIN simulation.

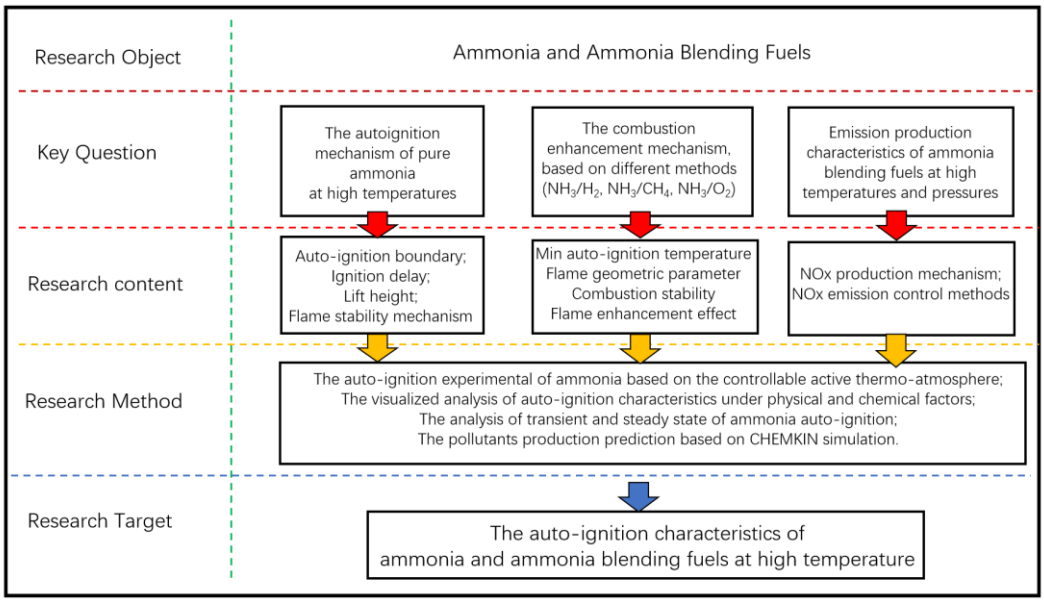

Figure 1.5.1: The main research route

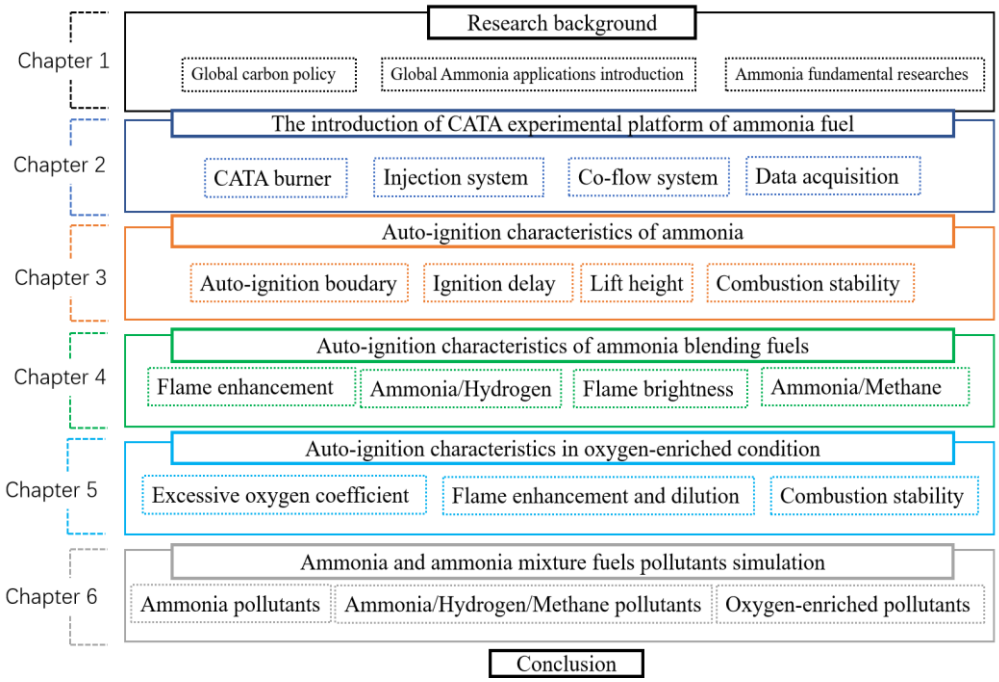

Figure 1.5.2: The outline of research

Chapter 2

Controllable Active Thermo-Atmosphere experimental platform of ammonia fuel

2.1 Overview of test platform based on Controllable Active Thermo-Atmosphere burner

The combustion experimental platform of ammonia and ammonia blending fuels is illustrated in figure 2.1.1, including four integral components: the Controllable Active Thermo-Atmosphere burner, the gas supply system (which includes the co-flow control system and the jet fuel control system), the cooling system, and the data acquisition system. Central to the test system is the Controllable Active Thermo-Atmosphere burner, capable of providing a stable co-flow temperature field essential for the ammonia and ammonia mixture jet flows. The gas supply system is divided into a co-flow air control system and a jet fuel control system. The former controls the co-flow supply, allowing for precise control over the flow field's temperature and velocity via adjusting the hydrogen blower and a float flowmeter. The latter system is designed to mix the ammonia blending fuels and controlling the jet flow injection, consisting of a premixing tank, a solenoid valve, pressure reducing valves, a float flowmeter, a high-pressure gauge, an electric relay and a flame arrester. The cooling system is connected to both the jet tube and the burner, designed to initiate a continuous recirculation of water once the experiment begins, which is critical for maintaining the operational integrity of the test apparatus. The role of data acquisition system is to monitor the co-flow temperature, as well as the pressure and temperature within the burner, to capture visual data via a high-speed camera and to control the electric relay. Each component in combustion test system is

detailed to facilitate a comprehensive analysis of the combustion properties of ammonia and ammonia blending fuels.

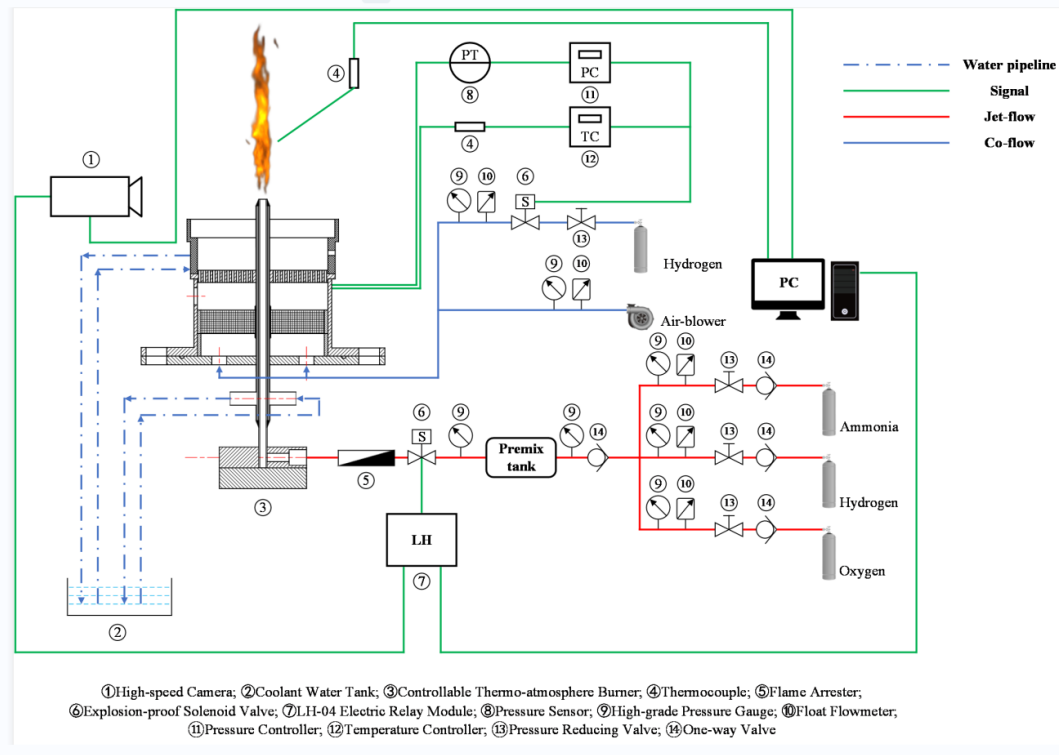

Figure 2.1.1: The test platform of ammonia and ammonia blending fuels, based on Controllable Active Thermo-Atmosphere burner.

2.1.1 The introduction of Controllable Active Thermo-Atmosphere burner

The conception of Controllable Active Thermo-Atmosphere burner has been proposed by Prof Robert in 2002. The burner in this work had been reformed in Tongji University and a series of liquid/gas fuels had been investigated [167-174]. Owing to its capacity to maintain a stable high-temperature field, the Controllable Active Thermo-Atmosphere burner is particularly suited for experimental investigating the auto-ignition characteristics of fuels with elevated temperatures.

The configuration of the burner comprises a central jet flow, encircled by a co-flow. The intake of the co-flow is a lean mixture of hydrogen and air, which is ignited by a pilot flame of hydrogen with a purity of 99.99%. A high and flat temperature co-flow is produced by hydrogen combustion, then ammonia and ammonia blending fuels are auto-ignited in the co-flow downstream area. It enables the exploration of auto-ignition dynamics and stabilization mechanisms of ammonia flames within a temperature range from 900 K to 1600 K. Furthermore, by modulating the co-flow velocity, a controlled turbulent flow field can be produced, allowing for an investigation into the auto-ignition of ammonia under conditions of high-temperature turbulence that is more closely to the real

combustion conditions in engine cylinder. Moreover, the simple coaxial structure of the burner makes it more convenient to study the relationship between chemical reactions and turbulence, and an open structure also provides convenience for the arrangement of various testing instruments.

The burner assembly structure is shown in figure 2.1.2. From top to bottom, it is mainly composed: the backfire control chamber, temperature flame stability chamber, porous combustion plate and the inlet of jet and co-flow.

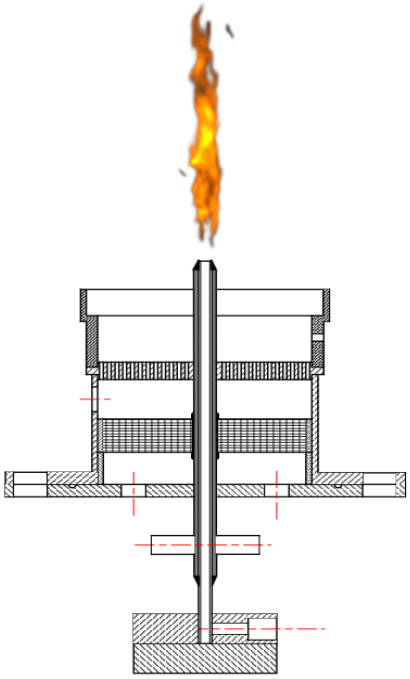

Figure 2.1.2: The structure drawing of burner assembly.

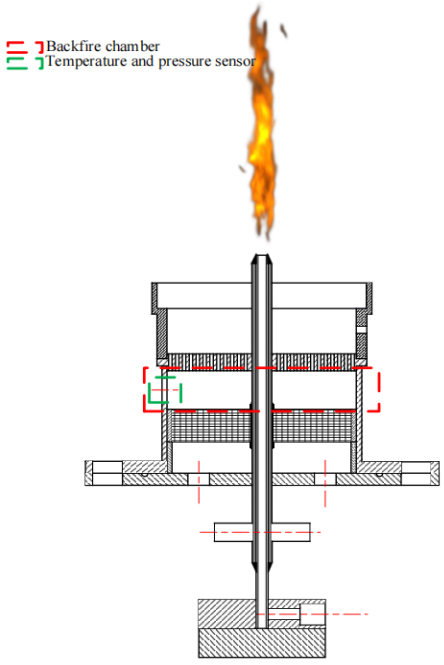

Figure 2.1.3: The structure drawing of backfire chamber.

In order to avoid the possible backfire and auto-ignition combustion of hydrogen/air, a thermocouple is used to monitor temperature and a pressure sensor is used to monitor pressure fluctuations in the backfire control chamber. Appropriate temperature and pressure threshold are established, ensuring that when these limits are surpassed, the control circuit will close the solenoid valve autonomously to ensure experimental safety.

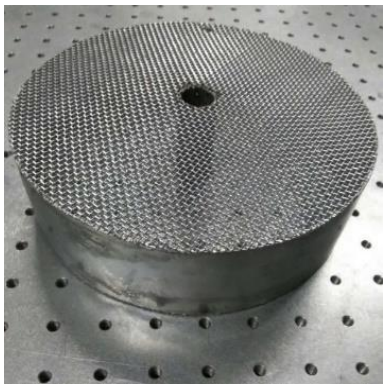

Figure 2.1.4: Flame trap

Complementing the temperature and pressure sensor, a flame trap (figure 2.1.4) situated between backfire chamber and co-flow inject chamber is filled with silica beads with a 2-3 mm diameter. This flame trap serves two critical functions: firstly, it extinguishes any flame that may occur in the backfire chamber, thereby inhibiting further propagation upstream; secondly, it induces a more uniform distribution of the co-flow mixture by constricting the flow area due to the interstitial spaces between the beads.

Figure 2.1.5: The porous combustion disk.

In order to keep the co-flow flame stability, a porous combustion disk, the flame stability chamber and a central tube consist the co-flow stable combustion system. Figure 2.1.5 is a physical diagram of a porous combustion disk. The combustion disk is manufactured with a porous structure, the co-flow hydrogen/air premixed gas can pass through the porous combustion disk and is ignited above the disk to form small premixed flow flames. The flat flame builds a stable high-temperature atmosphere for the center jet fuel gas. The porous disk has 874 uniformly distributed small holes, the diameter is 1.2 mm, and the

distance between the centers of every two small holes is 3 mm. Every 3 centers of the holes are the vertices of an equilateral triangle.

The flame stability chamber is an area in which the hydrogen/air premixed stable flame occurs. It includes outer retaining ring with cooling channel and a pilot flame outlet. The flame stability chamber is shown in figure 2.1.6.

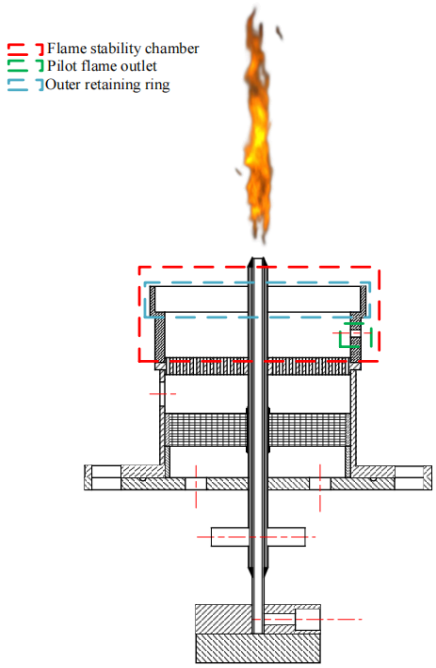

Figure 2.1.6: The structure drawing of flame stability chamber.

The outer retaining ring fabricated by stainless steel serves a critical role in maintaining a consistent combustion environment for the co-flow gas. It is designed to isolate the co-flow flame from external air currents, thereby preventing the flame from radially spreading towards the burner apparatus, which could potentially disturb the temperature field structure and stability. To mitigate excessive heat accumulation within the outer retaining ring, a copper tube is coiled around its circumference, using as a channel for coolant circulation. Water, selected for heat transfer properties, flows through this copper tubing, effectively removing excess heat from the retaining ring through convective heat exchange, thus maintaining a safe operational temperature of device.

Additionally, a pilot flame outlet is positioned on the inner wall of the burner. The purpose is to ignite the co-flow, utilizing pure hydrogen (with a purity of 99.99%) as the pilot fuel. The pilot tube has a diameter of 2 mm, ensuring a stable and controlled pilot flame. Once the co-flow combustion occurs, the pilot flow is terminated to eliminate any potential interference or measurement errors that could affect the experimental results. This setup is instrumental in enabling a stable combustion of the co-flow combustion while ensuring the accuracy of the combustion process.

The central injector is shown in figure 2.1.8. A cooling water path is welded to the outer layer of the central injector. In order to avoid the impact of gas fuel

leakage on the test, a machined base is made to connect the injector to the base to ensure the safety and accuracy of the test. The outlet of the central nozzle is 40 mm away from the upper surface of the combustion plate. This height is about twice the height of the co-flow flame, which ensures that the co-flow flame cannot interfere with the jet flame.

Figure 2.1.7: The outer retaining ring.

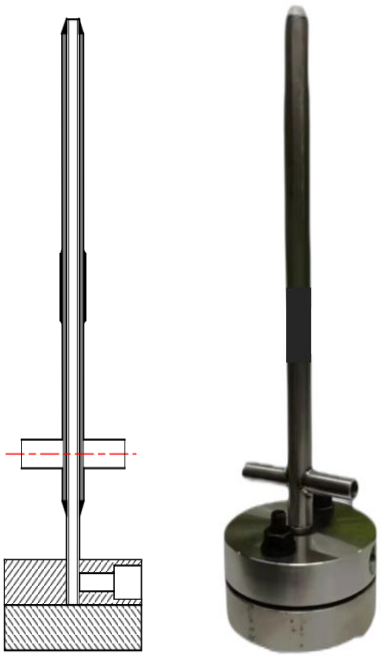

Figure 2.1.8: The jet flow injector.

2.1.2 The introduction of co-flow control system

The co-flow gas supply system, shown in figure 2.1.9 includes three parts: co-flow hydrogen pipeline, co-flow air pipeline and pilot pipeline. The hydrogen of co-flow is supplied by a hydrogen tank group. High-pressure hydrogen pipelines and low-pressure hydrogen pipelines are arranged in the laboratory to supply co-flow and pilot respectively. An explosion-proof solenoid valve is used to control the open and close, and a float flowmeter is used to adjust the hydrogen flow rate of the hydrogen pipeline. The blower supplies co-flow air with a max flow rate of

600 m^3/h, and a flowmeter is installed in the co-flow air pipeline to measure the temperature and flow rate of the co-flow. The co-flow hydrogen pipeline and the air pipeline are connected through a three-way valve, thereby forming a uniformly mixed co-flow gas in the pipeline. Finally, the hydrogen/air mixed gas is divided into four channels through the pipeline and then enters the burner. The gas supply method of the pilot hydrogen pipeline is the same as that of the co-flow hydrogen pipeline. A solenoid valve is used to control the gas pipeline, and the pilot hydrogen flow is controlled by a float flow meter.

The co-flow temperature is obtained by controlling the hydrogen content in the co-flow pipeline. Varying the volumetric flow rate of hydrogen alters the temperature within the co-flow. The temperature conditions during experimentation are monitored via a thermocouple, interfaced with an intelligent temperature control unit. To diminish the thermal influence of the combustion processes on the thermocouple, it is positioned 30 mm downstream from the jet nozzle's exit.

In order to verify the uniformity of the co-flow temperature field, the thermocouple has been installed on a three-dimensional moving platform and the temperature has been measured at different locations. When the thermocouple is moved, the temperature is recorder after 30 seconds to let the thermal regime to be reached. For all the considered experimental conditions, the autoignition occurs in the uniform part of the co-flow field, which consists of a cylinder with a diameter of around 90 mm a height of around 180 mm. The co-flow thermal field has been empirically characterized and documented in ref [169].

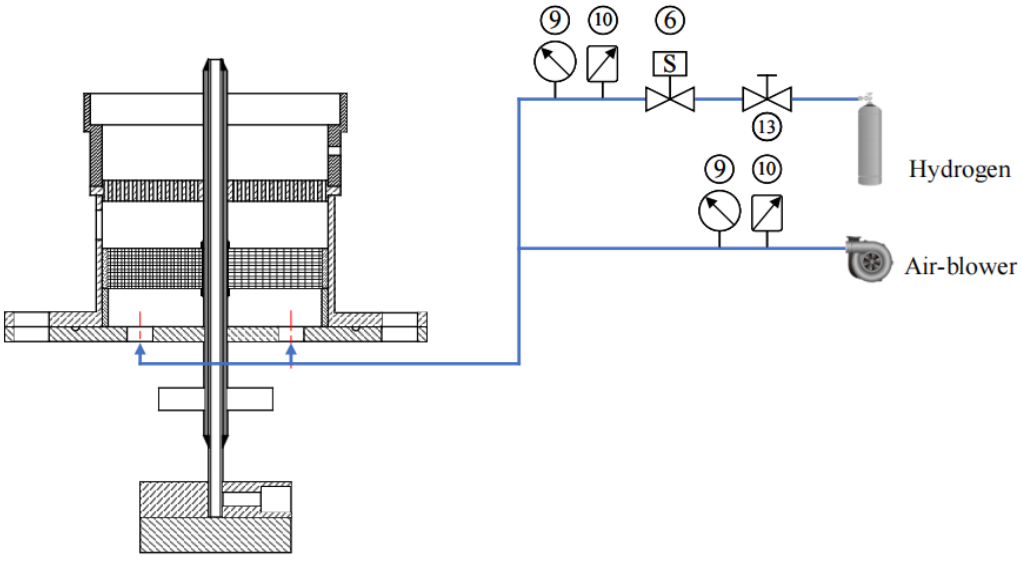

Figure 2.1.9: The structure of co-flow system.

Table 2.1 reports the co-flow chemical constituents determined by CHEMKIN software with the GRI-Mech 3.0 mechanism and corresponding to the reported co-flow temperature values (Y stands for the mass fraction). As can be inferred, when the co-flow temperature increases, the H_2O concentration, namely

Y_{H2O}, augments slightly, while the nitrogen and oxygen mass fractions slightly reduce (the Y_{O2} reduction is around 5% if the co-flow temperature passes from 973 K to 1223 K).

Table 2.1: Co-flow chemical constituents at different co-flow temperatures.

T_{cf}	Y_{H2O}	Y_{N2}	Y_{O2}
973 K	0.057	0.761	0.181
1023 K	0.061	0.761	0.177
1073 K	0.065	0.761	0.174
1113 K	0.069	0.761	0.170
1123 K	0.071	0.761	0.168
1148 K	0.074	0.761	0.165
1173 K	0.076	0.761	0.164
1198 K	0.079	0.761	0.161
1223 K	0.081	0.761	0.159

The co-flow velocity is determined, based on the volumetric flow rate of the blower (measured at T=20 °C and p=1 atm), therefore the corresponding mass flow rate can be calculated. Then, by the mass conservation law, since the burner is exposed to the environment, the co-flow velocity can be determined by knowing both the burner cross section area (this is determined based on the burner diameter) and the co-flow density, the latter determined by means of the perfect gas law with the measured co-flow temperature (a static pressure equal to 1 atm is taken). For each set of air volumetric flow rate and co-flow temperature, because of the great excess of air flow rate with respect to the hydrogen one, air properties have been used to determine the co-flow velocity. Figure 2.1.10 reports the co-flow velocities at different temperatures, for fixed values of the blower volumetric flow rates. As can be inferred from figure 2.1.10, the co-flow velocity is mainly controlled by the blower flow rate. However, for a fixed blower flow rate, the co-flow velocity is also a function of the co-flow temperature (since the co-flow pressure is fixed, the density reduces when the temperature augments) and the latter is increased by augmenting the hydrogen flow rate. The co-flow temperature measured with the thermocouple is used as a feedback signal that acts on the hydrogen pressure reducing valve to reach the co-flow temperature target value.

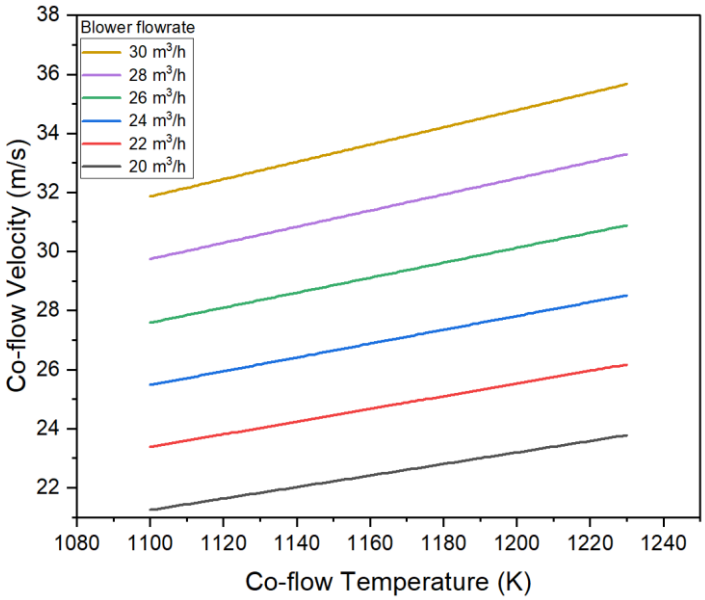

Figure 2.1.10: Co-flow velocities at different temperatures.

2.1.3 The introduction of jet control system

The jet fuel control system has shown in figure 2.1.11. The jet gas is mixed by a premixed tank which is made by stainless steel and can withstand a maximum pressure of 2 MPa. The premixed tank is equipped with a safety valve and pressure gauge. Mixture fuels method of different blending ratios is based on the partial pressure law. When the preparation of ammonia-hydrogen blending fuels starts, the preparation operations are shown as follow: (1) close the outlet valve of the premix tank; (2) open the ammonia inlet switch of the premix tank; (3) adjust the gas pressure reducing valve to adjust the pressure of the gas in the premix tank; (4) observe the pressure gauge of the premix tank to make the ammonia pressure in the premix tank reach the predetermined value; (5) close the ammonia gas inlet switch and open the hydrogen gas inlet switch, and repeat the above operations, so that the hydrogen pressure in the premix tank reaches the predetermined value; (6) close the hydrogen inlet switch, disconnect the connecting pipeline between the gas cylinder and the premix tank after the preparation of ammonia-hydrogen blending fuel is completed. Once the outlet valve of the premixed tank opens, a solenoid valve in the jet pipeline controlled by the LH-04 relay module can be used to adjust different injection pulse width to realize the different injection time of ammonia-hydrogen blending fuel. In order to synchronize the injection of ammonia-hydrogen blending fuel and the operation of the high-speed camera, a synchronous trigger method is designed. The two signals are controlled simultaneously to ensure that the high-speed camera can begin to record the injection beginning moment once the solenoid valve is opened to inject fuel.

As far as the evaluation of jet velocity is concerned, the presence of a water layer around the fuel pipe makes virtually null the heat transfer from the co-flow

to the fuel during the working conditions of the burner. The fuel jet outlet velocity can be consistently determined by assuming that its temperature is almost equal to the water-cooling temperature. Therefore, for each tested inject pressure, velocity of the ammonia jet has been determined, based on the measured fuel mass flow-rate, the pipe cross section area and the fuel density (the density of the ammonia is calculated at the environment pressure and at the water-cooling temperature).

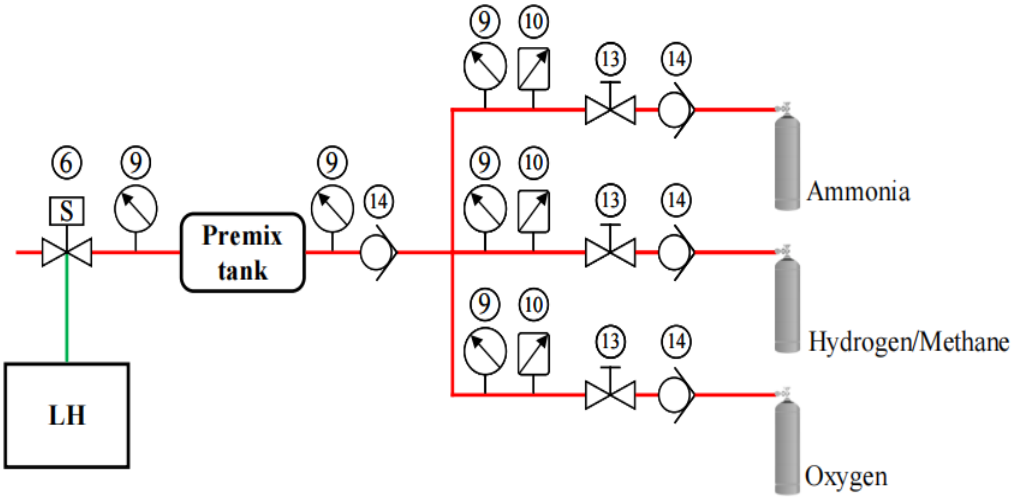

Figure 2.1.11: Jet fuel control system.

2.1.4 The introduction of cooling system

The cooling system shown in figure 2.1.12 is designed to consist of two distinct channels, each with a function to dissipate heat effectively from critical components of the burner assembly. The first channel is integrated into the design as an annular passage surrounding the fuel jet tube, with its inlet located at the base of the jet tube. The second channel encompasses the outer retaining ring, with its inlet mounted onto the ring's structure. During experimental operations, the cooling water inlet temperature is maintained at an approximate 10 °C. The first cooling channel operates in close proximity to the fuel jet tube, forming a concentric arrangement that facilitates the removal of heat via convection directly from the tube's surface. This design allows for a high degree of thermal transfer efficiency due to the minimized thermal resistance between the hot surface and the cooling medium. The second cooling channel, encircling the outer retaining ring, is important for sustaining the ring by preventing thermal overload. The design of both cooling channels takes into account the flow rate that can be regulated based on real-time thermal load assessments.

In summary, the cooling system's dual-channel approach is optimized to provide targeted cooling to the jet tube and outer retaining ring, ensuring that these components operate within their thermal design limits. The precise control

of water temperature and flow rate, with the design of the cooling channels, are critical to the successful mitigation of heat, thereby safeguarding the burner's performance and longevity.

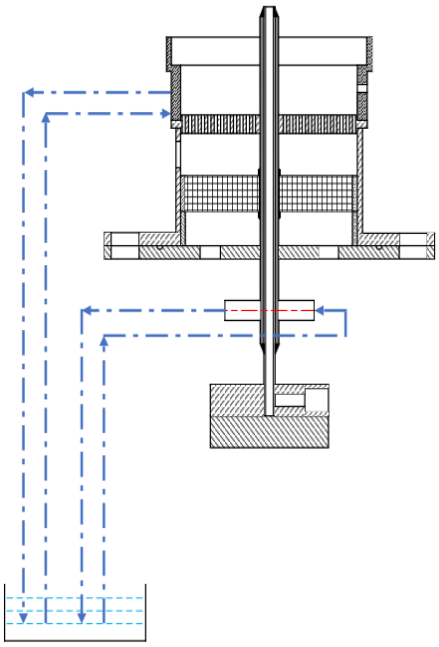

Figure 2.1.12: The cooling system.

2.1.5 Data acquisition method

The original flame images are captured by the Phantom V7.3 high-speed camera from American VRI Company. The camera has a maximum resolution of 800×600, uses an SR-CMOS sensor, 14-bit depth of field, a full-frame shooting rate of 6688 frames/second, and a frame rate of up to 500,000 frames/second. The control software with the high-speed camera can be used to control camera performances, such as resolution, frame rate, and exposure time. In this work, the parameter settings of the high-speed camera were as follows: The resolution is 512×512 pixels, the shooting frequency is 500 Hz, and the exposure time is 2 ms.

In order to obtain the full flame data, a figure data extraction method is proposed, based on Python software. The detailed steps are shown in figure 2.1.13 and 2.1.14 and can be summarized as follow: (1) in order to reduce the subsequent processing time, the original figure is converted to a grayscale flame image. The storage of each pixel only requires one byte, so converting flame images into grayscale images can reduce the subsequent processing time. The amount of calculation is reduced, and the grayscale image can still accurately express the characteristics of the image. (2) Based on the same method, a color image can be obtained to observe the flame combustion beginning point and flame brightness clearly. (3) Then the grayscale flame image is converted to a Binarization flame

image to get a clear flame morphology boundary. The threshold value of binarization need to be chosen. The main difference between real flame and obtained area (red line in 2.1.13e) is the key judgment to choose the optimal threshold. A brightness point in right corner of the flame in the original image, which is the thermocouple used to measure the temperature of the co-flow field, may be occurred sometimes. This point is relatively blurry in the original image and the grayscale image, but can be clearly seen after binarization. The image processing system can remove this point during the data extraction process to ensure that it does not affect the extraction of flame characteristic parameters and ensure the accuracy of test data extraction.

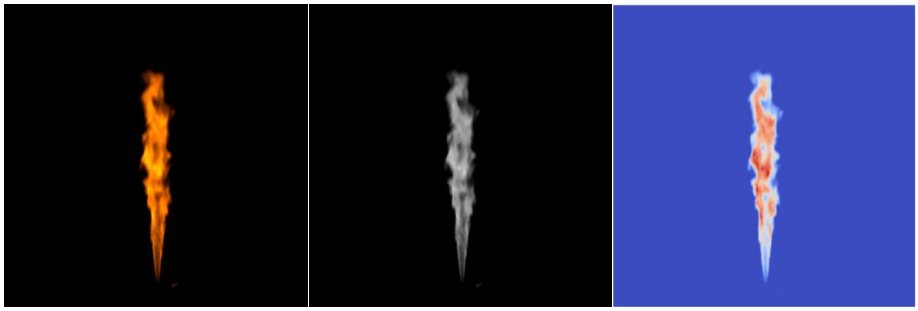

(a) Originally figure (b) Grayscale (c) Colored grayscale

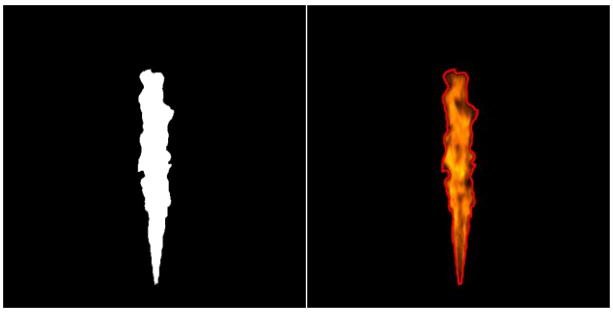

(d) Binarization (e) Flame data extraction

Figure 2.1.13: Data processing method.

The characteristic parameters extracted are shown in figure 2.1.15 (the horizontal dashed line represents the fuel pipe outlet position). By measuring the distance from the lowest point of the extracted jet flame to the injection outlet, namely H, the normalized flame lifted height can be calculated as H/d, where d is the fuel pipe inner diameter. The flame length is the distance L between the highest point and the lowest point of the extracted flame, while the flame perimeter is the length C of the extracted flame edge. Finally, the flame area is the area S enclosed by the extracted flame edge, and the flame perimeter-to-area ratio is the value of S/C. Since steady-state flames should be considered, 50 consecutive flame pictures with visible flame have been selected for the experimental analysis, and the average value of each parameter is calculated as the characteristic parameter of the flame to ensure the reliability of the data. Finally, the contour information and the characteristic parameters, such as the lifted height, flame length, flame area and perimeter have been obtained.

Besides the flame geometric parameters, the flame brightness and ignition delay also can be obtained. The gray value is used to present the flame brightness. The gray value has been defined in Eq 2.1. The ignition delay can be recorded from the first image recorded by camera to the first image in which the flame can be observed in stable flame. The camera and electric relay have a synchronous control, so the first figure can be seemed the starting time of injection.

Gray value=0.299×R value+0.587×G value+0.114×B value (2.1)

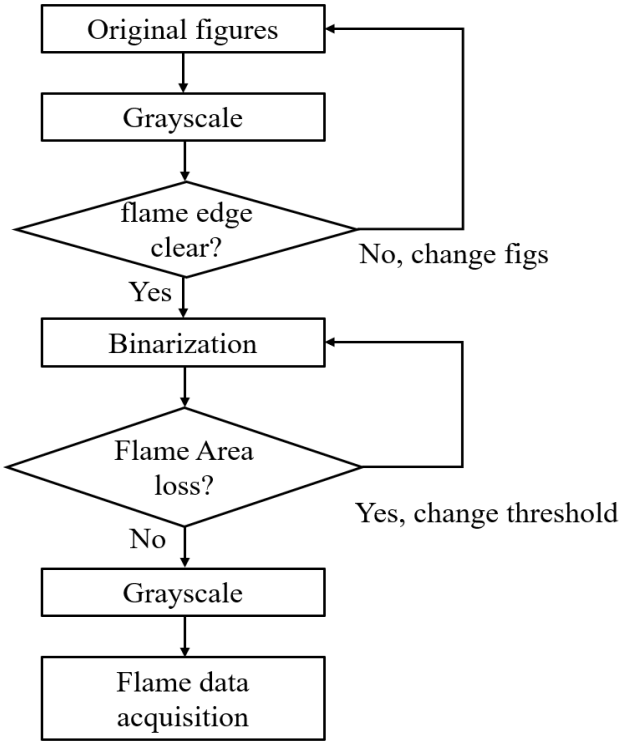

Figure 2.1.14: Data processing flow diagram.

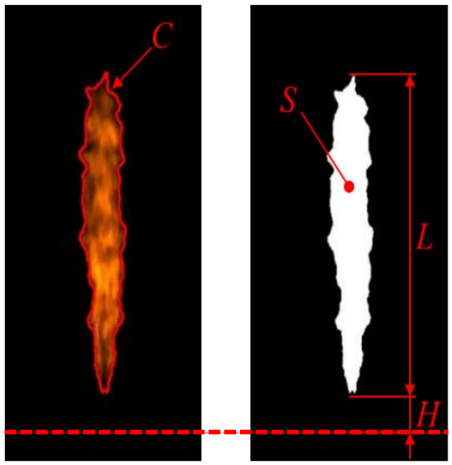

Figure 2.1.15: Schematic diagram of characteristic parameters of the jet flame

2.2 Experimental and simulation methods

The experimental method and process are shown in figure 2.2.1 and 2.2.2. As an example of ammonia-hydrogen, the ammonia and hydrogen are blended homogeneously in a premixed storage tank controlled by jet flow control system

(cf. chapter 2.1.3); then jet flow is injected into a controllable thermal co-flow which is controlled by co-flow system (cf. chapter 2.1.2). Flame behaviors are recorded by a camera from the initiation of injection to close of the jet valve. Autoignition sequences are captured as video recordings. The flame characteristic parameters are extracted from each image frame employing the data acquisition method (cf. 2.1.5).

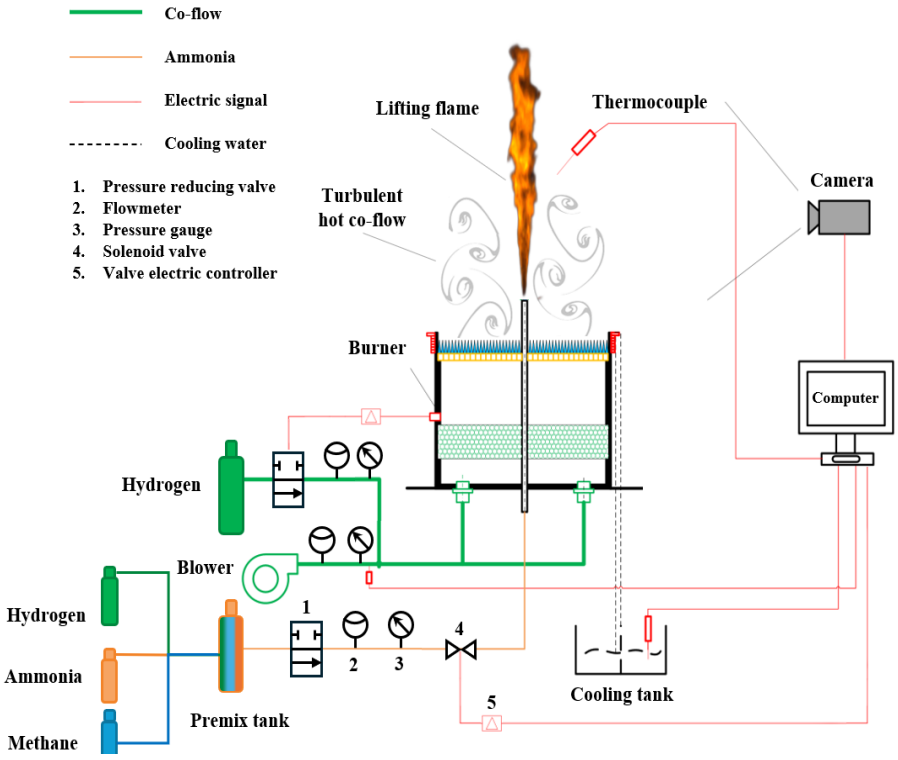

Figure 2.2.1: Experimental test platform.

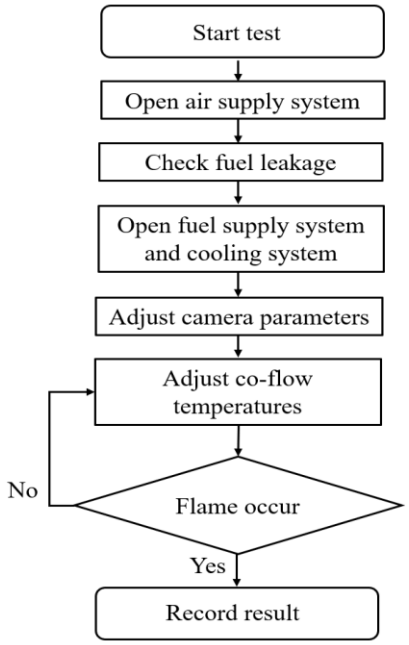

Figure 2.2.2: Experimental test process.

To investigate the auto-ignition characteristics and emission production mechanism of ammonia and ammonia blending fuels, simulation tool of CHEMKIN is used. CHEMKIN is a computational software package designed to solve complex chemical kinetics problems and simulate various chemical reactions, including combustion processes in different reactor models. The software is capable to model closed homogeneous batch reactors, which are commonly used to calculate auto-ignition characteristics for different fuels under a wide range of temperatures, environmental pressures, and fuel types.

In order to define chemical mechanism, the CUE and MEI mechanism have been selected by an extensive simulation from 1100K to 1500K, shown in figure 6.2.1. Moreover, the pure ammonia in oxygen-enriched condition has been validated shown in figure 6.5.1. The simulation results show that the MEI mechanisms provide a good match with the experimental data, particularly at temperatures above 1200 K and excess oxygen coefficients near 0.2.

2.3 Chapter Summary

In this chapter, the experimental platform has been introduced and the main works have shown: based on the controlled thermal atmosphere burner, the combustion experimental system of ammonia and ammonia blending fuels had been designed and built, and the working process and components of the experimental system are introduced. The co-flow supply system, the jet system and the cooling system have been introduced in detail. The data acquisition system and data obtained method have been introduced. The parameters of combustion characteristics have been defined.

Chapter 3

Autoignition boundary and stability mechanism of pure ammonia turbulent flames under high-temperature co-flow

3.1 Experiment conditions of pure ammonia auto-ignition

The auto-ignition characteristics of pure ammonia have been investigated based on the experimental platform. The gas in premixed tank is pure ammonia (99.9%). In experimental test, the plastic pipelines and joints are replaced every 2 days to avoid the ammonia leakage because of high corrosivity of ammonia. A specialized ammonia gas leakage detector is used to detect the leakage of ammonia in every pipeline and joint from the beginning to the end of test. The detector can be used continuously to detect the ammonia concentration to ensure the safety of human healthy. In order to form a turbulent co-flow with high temperature, the experimental conditions have shown in table 3.1.

The auto-ignition performance of ammonia necessitates investigation due to its lower flame speed, higher ignition energy, longer ignition delay, and worse stability. Due to the challenges associated with the application of pure ammonia in internal combustion engines (ICEs), defining its combustion performance is critical for evaluating different flame enhancement methods. Furthermore, clarifying the auto-ignition characteristics of ammonia in turbulent conditions is significant for informing the design of ammonia burners and compression ignition (CI) engines. But the turbulence characteristics of ammonia auto-ignition remain insufficiently characterized globally. Consequently, experimental tests targeting auto-ignition characteristics of pure ammonia, aim to define the auto-ignition boundary, investigate the mechanisms of combustion stability, and analyse auto-ignition characteristics within high-temperature turbulent fields. Subsequent

analysis will integrate results on flame morphology, geometric parameters, combustion boundaries, and stability to facilitate the advancement of ammonia combustion applications. The flame morphology, combustion boundary and combustion stability have been summarized in next section.

Table 3.1: Experimental conditions of pure ammonia.

Parameters	Value
Co-flow velocity (U_{cf}) [m/s]	23, 25, 27, 29, 32, 34
Injection pressure (P_{inj}) [bar]	1.3, 1.6, 1.9, 2.2, 2.5
Injection velocity (u_{inj}) [m/s]	3.4, 9.4, 15.5, 21.5, 27.6
Co-flow temperature (T_{cf}) [K]	1113-1223

3.2 Morphology characteristics of ammonia jet flame

Flame morphology is a fundamental parameter in the analysis of flame propagation and combustion efficiency. The jet flame combustion process of pure ammonia has shown in figure 3.2.1. The auto-ignition full process of ammonia jet flame can be recorded by high-speed camera from auto-ignition to extinction. Once the electric valve open, the ammonia injection begins and the cold ammonia flow jets into the high temperature co-flow. Then ammonia will mix with oxygen and absorb the energy from the high temperature co-flow. The temperature of ammonia/air gas increases until the auto-ignition occurs, as figure 3.2.1(a) shown. With the flame propagates, the flame length, flame brightness, flame area and flame perimeter increase from minimum to maximum. Once the jet flame parameter has not been increased, it means the combustion propagate to the max, shown as figure 3.2.1(b). After auto-ignition of the ammonia jet flow occurs, the flame length, flame area and flame brightness increase rapidly, and a stable lifted flame is formed. After the ammonia jet forms a stable lifted flame, the flame will continue for a period of time which is mainly determined by the pulse width of the ammonia jet solenoid valve. Finally, the electric valve close and the residual ammonia form injection system inject into co-flow. The flame length and area decrease rapidly, then jet flame is gradually extinguished, shown as figure 3.2.1(c). According to the images of the ammonia continuous lifted flame taken by the high-speed camera, it can be seen that the ammonia jet flame presents obvious turbulent flame corrugation characteristics.

The ammonia jet flame at different co-flow temperatures have been reported in figure 3.2.2. The overall color of ammonia jet diffusion flame is orange with brighter yellow zone, the main reason for the formation of ammonia flame is the spectrum of the NH_2 free radicals and water vapor in the ammonia flame [77,78]. With the T_{cf} increases, the flame brightness increases. The RGB average value and brightness can be used to evaluate the flame brightness, shown in figure 3.2.3.

The flame brightness shows an obvious increment once the T_{cf} >1173 K. A higher T_{cf} can form a brightness area at the center of jet flame. The center brightness area represents an intense combustion occurs. A higher T_{cf} can improve the combustion chemical reaction and form an intense lifted flame. When the T_{cf} increases, ammonia flame becomes longer, the overall injected ammonia can be burned, the jet flame become completer and more stable.

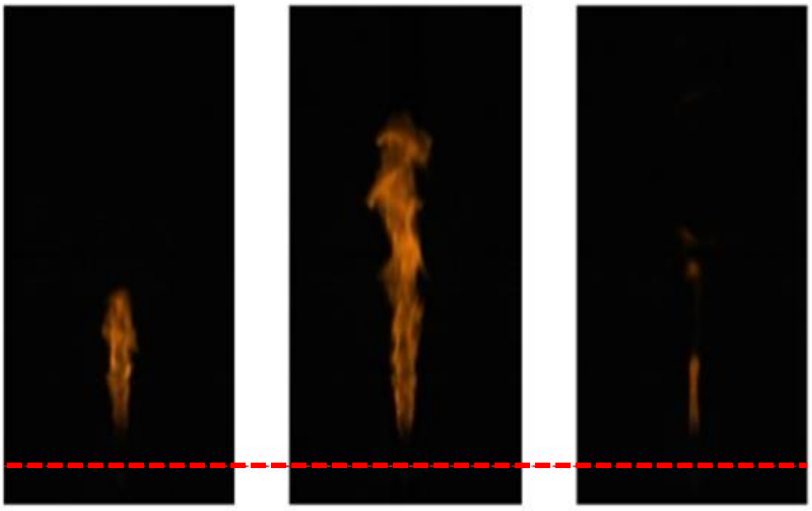

(a) Auto-ignition (b) Combustion (c) Extinction

Figure 3.2.1: Ammonia auto-ignition in the co-flow field captured by high-speed camera.

(T_{cf} = 1223 K, U_{cf} = 25 m/s, and P_{inj} = 1.9 bar)

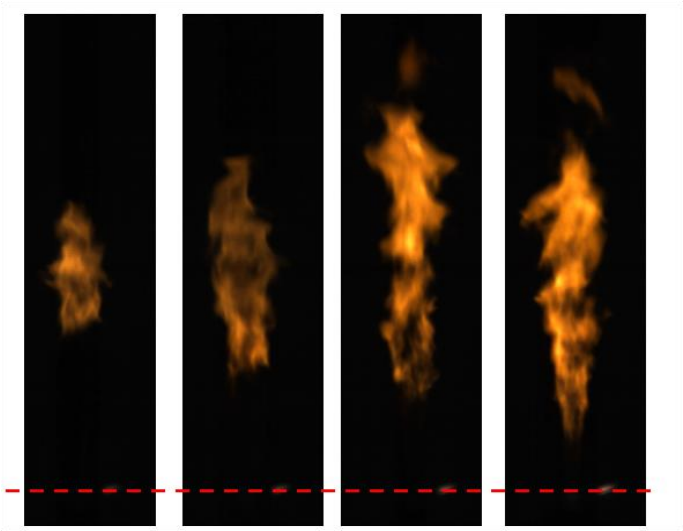

1148 K 1173 K 1198 K 1223 K

Figure 3.2.2: Ammonia jet flame at different co-flow temperatures.

(U_{cf} = 25 m/s, P_{inj} = 1.9 bar)

When the T_{cf} is lower (1148 K), the overall brightness of the flame is low, and the flame length is also significantly small. The reason is that only part of ammonia can be ignited in lower T_{cf} (1148 K) compared to higher T_{cf} (1223 K).

The unstable auto-ignition due to the low co-flow temperatures lead to a large amount of unburned ammonia. When the co-flow temperature reaches to 1223 K, the orange brightness of the flame is significantly enhanced, because the high temperature makes the high vibrational excited states of the molecule in the ammonia flame more pronounced [77, 96, 175].

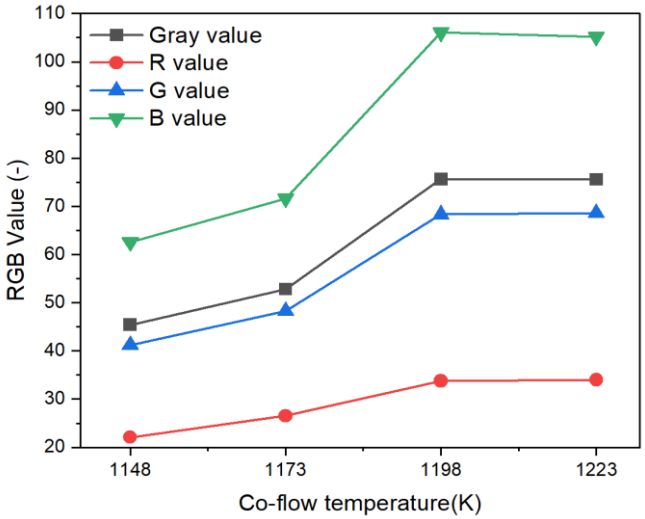

Figure 3.2.3: The flame brightness of ammonia at different co-flow temperatures.

(U_{cf} = 25 m/s, P_{inj} = 1.9 bar)

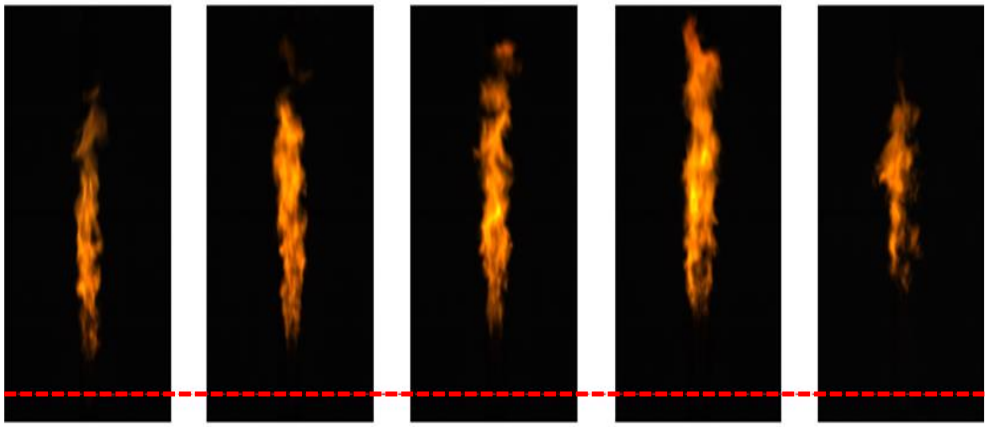

1.3 bar 1.6 bar 1.9 bar 2.2 bar 2.5 bar

Figure 3.2.4: Ammonia jet flame at different injection pressures.

(U_{cf} = 25 m/s, T_{cf} = 1173 K)

Figure 3.2.4 shows the original images of the ammonia jet flames with different injection pressures under T_{cf} = 1173 K and U_{cf} = 25 m/s. It can be seen that the lifted height of the flame increases with an increase in injection pressure. When P_{inj} reaches to 2.5 bar, the overall brightness of flame become lower, compared to the brightness at P_{inj}= 2.2 bar. The flame length is significantly lower at P_{inj}= 2.5 bar, which indicates that the auto-ignition of the ammonia jet is incomplete. The reason is that the large amount of ammonia injects into the co-

flow field, which cannot completely burn, leading to a large amount of unburned ammonia.

According to the overall observation at different combustion conditions: the flame combustion efficiency and stability have an obvious influence by different co-flow temperatures, co-flow velocities and jet pressures. So, in order to control the ammonia auto-ignition with a higher combustion efficiency and a better stable flame, the characteristics of ammonia auto-ignition need a further analysis.

In figure 3.2.5, the flame length and the flame area are reported at different co-flow temperatures, while figure 3.2.6 shows the corresponding flame perimeter and aspect ratio S/C. For both the figures, U_{cf} has been kept constant at 25 m/s, and P_{inj} is equal to 1.9 bar. As can be inferred from figure 3.2.5 and 3.2.6, the length, area and perimeter of the ammonia flame increase with T_{cf}. The flame length of ammonia combustion is primarily affected by the flame speed of ammonia. If the T_{cf} increases, the flame speed of ammonia augments [176], thus promoting the faster development of the ammonia flame in the axial direction; therefore, the diffusion ability of ammonia becomes stronger with an increment in the T_{cf} value, leading to an augmented flame area. The flame perimeter will also increase together with the value of T_{cf}, due to the more pronounced flame length and wrinkle. Froude number (Fr), the ratio of the initial momentum of the jet to the buoyancy force, is one of the important factors affecting the flame length. For turbulent jet flame, Fr and flame length are defined by the following Eq 3.1 and 3.2 [173,177]:

$$\mathrm{Fr} = \frac{u_n \cdot \varphi^{1.5}}{\left(\frac{\rho_n}{\rho_\infty}\right)^{0.25}\left(\frac{\Delta T_f}{T_\infty} g d\right)^{0.5}} \quad (3.1)$$

Where, $\Delta T_f = T_f - T_\infty$ represents the temperature difference caused by combustion, T_f is flame temperature, and T_∞ represents ambient temperature, it refers to the co-flow temperature. ρ_n is the density of the jet, ρ_∞ is the density of the environment gas, refers to the co-flow atmosphere gas density(ρ_{CO}); u_n is the velocity of jet, g is the local gravitational acceleration, and d is diameter of the jet nozzle. φ represents the chemical equivalent.

$$L \propto \left(\frac{\rho_n}{\rho_\infty}\right)^{0.5} \quad (3.2)$$

With jet pressure increases, the velocity and momentum of the jet increase, in the meanwhile, the Froude number increases. When the Froude number is large, the effect of buoyancy on the flame is weakened, and the momentum of the jet is the dominant factor. As the jet momentum increases, the flame length starts to increase. That the reason why flame length increases at 1.3-2.2 bar.

The dashed curve plotted in figure 3.2.5, which follows Eq.3.2, has been determined, based on experimental data of co-flow temperatures, up to 1198 K. In fact, for a certain value of initial axial jet momentum, a fixed fuel flow-rate, an asymptotic flame length value exists: such a value is reached as the fuel jet can absorb enough heat from the co-flow to ensure a complete combustion. A knee occurs in figure 3.2.5 when T_{cf} =1198 K and for T_{cf}>1198 K the flame length

starts to be less sensitive to T_{cf}, and any further increment only reduces the lifted height.

As can be inferred when examining figures 3.2.5 and 3.2.6, flame geometric features augment modestly as co-flow temperature surpasses 1198 K. This implies that at T_{cf} = 1198 K, U_{cf} =25 m/s and P_{inj} =1.9 bar, the jet ammonia already has acquired the sufficient heat energy from the co-flow field for thorough combustion fulfilment. The increment become slightly in flame parameters at T_{cf} =1223 K, due to ignition delay reduction. A smaller ignition delay represents the fuel jet reaches the auto-ignition state closer to the nozzle exit to diminish lifted height.

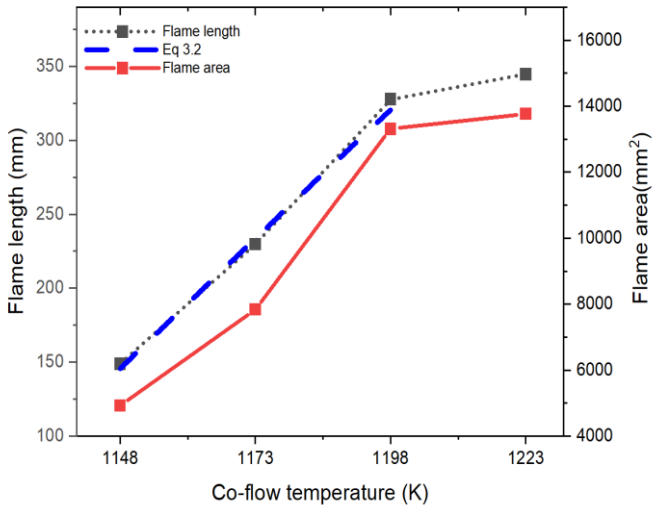

Figure 3.2.5: Flame length, flame length model based on Eq. 3.2 and flame area of ammonia gas at different co-flow temperatures.

(U_{cf} =25 m/s, P_{inj} =1.9 bar)

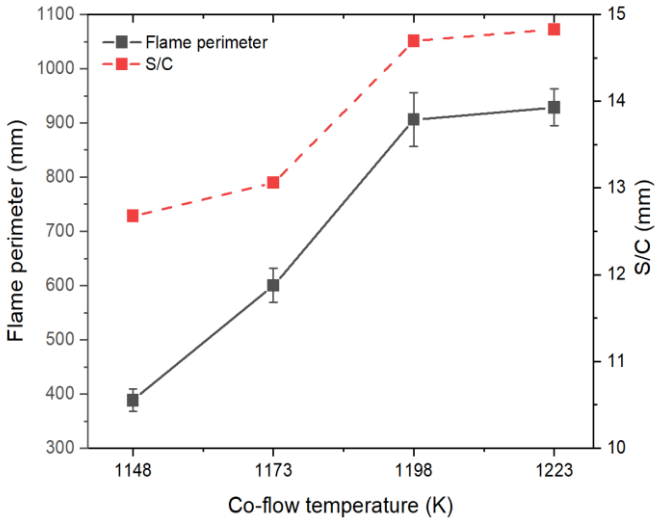

Figure 3.2.6: Ammonia flame perimeter and S/C at different co-flow temperatures. (U_{cf} = 25 m/s, P_{inj} =1.9 bar)

Figures 3.2.7 and 3.2.8 compare geometrical parameters of ammonia jet flame under different injection pressures. In particular, the experimental T_{cf} is 1223 K,

and the different curves refer to two co-flow velocities equal to 23 m/s (continuous lines) and to 32 m/s (dashed lines). The higher co-flow velocity generally augments the turbulence of the co-flow field around the ammonia jet; therefore, it promotes the heat transfer between the fuel and the co-flow field, leading to a growth in the length, area and perimeter of the jet flame. The rise in the ammonia jet speed (a higher P_{inj}) obviously corresponds to an increment in the ammonia volumetric flow rate: this enhances the mixing rate with the oxygen, and the temperature of the flame combustion will rise, thus improving the diffusion of the ammonia jet gas and promoting the chemical reactions. Furthermore, due to the increase in the jet momentum, the diffusion distance of the ammonia jet in both the axial and radial directions increase and lead to a flame morphology change.

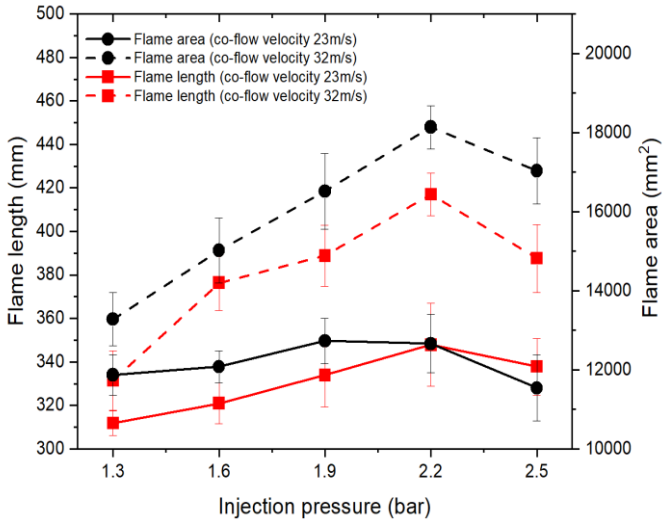

Figure 3.2.7: Length and area of ammonia flame at different jet velocities. (T_{cf} = 1223 K)

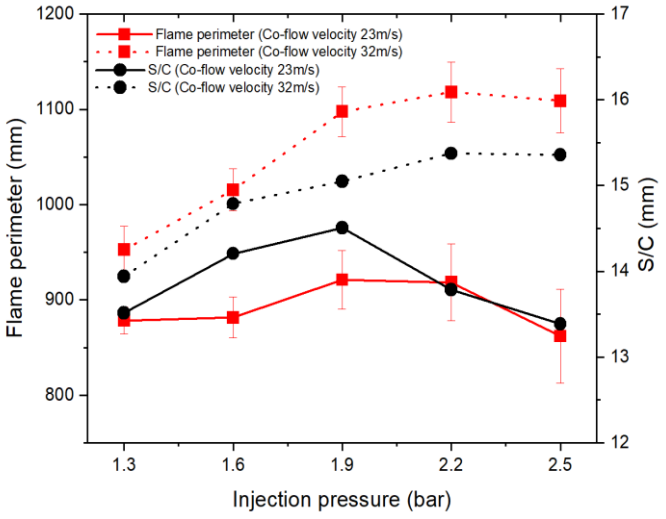

Figure 3.2.8: Ammonia flame perimeter and aspect ratio at different jet velocities. (T_{cf} = 1223 K)

However, when the jet pressure exceeds 2.2 bar, as reported in figure 3.2.7 and 3.2.8, a rapid decline in the length, area and perimeter of the ammonia flame

can be noticed. In fact, the amount of ammonia injected into the co-flow field is high and cannot be fully burned [178]. Therefore, there may be a large amount of unburned ammonia in the co-flow field, which leads to the reduction in the length, area and perimeter of the ammonia flame.

3.3 Auto-ignition boundary

In order to find a better control strategy to avoid the unstable combustion, auto-ignition boundary of ammonia should be investigated and clarified. A definition auto-ignition boundary of ammonia is very important for its application.

The ammonia auto-ignition boundary has shown in figure 3.3.1 at P_{inj}=1.9 bar. Every point has been tested at least 3 times to improve accuracy. The blue triangles, named "Auto-ignition", represents a stable lifted flame can be formed in every times. The red circle, named "No combustion" represents no flame can be obtained by camera and data acquisition method. The black square, named "Auto-ignition boundary" represents the flame can be observed sometimes which means it is difficult to form a stable flame at the boundary condition. With the co-flow velocities increases, a stable flame needs a higher co-flow temperature. The reason is that the heat exchange time between jet flow and co-flow decreases due to co-flow velocity increases. The jet flow does not have enough time to mix with oxygen and absorb energy from high temperature co-flow. As an example, by considering a co-flow speed of 23 m/s, the ammonia jet can be ignited at a co-flow temperature beyond 1163 K, forming a stable lifted flame.

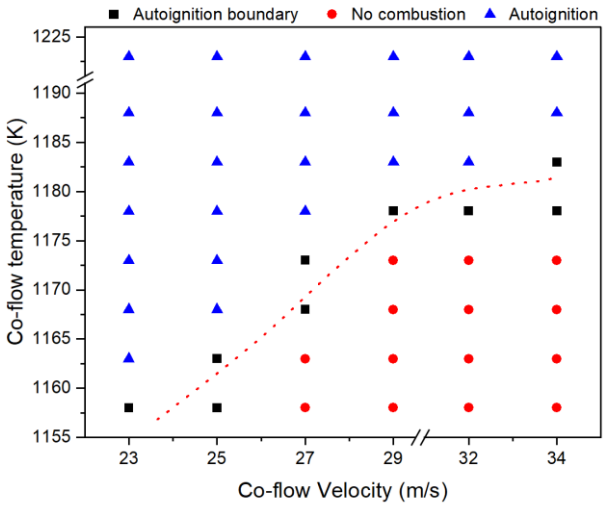

Figure 3.3.1: Auto-ignition of ammonia at different co-flow velocities.

(P_{inj}=1.9 bar)

Figure 3.3.2 shows the auto-ignition boundary of ammonia under different P_{inj} with a fixed co-flow velocity equal to 25 m/s. With the jet pressure increases, the lowest auto-ignition temperature increases. For example, if P_{inj}=1.6 bar, the ammonia jet can be ignited and a stable lifted flame can be formed when the co-flow temperature is beyond 1158 K. At the same co-flow temperature, a higher

injection pressure leads to a higher initial momentum and a higher jet velocity. In fact, a higher jet velocity reduces the mixing time between the jet flow and the co-flow, therefore the ammonia cannot reach the auto-ignition temperature. Similar trends to the one reported in figure 3.3.1 have been obtained for different co-flow velocities.

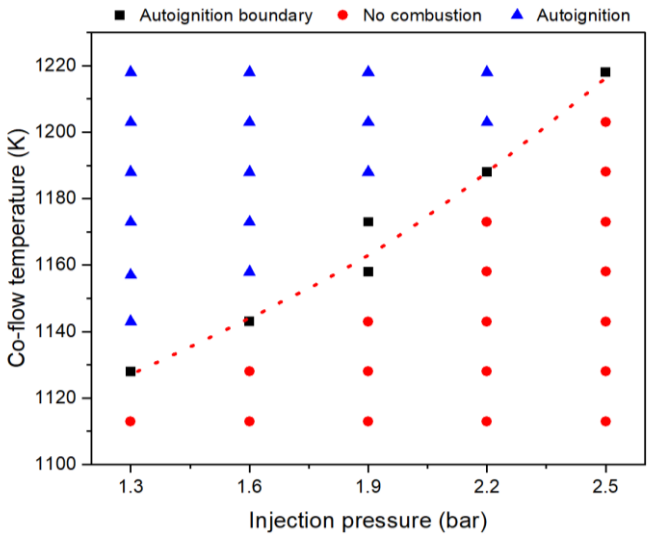

Figure 3.3.2: Auto-ignition of ammonia at different jet pressures.

(U_{cf} = 25 m/s)

3.4 Ignition delay and auto-ignition point

Ignition delay is an important parameter to evaluate fuel combustion characteristics. A shorter ignition delay usually represents the fuel has a higher combustion efficiency and a better flammability. The figure 3.4.1 shows the ignition delay at T_{cf} = 1148-1123 K, U_{cf} = 25 m/s and P_{inj} =1.9 bar. When the co-flow temperature is closer to 1148 K, ammonia is still in the unstable region of the combustion boundary (cf. figure 3.3.2). Therefore, a higher co-flow temperature lead to a higher the combustion stability, leading to a pronounced drop in the ignition delay up to T_{cf} = 1173 K. A lower co-flow temperature and a higher injection pressure let the ammonia cannot absorb enough energy from the co-flow at T_{cf} = 1148 K, leading to a high value of flame lifted height and to the presence of unburned ammonia. When the T_{cf} rises to 1173 K, the fuel reaches a stable lifted flame, and the ignition delay further decreases. Beyond this temperature, the energy exchange between the fuel and the co-flow is enough to ensure a stable flame. When the co-flow temperature exceeds 1198 K, the ammonia flame is always stable, and the influence of the co-flow temperature on the ignition delay of ammonia is reduced. The ignition delay has a stronger temperature sensitivity when co-flow temperature is lower than 1198 K, which means the chemical reaction control the ignition in a lower co-flow temperature. When T_{cf} >1198 K, the ignition decline trend decrease, which means the temperature effect on chemical reaction is not the key factor at high temperature. At the high co-flow

temperature, the physical gas mixing effect become the dominated factor on ignition delay because the temperature effect on chemical reaction has been reach to maximum. The temperature turning point is 1198 K of pure ammonia at U_{cf} = 25 m/s, P_{inj}=1.9 bar and it also can be called temperature sensitivity limitation point. The ignition delay shows a near 18% decline once the T_{cf} increases form 1148 K to 1173 K. But the decline is only near 6% when the T_{cf} increases form 1198 K to 1223 K

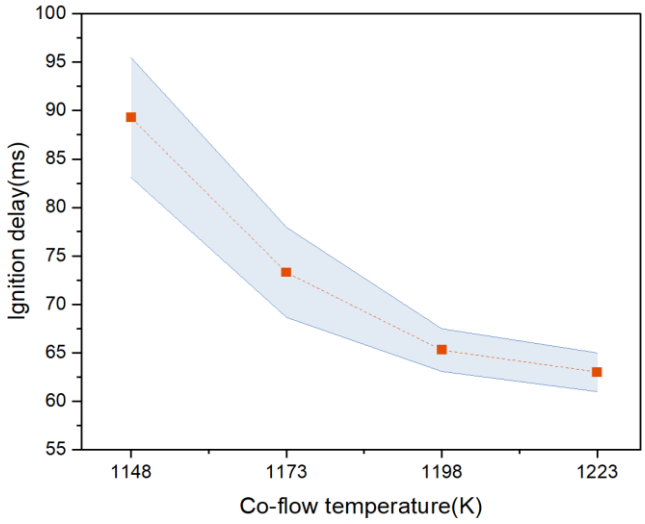

Figure 3.4.1: Ignition delay of ammonia at different co-flow temperatures.

(U_{cf} = 25 m/s, P_{inj}=1.9 bar)

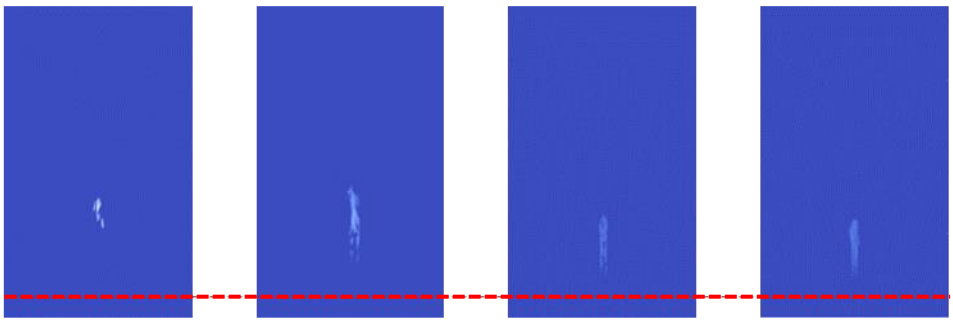

Figure 3.4.2: Location of auto-ignition point of ammonia gas at different co-flow temperatures.

(U_{cf} = 25 m/s, P_{inj}=1.9 bar)

The auto-ignition point has shown in figure 3.4.2, which represents the flame core formation. In order to a better observation, the background color change to blue and a red line represent the injection position. At a lower co-flow temperature (1148 K), the flame core location is far away from injection outlet and the core boundary fuzzy. The fire cores are small and scattered even unconnected, showing a multi-point distribution accompanied by wrinkles. It means the combustion is unstable and easy to extinct at 1148K. As the co-flow temperature increases to 1173 K, the flame cores gradually concentrate, the fuzzy

boundary disappears, the fire core is closer to the nozzle exit, flame core area increases and the core structure is close to a preliminary flame. In fact, the augmented co-flow temperature provides the ammonia jet with a higher energy, which promotes the auto-ignition and makes the position of the auto-ignition point closer to the nozzle outlet. Once the co-flow temperature increases to 1198 K and 1223 K, the flame core structure and position nearly has a slightly change. The flame core boundary become flat and core is closer to injection outlet, which means the flame core formation is smoother to ignite and diffuse. Thus, a higher co-flower temperature (T_{cf} >1198 K) can improve combustion stability.

3.5 Lifted height and auto-ignition stability

The normalized flame lifted height (H/d), corresponding to an average position of the flame, can be used to quantify the flame stability because it is sensitive to several flow and flame parameters, especially to the co-flow temperature [157]. Thus, lifted height has been used to evaluate the combustion stability in different T_{cf}, U_{cf} and P_{inj}.

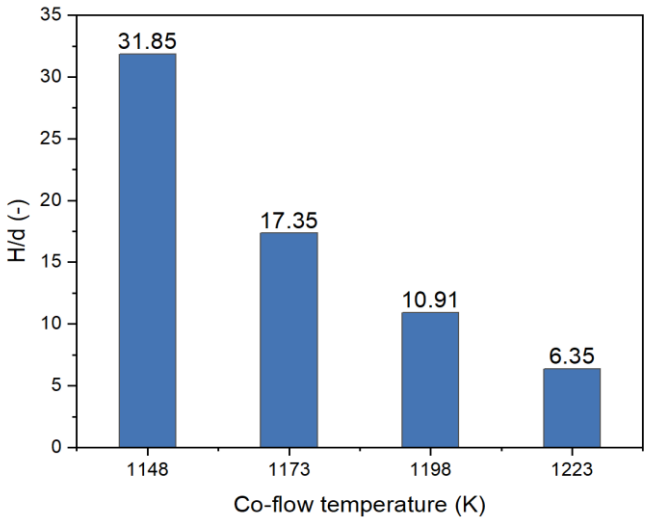

Figure 3.5.1: Ammonia flame lifted height at different co-flow temperatures. (U_{cf} =25 m/s, P_{inj}=1.9 bar)

Many fuels show a co-flow temperature threshold beyond which its influence on flame lifted height drastically reduces [30]. The temperature threshold for the ammonia under the considered experimental conditions can be identified at T_{cf}= 1198 K, for both the ignition delay and flame lifted height. In figure 3.5.1, the lifted height declines with the T_{cf} increases. It is similar to the trend of ignition delay, which the turning point is near to 1198 K. When the T_{cf} <1198K, the lifted height has obvious decline and a higher sensibility to T_{cf}. Whereas, when the T_{cf} >1198 K, although the lifted height still decreases, the lifted height is lower sensitive to T_{cf}. The one reason is that the ignition delay has a strong effect on lifted height in a lower T_{cf}. A lower ignition delay represents a fast chemical reaction to lead the combustion occurs close to the tube outlet. The other reason is

that for the flame lifted height, an augmented co-flow temperature increases the flame stability, due to an enhanced heat exchange.

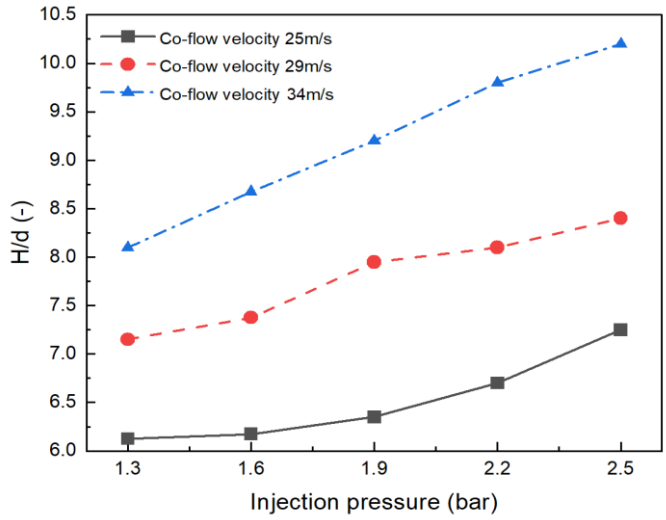

Figure 3.5.2: Lifted height versus injection pressures at different co-flow velocities.

(T_{cf} = 1223 K)

Co-flow velocity and injection pressure have an important effect on ammonia lifted height [179]. The lifted height trends with respect to the injection pressure for different co-flow velocities in T_{cf}=1223 K. In order to eliminate the co-flow temperature effect, the T_{cf} has been chosen to the max temperature in which a stable flame can be formed. The figure 3.6.2 shows that a higher P_{inj} and U_{cf} lead to a higher lifted height. A higher P_{inj} increases the concentration of ammonia in the area near to the ammonia injection tube, leading to augmented local equivalence ratios, therefore, the auto-ignition is not promoted and the ammonia flame will be settled further away from the injector tube outlet. A higher U_{cf} decreases the heat exchange time and the ammonia gas does not absorb enough thermal to auto-ignite. A higher U_{cf} also lead to the ammonia gas energy dissipate too fast to concentrate energy. Thus, a suitable P_{inj} and U_{cf} is very important to ammonia combustion control strategy.

A modified large-scale mixing model suitable for auto-ignited flame in a high-velocity co-flow field has been developed in [133]. In particular, the lifted height ca be expressed as Eq. (3.3):

$$\frac{H}{d} \propto \tau_{ign,ad} \frac{(k_{st})^{\alpha}}{\tau'^{\,1-\alpha}_{mix}} \quad (3.3)$$

Where $\tau_{ign,ad}$ is the ignition delay determined by CHEMKIN at adiabatic stoichiometric conditions, k_{st} is the strain rate, τ'_{mix} is the mixing time, which also accounts for shearing effects, and α is a parameter in the range of [0, 1]. When α = 1, small-scale strain completely dominates the lifted height, while if α = 0, large-scale mixing entirely controls the lift-off height. The flame strain rate is calculated as Eq. (3.4):

$$k_{st} \propto \frac{u_{inj}}{d}(Re_{co} \cdot f_M)^{0.5} \quad (3.4)$$

where u_{inj} is the fuel velocity, d is the injector pipe diameter and Re_{co} stands for the Reynolds number of the co-flow and f_M is defined as Eq. (3.5):

$$f_M = \left[1 + \frac{1-M}{\left(\frac{d_{cf}}{d}\right)^2 M}\right]^{0.5} \quad (3.5)$$

Where d_{cf} is the diameter of the burner disk (equal to 100 mm) and M is the specific co-flow-to-jet momentum flux ratio, defined as Eq. (3.6):

$$M = \left(\frac{u_{cf}}{u_{inj}}\right)^2 \frac{\rho_{cf}}{\rho_{jet}} \quad (3.6)$$

In which ρ_{cf} and ρ_{jet} stand for the co-flow and fuel jet density, respectively.

Due to the absence of a flowmeter suitable for ammonia, the fuel flow rate and the fuel velocity, have been determined by means of a characterization of the fuel line when air flows through it. In particular, for the same injection pressures, air flow rate has been measured when the solenoid valve is opened and there is not any co-flow in the burner. Based on the measuring principle of the employed Alicat flowmeter, the corresponding mass flow rate of ammonia can be determined from the air flow rate based on dynamic viscosity and density of the two gases. The presence of a water layer around the fuel pipe shields the fuel from heat transfer due to the co-flow presence during normal working conditions of the burner. Therefore, effects of heat transfer which can modify the fuel flow-rate, based on the Rayleigh flow theory, when co-flow laps the fuel pipe can be disregarded, and the flow rate can be consistently assumed equals to the one determined when the burner is turned off and outlet temperature is almost equal to the environment one. Therefore, for each tested P_{inj}, velocity of the ammonia jet has been determined.

The mixing time τ'_{mix} in Eq. (3.7) can be expressed as

$$\frac{1}{\tau'_{mix}} \propto \frac{u_{inj}}{L_P}\left[1 + C\left(\frac{\Delta u}{u_{cf}}\right)\right] \quad (3.7)$$

Where C is a positive coefficient representative of the degree of shearing effect on the mixing time, $\Delta u = u_{inj} - u_{cf}$ and L_p is the potential core length, evaluated as Eq. (3.8):

$$\begin{cases} \frac{L_p}{d} = 4 + 12\left(\frac{u_{cf}}{u_{inj}}\right) & \text{if } u_{cf} < u_{inj} \\ \frac{L_p}{d} = \frac{16}{\left(\frac{u_{cf}}{u_{inj}}\right)} & \text{if } u_{cf} > u_{inj} \end{cases} \quad (3.8)$$

Lifted height data has been plotted using the modified mixing-strain model given by Eq. (3.3) in figure 3.5.3, with C = 0.167 and $\alpha = 0$, meaning that ammonia diffusive combustion in high-temperature co-flow is controlled by the large-scale mixing.

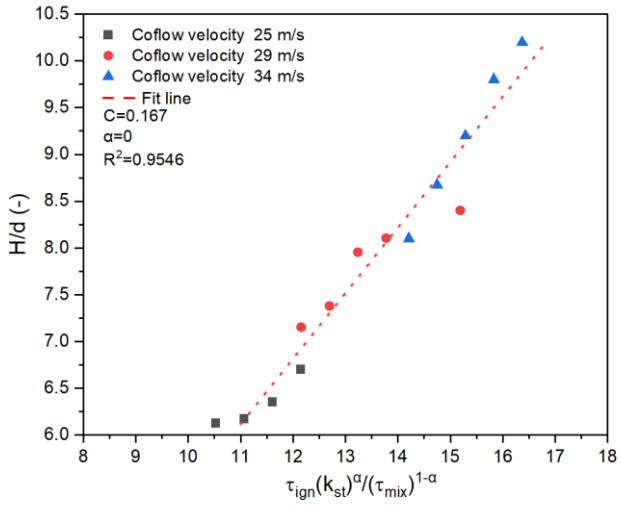

Figure 3.5.3: Modified mixing-strain model correlation of lifted height at different co-flow velocities.

(T_{cf} = 1223 K)

Besides the lifted height (H/d) combustion model, the time-fluctuations of the flame lifted height also can evaluate the combustion stability. The lifted height fluctuation at different T_{cf} in 200-260 ms has shown in figure 3.5.4. In order to form a stable flame, the co-flow velocity and injection pressure have been controlled to 25 m/s and 1.9 bar. As the co-flow temperature increases, the maximum and average value of flame lifted height reduces overall which means flame becomes more stable. The standard deviation of the flame lifted height (H/d) in the considered time interval is reported in figure 3.5.4: it dramatically reduces when the co-flow temperature increases. Because of faster flame speed and lower ignition delay with a higher co-flow temperature, both the flame diffusion and chemical reaction have been enhanced, improving the flame stability of the ammonia diffusive combustion. In fact, when the co-flow temperature is high, the mixing process between ammonia in the jet and oxygen in the co-flow is accelerated, which is more conducive to the formation of combustible gas mixture, making the combustion become more stable, and there is no obvious multi-point auto-ignition phenomenon. Instead, when the co-flow temperature is low, the combustion of the ammonia jet is very unstable and accompanied by a sharp burst sound (as soon as the co-flow temperature exceeds a certain value, the burst sound disappears). The flame front is uneven, the shape is very irregular, and the direction and speed are frequently changed in the combustion process: unburned ammonia can be diffused and heated from all directions, and the resulting small explosions emit sharp pressure pulses, causing ringing.

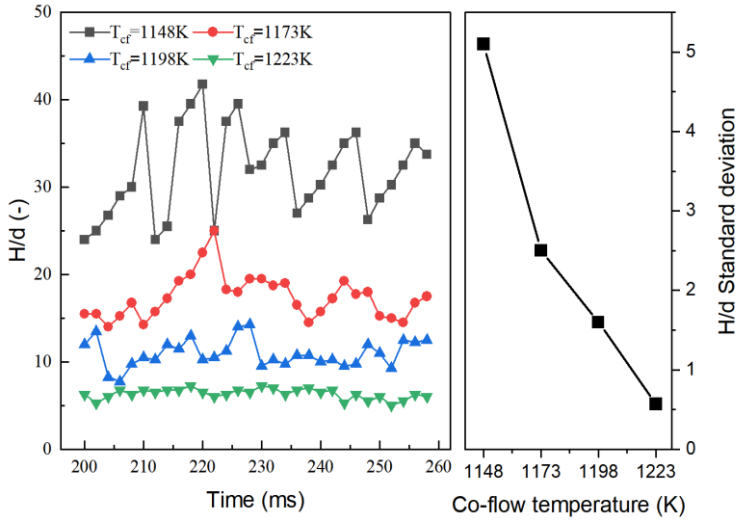

(a) Lifted height at different T_{cf} (b) Standard deviation of H/d at different T_{cf}

Figure 3.5.4: The lifted height time fluctuations at different co-flow temperatures.

(U_{cf} = 25 m/s, P_{inj}= 1.9 bar)

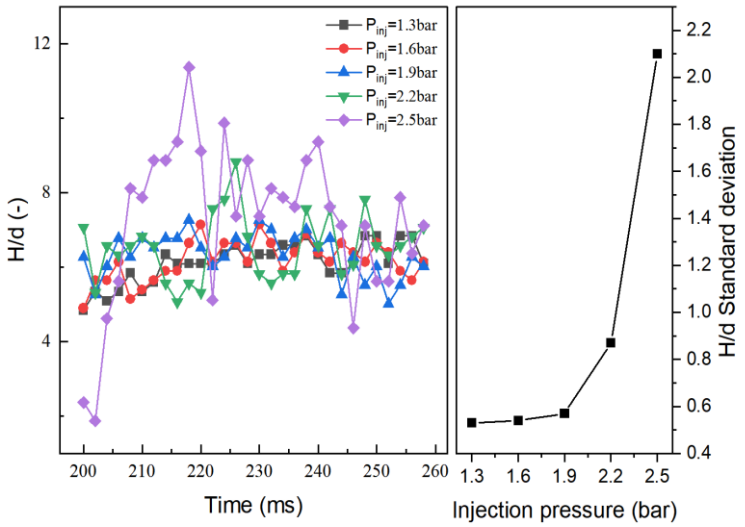

(a) Lifted height at different P_{inj} (b) Standard deviation of H/d at different P_{inj}

Figure 3.5.5: The lifted height time fluctuations at different injection pressures.

(U_{cf} = 25 m/s, T_{cf}= 1223 K)

The lifted height (H/d) fluctuations for different injection pressures have been reported in figure 3.5.5. The standard deviation of the flame lifted height in the considered time interval increases with the injection pressure increases. A higher pressure leads to higher fluctuations, due to intensified turbulence disturbance because of the augmented fuel Reynolds number. With an injection pressure increase, the injection velocity rises, and the flame morphology continuously

changes from lift-off to blow-off: for P_{inj}=2.5 bar, the ammonia lifted flame shows a critical auto-ignition (CA) behaviour, that is represented by the repetition of flame extinction and re-ignition [180]. In order to a further analysis the flame extinction and re-ignition phenomenon, the blow off flame can be observed at a higher condition: P_{inj}=2.5 bar and U_{cf}=34 m/s. As reported in figure 3.5.6, a series consecutive photo in 200-260 ms report a critical auto-ignition behaviour in which the lifted height is high with a high fluctuation. A higher fluctuation means the flame combustion is unstable with repetition of extinctions and re-ignition. In fact, the burnt gas could induce local acceleration in the streamwise velocity, due to the buoyancy, thus leading to blowout. As the local velocity decelerates, as a result of the mitigation in the buoyancy effect, an auto-ignition can again occur [180].

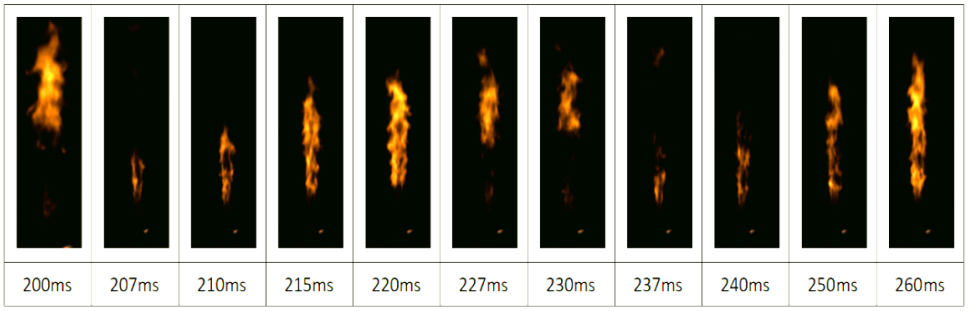

Figure 3.5.6: The flame fluctuation and reignition phenomenon in the time range 200-260 ms after the beginning of the fuel flow.

(T_{cf} = 1223 K, P_{inj}= 2.5 bar, U_{cf} = 34 m/s)

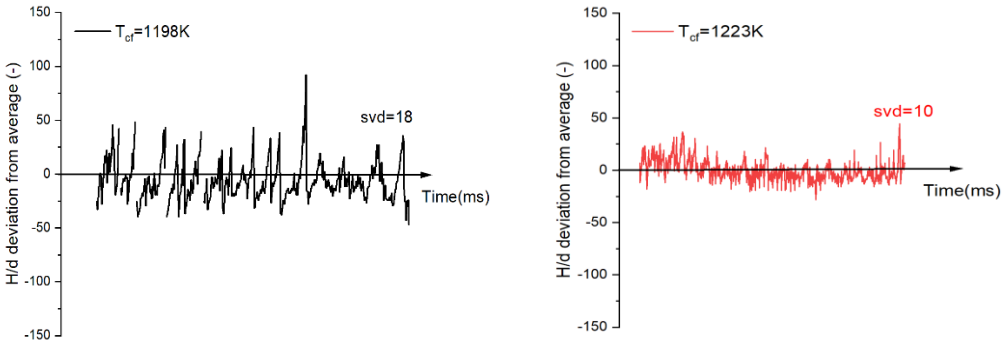

(a) The lifted height at 1198 K (b) The lifted height at 1223 K

Figure 3.5.7: The flame stability at different co-flow temperatures.

The unstable flame with repetition of extinctions and re-ignition behaviour has a critical effect on flame stability. The figure 3.5.7 show the flame H/d fluctuations from the injection to extinction at different co-flow temperatures. Different with figure 3.5.4, both the stable and unstable combustion have been summarized that is the reason why the svd is higher. In figure 3.5.7, the flame fluctuation declines with the co-flow temperature increases. When the T_{cf} reach to 1223 K, the flame standard deviation close to 10 which show a 44% decline compare to T_{cf} = 1198 K. Thus, a higher T_{cf} can improve the flame stability.

3.6 Chapter Summary

In this chapter, the turbulent jet flame characteristics of pure ammonia within a high-temperature co-flow, measured by the Controllable Active Thermo-Atmosphere (CATA) burner, has been investigated. The non-premixed jet flame morphology of ammonia, the auto-ignition boundary, the ignition delay, the combustion stability mechanism and flame fluctuation have been explored and summarized. The main conclusions are shown as follow:

The overall color of ammonia jet flame is orange with brighter yellow zone. With the T_{cf} increases, the flame brightness, flame length and flame area increase. The reason is that only part of ammonia can be ignited in lower T_{cf} (1148 K). The unstable auto-ignition due to the low co-flow temperatures lead to a large amount of unburned ammonia. When P_{inj} reaches to 2.5 bar, the overall brightness of the flame is lower than the brightness at P_{inj} = 2.2 bar and the flame length is significantly lower. The reason is that a large amount of ammonia injects into the co-flow field, which cannot completely burn, leading to a large amount of unburned ammonia. With the jet pressure increases, the lowest auto-ignition temperature increases. At the same co-flow temperature, a higher injection pressure leads to a higher initial momentum and a higher jet velocity. A higher jet velocity reduces the mixing time between the jet flow and the co-flow; therefore, the ammonia cannot reach the auto-ignition temperature.

At a lower co-flow temperature (1148 K), the flame core location is far away from injection outlet and the core boundary fuzzy. The fire cores are small and scattered even unconnected, showing a multi-point distribution accompanied by wrinkles. It means the combustion is unstable and easy to extinct at 1148 K. As the co-flow temperature increases to 1173 K, the flame core gradually concentrates, the fuzzy boundary disappears, the fire core is closer to the nozzle exit, flame core area increases and the core structure is close to a preliminary flame.

A higher co-flow temperature lead to a lower ignition delay. Once co-flow temperature beyond 1198 K, the decline trend of ignition delay decreases. The ignition delay shows a 6% decline once the T_{cf} increases form 1198 K to 1223 K. At the high co-flow temperature, the physical gas mixing effect become the dominated factor on ignition delay due to the temperature effect on chemical reaction has been reach to maximum.

The distance from the position of the auto-ignition point to the outlet of the central nozzle and the ignition delay both decrease when the co-flow temperature increases. In addition, the flame lifted height of the ammonia gradually decreases with an augment in the co-flow temperature, and there is a critical temperature at 1198 K beyond which the effect of T_{cf} on H/d dramatically reduces. Lifted length data are satisfactorily fitted by a modified mixing-strain model, showing that the combustion is controlled by the large-scale mixing.

With the increase of co-flow temperature, the flame stability of the ammonia increases significantly, and the fluctuations of the flame lifted height with respect to time decrease obviously. Conditions characterized by high injection pressures and high co-flow velocities show an unstable critical auto-ignition behavior, featuring the repetition of extinctions and re-ignition.

Chapter 4

Auto-ignition characteristics and flame enhancement mechanism of ammonia blending fuels

4.1 Experimental conditions of ammonia blending fuels auto-ignition

The blend homogeneity is a key factor for ammonia-hydrogen blending fuel. A premixed tank has been used to blend the ammonia with active gas fuels. In addition to the ammonia detection system discussed in Chapter 3, a specialized hydrogen gas leakage handheld detector has been implemented to keep experimental process safety. The test conditions of ammonia-hydrogen combustion test have shown in Table 4.1. The co-flow velocity and jet flow injection pressure ensure Reynolds number beyond 4000 to form a high temperature turbulent co-flow field. The parameters definition of (U_{cf}, P_{inj} and T_{cf}) are same with pure ammonia experimental test (cf. table 3.1).

Table 4.1: Experimental conditions of ammonia blending fuel fuels

Parameters	Value
Co-flow velocity (U_{cf}) [m/s]	23, 25, 27, 29, 32,
Injection pressure (P_{inj})[bar]	1.3, 1.6, 1.9, 2.2, 2.5
Co-flow temperature (T_{cf}) [K]	973-1173
H_2 ratio(X_{H2}) [%]	0-25
CH_4 ratio(X_{CH4}) [%]	7

4.2 Morphology characteristics of ammonia-hydrogen jet flame

According to multiple investigations conducted on the combustion properties of ammonia-hydrogen blends in various combustion burners [61,72,79,81], a hydrogen fraction ranging from 5% to 25% into pure ammonia has been found to accelerate the combustion process in ICEs. Figure 4.2.1 compares the flame characteristics of the ammonia-hydrogen blending fuels with that of pure ammonia. Compared to pure ammonia, ammonia-hydrogen flame has a higher flame brightness, a large flame area and a crinkly flame morphology at the same experimental conditions. Additionally, the lifted height (H/d) of ammonia-hydrogen is smaller than that of pure ammonia.

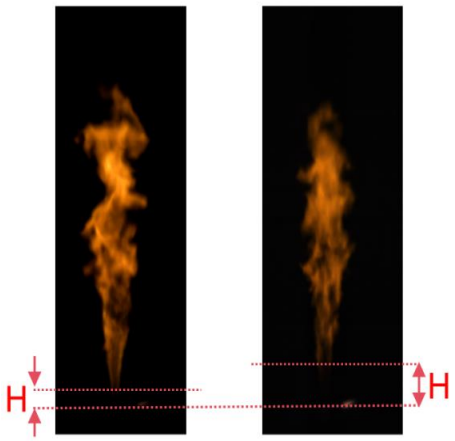

10% H_2/90%NH_3 100% NH_3

Figure 4.2.1: Comparison of ammonia-hydrogen and pure ammonia.

(U_{cf} = 23 m/s, P_{inj} = 1.6 bar, T_{cf} = 1173 K)

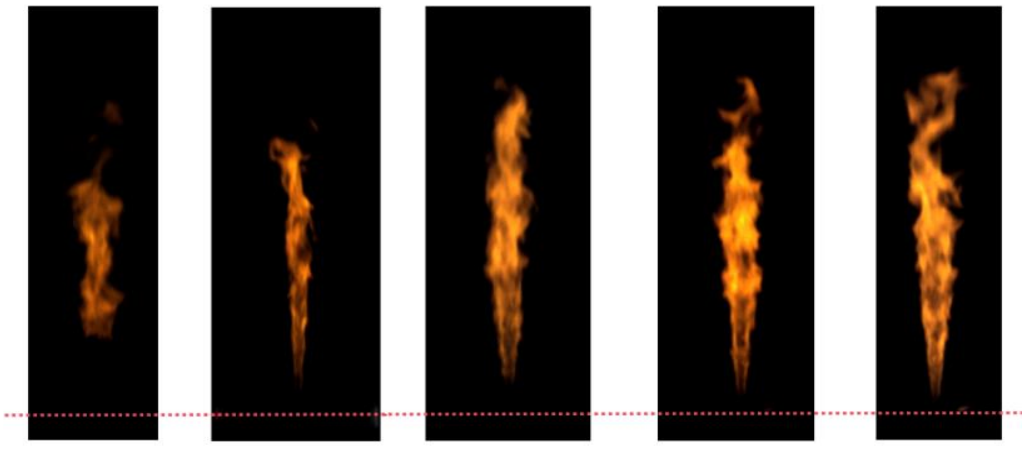

5% 10% 15% 20% 25%

Figure 4.2.2: The flame morphology at different hydrogen ratios.

(U_{cf} = 23 m/s, P_{inj} =1.6bar, T_{cf} = 973K)

The flame morphology at different hydrogen ratios have shown in figure 4.2.2. The pure ammonia can maintain a stable flame when the $T_{cf} \geq 1173$ K, however,

at the same conditions (U_{cf} = 23 m/s, p_{inj} = 1.6 bar), by adding a fraction of 10% to 20% hydrogen into the ammonia, the ammonia-hydrogen blending fuels are capable to maintain a stable lifted flame at a significantly reduced co-flow temperature of 973 K. The effect of hydrogen markedly lowers the threshold temperature required for stable auto-ignition combustion, thus enhancing the flammable limitation of ammonia and potentially broadening its applicability in combustion systems.

Ammonia flame with a low hydrogen addition ratio exhibits an orange color, similar to that of pure ammonia combustion. As the proportion of hydrogen is augmented, the flame becomes brighter, which means that the increasing of hydrogen lead to an augmented production of NH_2. NH_2 is the main factor to control the flame spectrum [18,34]. This enhanced brightness is quantitatively captured by an increase in the flame gray value, a trend that is clearly illustrated in figure 4.2.3. Two principal mechanisms contribute to this elevation in gray value: Firstly, the presence of hydrogen, due to a higher concentration of OH and H, accelerates the NH_2 production [36,37]. Secondly, hydrogen augments the mixture gas combustion temperature, leading to an enhanced chemical ionization. Figure 4.2.4 show the average value of gray value in every 50 pictures from the open time of electric valve to the close time, thereby encompassing the entirety of the injection cycle. The flame average gray value increases with increasing hydrogen ratios.

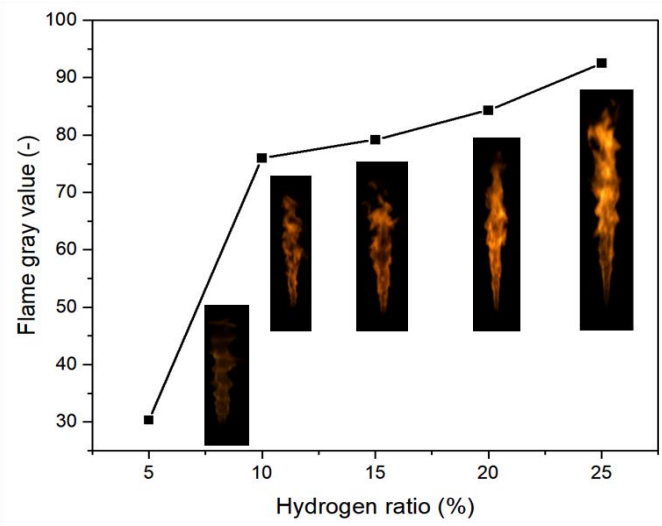

Figure 4.2.3: Flame average gray value at different hydrogen ratios.

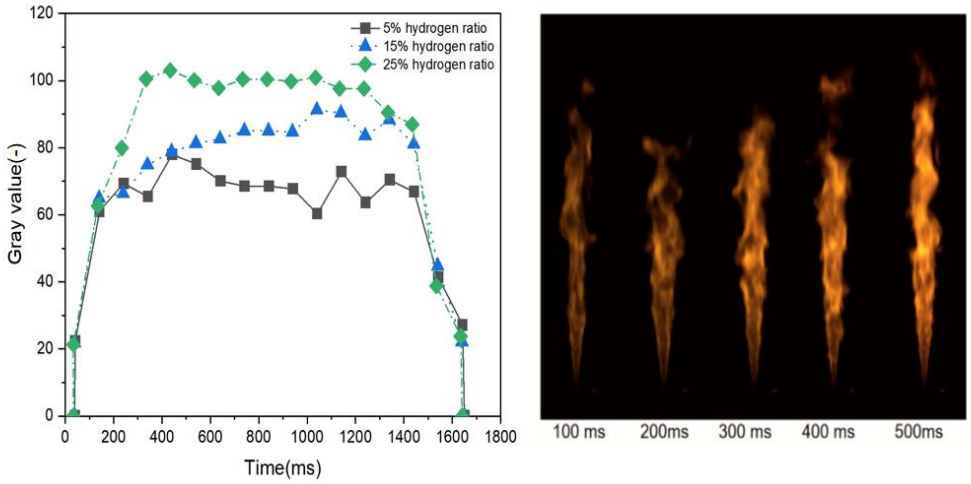

Figure 4.2.4: Flame gray values fluctuation with time at different hydrogen ratios (left); The flame images of 25% hydrogen ratio with time (right).

(U_{cf} =23 m/s, P_{inj} =1.6 bar, T_{cf}=1173 K)

There exists an interesting phenomenon at 25% hydrogen ratio that the gray value growing time from 0 to Max is longest, nearly 350 ms in figure 4.2.4. Conversely, at lower hydrogen ratios of 5% and 15%, this ramp-up period is considerably shorter, approximating 150 ms. The underlying dynamic driving this phenomenon is the differential reactivity of hydrogen relative to ammonia. The reason is that hydrogen is main burned fuel at the beginning because hydrogen is more active than ammonia, so only part of ammonia fuel has been auto-ignited because the hydrogen combustion increases the temperature of mixture flow. And with the more ammonia fuel beginning to be ignited, the mixture flow temperature has an obvious enhancement and lead to ammonia combustion fully. Auto-ignition process ultimately manifests in the observed variations in the temporal development of the flame gray value.

Figure 4.2.5 shows the flame morphology of ammonia/10% hydrogen mixture fuel combustion at T_{cf}= 973-1173 K. As the co-flow temperature increases, the lifted height exhibits a decreasing trend, whereas its length, area, perimeter, and brightness show a concurrent increase. Notably, the combustion flame of the ammonia-hydrogen mixture displays a region of diminished brightness along the axial direction, present at the flame root region (as demarcated by the red rectangle at 1023 K). This localized reduction in brightness can be ascribed to a combination of factors: initially, a lower temperature leads to auto-ignition incompletely. Furthermore, due to its higher chemical reactivity, hydrogen ignites more readily than ammonia, a phenomenon that corroborates the differential brightness observed in figure 4.2.4. With the combustion development and propagation, the middle and upper parts of the ammonia-hydrogen blending fuel flame become brighter and the flame width is larger. The ammonia-hydrogen mixture gas and the oxidant achieve a homogeneous mixture conducive to intense combustion, with the peak brightness situated at the flame's core. With the T_{cf} increase, the ammonia-hydrogen flame brightness maximum increases and flame core become lighter, which means a higher co-flow temperature can enhance the

combustion. The correlation between co-flow temperature and the various parameters of flame morphology emphasizes that the co-flow temperature plays an important role in the combustion of ammonia-hydrogen mixtures, and highlights the critical role of temperature in optimizing the combustion characteristics for such fuel blends in practical applications.

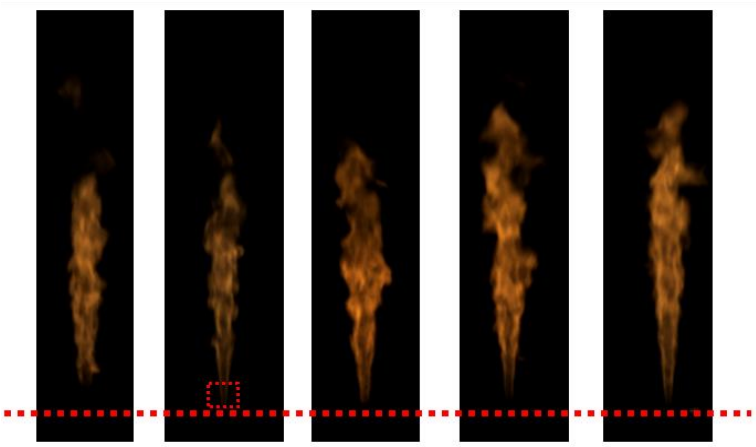

Figure 4.2.5: Ammonia/10% hydrogen flames at different co-flow temperatures. (U_{cf} =23 m/s, P_{inj} =1.6 bar)

In figure 4.2.6, the flame length of ammonia-hydrogen increases gradually with the increase of hydrogen ratio. Mixing hydrogen into ammonia can enhance the mixture flame speed, so that the jet flame can be propagated far away in the axial direction. The hydrogen combustion promotes the ammonia combustion, making the combustion more intense. Hydrogen addition into ammonia has a stronger effect at lower co-flow temperatures. The reason is that hydrogen has a lower ignition delay and lead to decrease the minimum ignition energy of the mixture fuel. Even T_{cf} is lower to 973 K, the T_{cf} is enough for hydrogen ignition, but for ammonia, 973 K is not enough to form a flame. Consequently, the addition of hydrogen effectively broadens the flammability limits of the flame in comparison to pure ammonia, even when the hydrogen mix ratio is as low as 5%. At higher co-flow temperatures, the impact of hydrogen becomes less significant. High T_{cf} values approach or exceed the auto-ignition temperature of ammonia, which means the auto-ignition of ammonia can be occurred without the need for hydrogen. Therefore, the effect of hydrogen on facilitating auto-ignition is diminished at these higher temperatures.

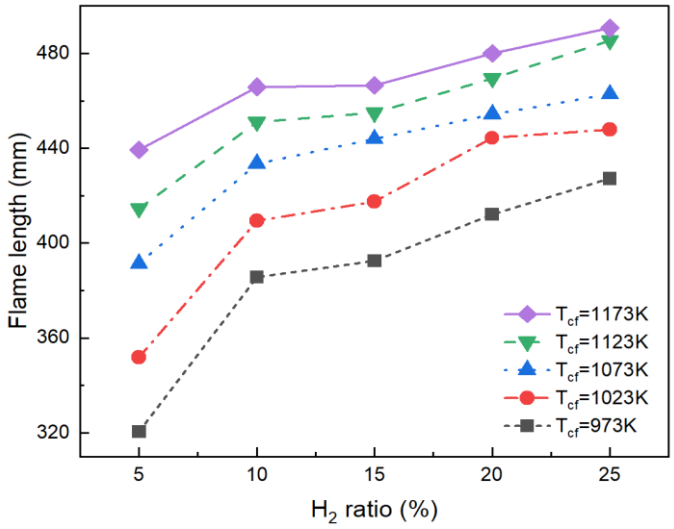

Figure 4.2.6: Flame length with different hydrogen ratios at different co-flow temperatures.

(U_{cf} = 23 m/s, P_{inj} = 1.6 bar)

The length of the flame of an ammonia-hydrogen blending fuel exhibits a gradual increase with a rise in co-flow temperature. Notably, when the hydrogen ratio exceeds 10%, the rate of increase in flame length diminishes, suggesting that a 10% hydrogen ratio may represent an optimal economic balance for enhancing the ammonia flame. The addition of hydrogen leads to a higher concentration of active free radicals, OH and H, which elevate the flame speed and temperature, as referenced in publications [61,72,79,81]. Therefore, on the one hand, hydrogen enhance the chemical reaction of overall mixture gas; on the other hand, the flame temperature increment from hydrogen combustion improves the ammonia combustion. The flame length increases with two reverse directions: towards the proximity of the tube, governed by the ignition delay, and away from the tube, associated with the flame speed. Consequently, both ignition delay and flame speed have influence on flame length. Under high T_{cf} condition (exceeding 1073 K), the combustion enhancement effect of hydrogen cannot be significantly improved, implying that flame propagation speed has minimal alteration. A higher T_{cf} can increase the heat exchange and lead to ammonia auto-ignition fully. Thus, the increase of T_{cf} can promote the combustion of ammonia gas in the mixture fuel, showing that flame length still continues to increase. From the perspective of flame length, hydrogen addition has a stronger effect than T_{cf} increment.

The flame area can be defined as a parameter to evaluate the flame propagation and combustion efficiency. A smaller flame area means a lower flame propagation and a lower combustion efficiency which means a lot of non-ignition ammonia occurs. Non-ignition is a kind of insufficient combustion and need to avoid. The figure 4.2.7 is ammonia/5% hydrogen at T_{cf} =973 K and T_{cf} =1173 K. The flame shows much different even the fuel is same. Thus, a higher T_{cf} have a sufficient combustion and it increases the combustion efficiency. In figure 4.2.8 and 4.2.9, the relationship between flame area and hydrogen ratios at different co-flow temperatures for ammonia-hydrogen blending fuel are quantitatively

reported. The data indicate a positive correlation between flame area and the hydrogen ratio, attributed to an increase in both flame velocity and axial length. A higher proportion of hydrogen improves the auto-ignition process, thereby improving the combustion efficiency of the ammonia-hydrogen mixture gas, which is reflected in an augmented flame area.

Figure 4.2.7: The ammonia/5%hydrogen jet flame at 973 K and 1173 K.

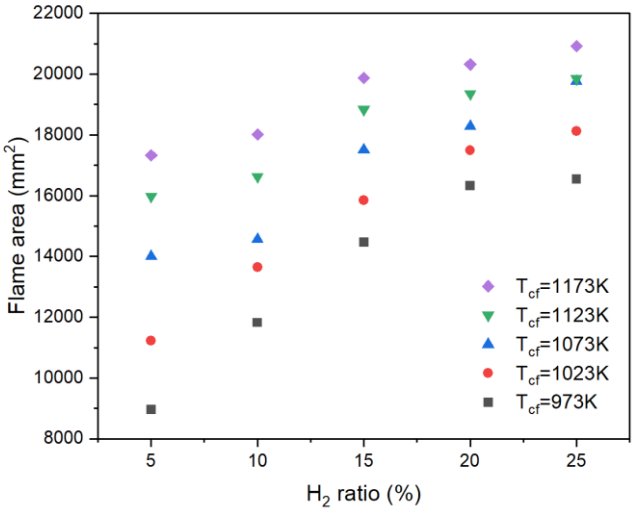

Figure 4.2.8: Effect of hydrogen ratio on flame area at different co-flow temperatures.

(U_{cf} = 23 m/s, P_{inj} = 1.6 bar)

The flame area has a higher sensibility in lower T_{cf}: When the co-flow temperature is 973 K, the mixing ratio of hydrogen increases from 5% to 25%, and the flame area increases by 84.6%. However, when the co-flow temperature is 1173 K, the mixing ratio of hydrogen increases from 5% to 25%, and the flame area only increases by 20.8%. It can be seen that the flame enhancement of mixing hydrogen into ammonia is better at lower temperature. Two factors control the flame area: one is the ignition delay and flame speed due to hydrogen addition (chemical factor); the other is heat exchanging enhancement from co-flow and jet

momentum (physical factor). The data further show the existence of a critical enhancement threshold of hydrogen ratio, close to 20% mixing ratio. When the hydrogen ratio increases to a certain ratio (20%), the flame length and area growth rate become slow, the small increases from the lifted height decline. Upon increasing the hydrogen ratio from 20% to 25%, the capacity of hydrogen to enhance combustion exhibits marginal change. The reason is that: although a higher hydrogen ratio increases the flame area due to the flame speed increases, the ammonia remains the main fuel in blending fuel. Once all the ammonia can be ignited easier, the potential for further expansion of the flame area is limited. This limitation is based on balance between the chemical and physical influences on the flame characteristics and the finite extent to which hydrogen addition can augment the combustion of ammonia within the mixture.

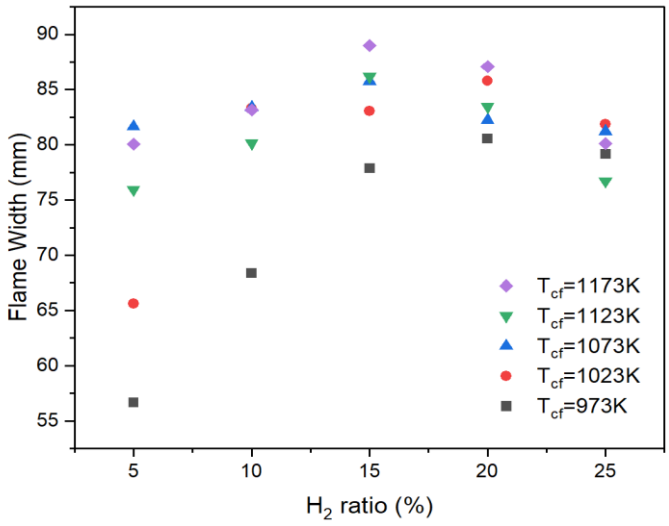

Figure 4.2.9: Flame max width at different hydrogen ratios and co-flow temperatures.

(U_{cf} = 23 m/s, P_{inj} = 1.6bar)

At T_{cf} = 973 K, the auto-ignition of blending fuel occurs because of hydrogen addition. Hydrogen ignites preferentially, followed by the combustion of ammonia because the temperature (973 K) is not reaching the min auto-ignition requirement temperatures for pure ammonia. Consequently, hydrogen ratio donates the flame efficiency (area and length) in lower T_{cf}. When the T_{cf} increase to 1173 K, both ammonia and hydrogen auto-ignition occurs. It is the reason why the flame area is much different at 973 K. The direct participation of ammonia in the ignition process, lessening the reliance on hydrogen to act as the primary ignition source. The higher T_{cf} narrows the discrepancy between the two fuels, hence diminishing the influence by hydrogen on flame characteristics at lower temperatures.

A similar phenomenon occurs at different T_{cf}: With the T_{cf} increases to temperature threshold, at a same hydrogen ratio, the area increments trend decline. The reason is that a higher T_{cf} increase the heat exchange efficiency which lead to improve the mixture gas combustion. Once auto-ignition of ammonia-hydrogen

both occurs, the combustion process is sufficiently optimized to the extent that further increases in flame area are limited. Thus, both adding hydrogen and increasing the co-flow temperature can improve the auto-ignition performance of ammonia. Increasing T_{cf} is more economical method than adding hydrogen increase. The flame area increment in every 50 K is similar with the flame area increment in every 5% hydrogen addition. It suggests that an appropriate balance between T_{cf} and hydrogen ratio can be selected to control over the flame area and combustion efficiency of an ammonia-hydrogen blending fuel.

Figures 4.2.10-4.2.12 reveal that both injection pressure and co-flow velocity leads to an improvement of flame area at different T_{cf}. In fact, the augmented injection pressure corresponds to a higher fuel flow rate. A higher injection pressure, in turn, amplifies the quantity of fuel/oxygen mixture involved in the combustion process, leading to an increment in the temperature of flame combustion. Moreover, a higher injection pressure lead to a higher fuel jet velocity and jet momentum, which promote fuel diffusion in the axial and radial directions.

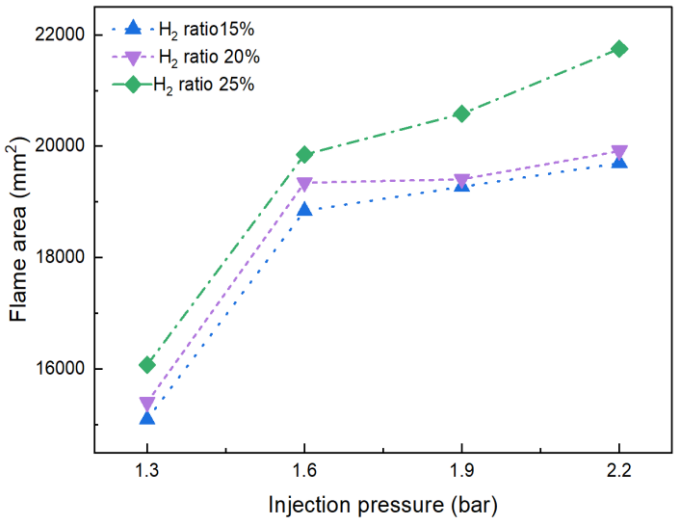

Figure 4.2.10: Flame area of ammonia-hydrogen at different injection pressures. (U_{cf} = 23 m/s, T_{cf} = 1123K)

If the injection pressure is above 1.6 bar, the flame area augment slope reduces, as can be inferred in figure 4.2.11. The increment of jet momentum lead to flame area increase. For example, when the hydrogen ratio increases, at 25% hydrogen, the minimum ignition energy decreases, combustion efficiency increment and momentum increment can both lead to a higher flame area, so the flame area of 25% hydrogen is greater than 5-10% hydrogen at P_{inj}> 1.6 bar.

The increasing of the co-flow velocity enhances the co-flow flow momentum and turbulent intensity of the high-temperature co-flow field. On the one hand, a higher flow momentum blows the jet flame far away from tube in axial direction; on the other hand, a higher co-flow enhances the heat exchange between the jet fuel and co-flow. With the co-flow velocity increases, the difference of flame area between different co-flow temperatures decreases shown as figure 4.2.12, which

means the flow momentum increase can make up combustion efficiency difference because of different T_{cf}.

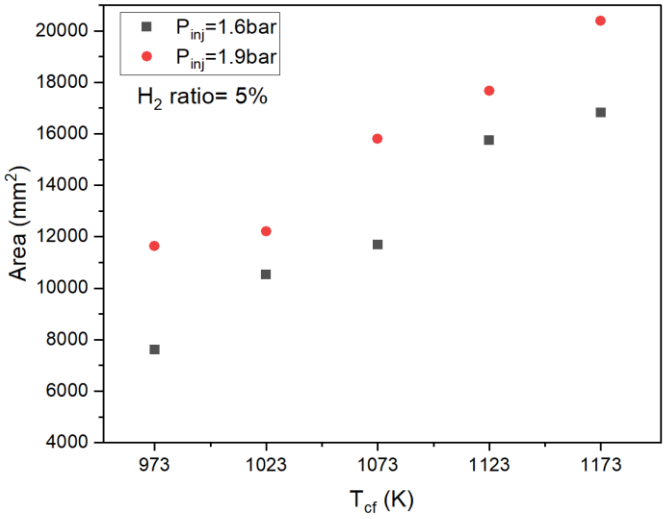

Figure 4.2.11: Flame area of ammonia-hydrogen at different temperatures.

($U_{cf} = 23$ m/s)

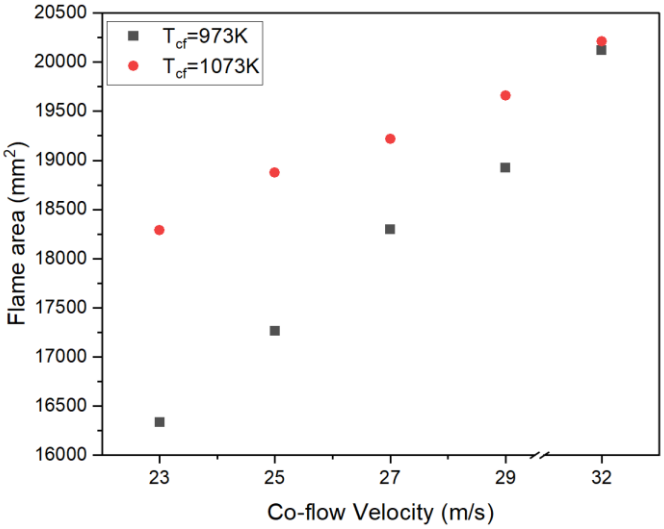

Figure 4.2.12: Flame area of ammonia-hydrogen at different co-flow velocities.

($P_{inj} = 1.6$bar)

4.3 Ignition delay and lifted height of ammonia-hydrogen blending fuel

The ignition delay at different hydrogen ratios and T_{cf} have been reported in figure 4.3.1. With T_{cf} increases, the ignition delay shows a downward trend due to the enhancement of heat transfer between jet fuel and co-flow. The ammonia-hydrogen jet fuel can reach the required auto-ignition temperature faster at a higher T_{cf}. With the hydrogen ratio increases, the ignition delay of ammonia-hydrogen mixture gradually decreases. Even a minor quantity of hydrogen markedly shortens the ignition delay. The hydrogen addition accelerates the

chemical claim of ammonia. Therefore, adding a small amount of hydrogen into pure ammonia let the related reaction of hydrogen to dominate the combustion of ammonia-hydrogen fuel [65]. On the one hand, a lower ignition delay of hydrogen can lead some local auto-ignition spots occur and increase the local temperature, which can promote the combustion of the whole jet fuel. On the other hand, the hydrogen addition enhances the chemical reaction due to active groups H and OH increases.

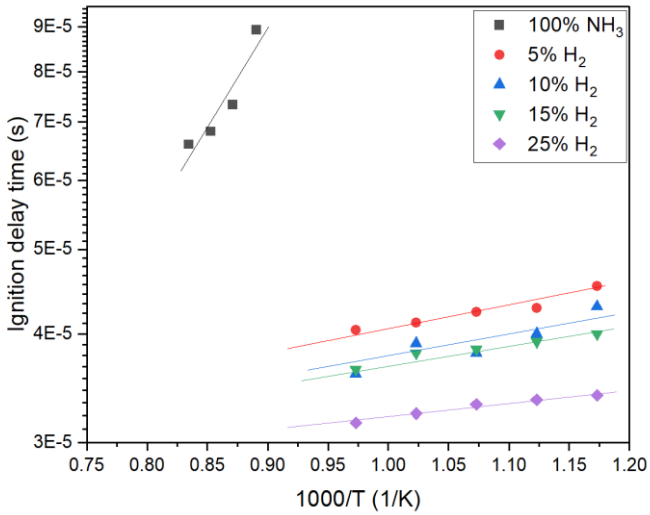

Figure 4.3.1: Ignition delay of ammonia and ammonia-hydrogen

(U_{cf} = 23m/s, P_{inj} = 1.6 bar, X_{H2} = 5%-25% and T_{cf} = 973-1173K.)

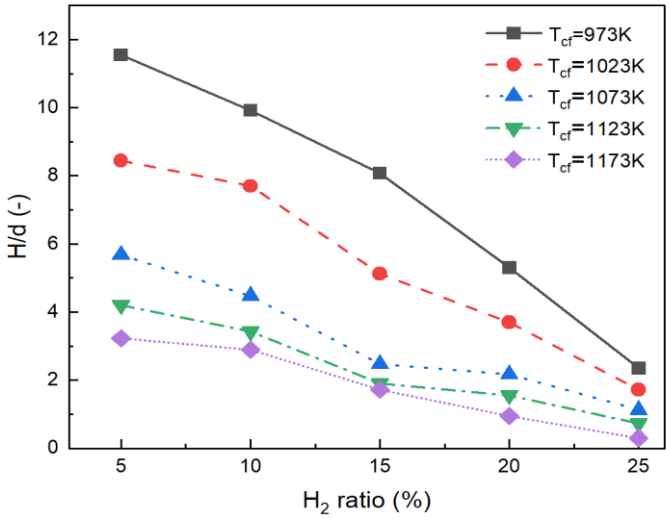

Figure 4.3.2: The flame lifted height at different hydrogen ratios.

(U_{cf} = 23 m/s, P_{inj} = 1.6 bar)

Figure 4.3.2 shows the hydrogen ratio effect on the lifted height of ammonia-hydrogen at different T_{cf}. At different T_{cf}, with the increase of hydrogen ratios, the lifted height shows a downward trend. The reason is that the ignition delay decline lead to auto-ignition occur closer to the tube outlet. At co-flow temperatures below 1073 K, the lifted height (H/d) experiences a pronounced decline; however,

as the co-flow temperature exceeds 1073 K, the decrement in lifted height exhibits a diminishing trend. When the hydrogen content is augmented from 5% to 25%, the lifted height is reduced by 9 at a co-flow temperature of 973 K. In contrast, at a co-flow temperature of 1173 K, the lifted height reduces to a mere 3, showing the more pronounced efficacy of hydrogen in enhancing combustion performance at lower thermal conditions.

Figure 4.3.3 shows the T_{cf} effect on the lifted height (H/d) of ammonia-hydrogen blending fuel at different hydrogen ratios. With the increase of T_{cf}, auto-ignition point is closer to the injector outlet because of a stronger heat exchange effect. The lifted height is less sensitive to the co-flow temperature change when T_{cf} excess the critical temperature (1073 K). It means the heat exchange efficiency has a limitation between and co-flow and jet flow. Actually, with the hydrogen increases, the critical temperature has a slightly decreases. When the hydrogen ratio increases to 25%, the lifted height line is near linear because the increasing of hydrogen ratio dominates the ammonia-hydrogen blending fuel combustion performance, even though the ammonia is the main fuel in mixture. The lifted flame is a combustion balance condition when the max laminar speed is equal to the turbulence flame speed. When the hydrogen ratio increases and the T_{cf} will also increase the mixture laminar speed. A faster flame speed lead to the bottom location of flame is closer to the fuel outlet.

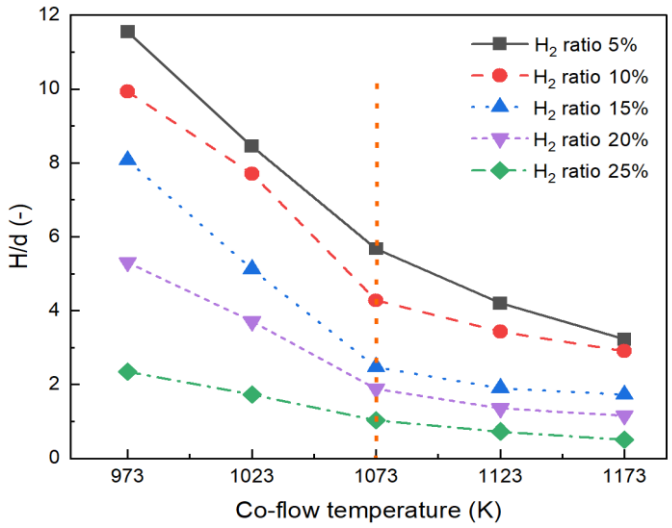

Figure 4.3.3: The lifted height at increasing co-flow temperatures and hydrogen ratios.

Figure 4.3.4 shows the influence of co-flow velocity on the lifted height of ammonia-hydrogen under different co-flow temperatures. With the increase of co-flow velocity, the lifted height of jet flame shows a slightly increase. However, compared to the effect of hydrogen ratio and co-flow temperature on the lifted height, the co-flow velocity effect is smaller. Although co-flow velocity has a stronger effect on pure ammonia, once addition hydrogen, the co-flow fact effect is smaller. It means hydrogen addition can enlarge the ammonia combustion boundary and the hydrogen flame enhancement is higher than hinder effect forms the co-flow increment.

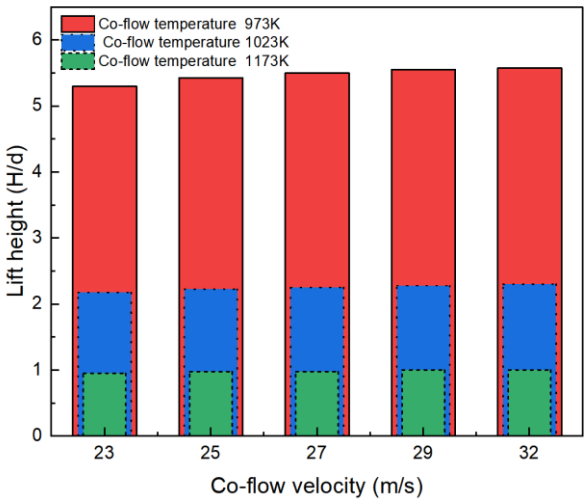

Figure 4.3.4: Flame lifted height at different co-flow velocities.

(P_{inj} =1.6 bar, X_{H2}=20%)

In figure 4.3.5, the lifted height (H/d) of the ammonia-hydrogen blending fuel increases as the injection pressure increases. Nonetheless, H/d shows a diminished sensitivity to change in injection pressure at higher hydrogen ratios. At low hydrogen ratio, the physical factor plays the dominant role: a higher initial jet momentum decreases the time for the heat absorption from the co-flow, leading the flame to develop far from the nozzle. On the contrary, at a high hydrogen ratio, the combustion limitation is mainly represented by the chemical ignition delay: when H_2=25%, although the fuel pressure increases, the auto-ignition initial point starts at almost the same distance from the fuel nozzle, showing that hydrogen has a stronger effect than jet momentum increment. This suggests that at sufficiently high hydrogen ratios, chemical effect from hydrogen is higher than physical effect from injection pressure on lifted height (H/d) [173].

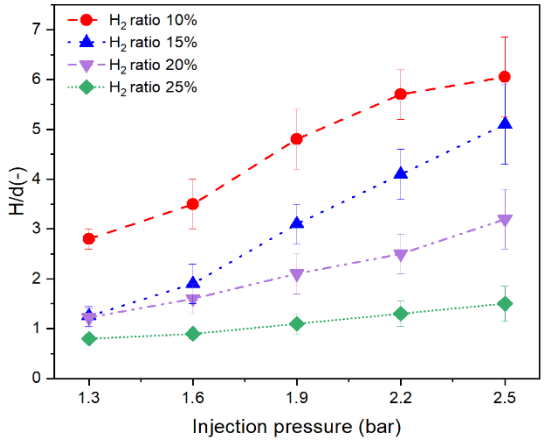

Figure 4.3.5: The lifted height at different injection pressures and hydrogen ratios.

4.4 Combustion stability of ammonia-hydrogen blending fuel

In order to explore the auto-ignition stability mechanism of ammonia-hydrogen blending fuel at different hydrogen ratios, co-flow temperatures, and jet velocities, lifted height fluctuation in the 200-300 ms range has been analysed. In 200-300 ms time range, the flame has a complete propagation, the flame brightness and flame area reach to max. This time range is so long to filtrate and delete the non-ignition and unstable flame. Figure 4.4.1 compares the fluctuation of the flame lifted height (H/d) of ammonia-hydrogen blending fuel. The standard deviation of the flame lifted height become significantly lower with hydrogen ratios increases. Hydrogen has a higher combustion stability than ammonia, so a higher hydrogen addition in ammonia has a much higher flame stability. When the hydrogen ratio is higher than 20%, the standard deviation decline tendency decreases and the standard deviation reaches a turning point. This suggests that the beneficial impact of hydrogen on enhancing combustion stability reaches a limit; further increases (hydrogen ratio above 20%） do not substantially improve stability. Therefore, a hydrogen ratio of 20% is identified as an optimal point for the combustion stability of ammonia-hydrogen mixtures.

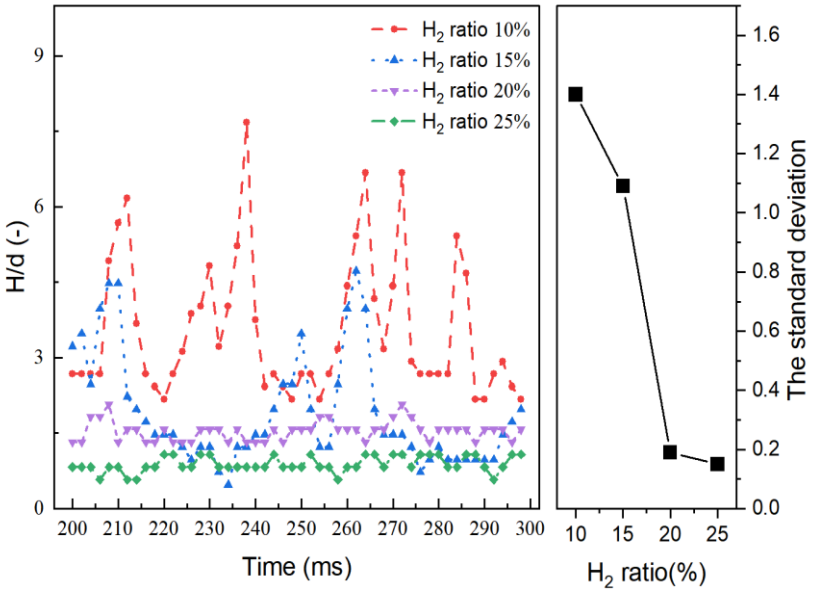

Figure 4.4.1: The flame lifted height of ammonia-hydrogen blending fuel at different co-flow temperatures.

(U_{cf} = 23 m/s, P_{inj} = 1.6 bar, T_{cf} = 1123 K)

To explore the effect of co-flow temperature on combustion stability, an ammonia/20% hydrogen flame was examined at temperatures ranging from 1023K to 1173 K. Figure 4.4.2 presents the variation in flame lifted height and its corresponding standard deviation within a time span of 200-300 ms. An increase in co-flow temperature shows decline in the standard deviations of lifted height, indicating enhanced flame combustion stability.

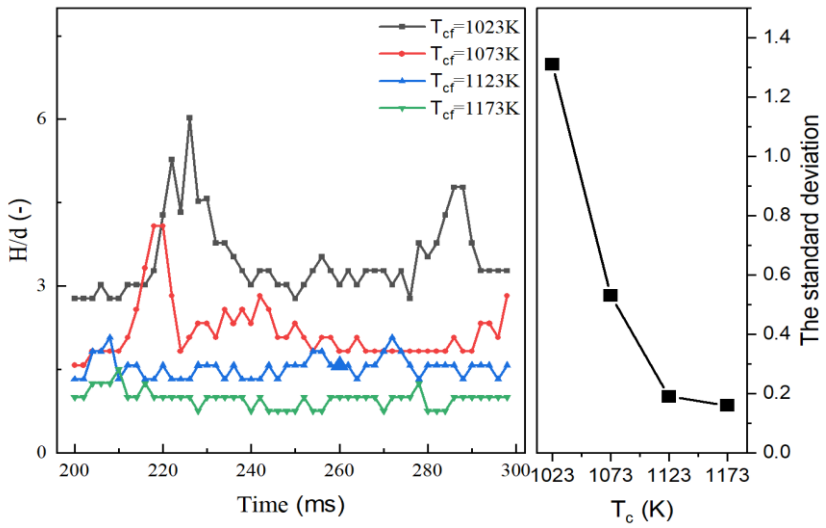

(a) H/d of ammonia-hydrogen flames at different T_{cf} (b) H/d standard deviation of ammonia-hydogen blending fuels

Figure 4.4.2: The ammonia-hydrogen flame lifted height of 20% hydrogen ratio at different co-flow temperatures.

(U_{cf} = 23 m/s, P_{inj} =1.6 bar)

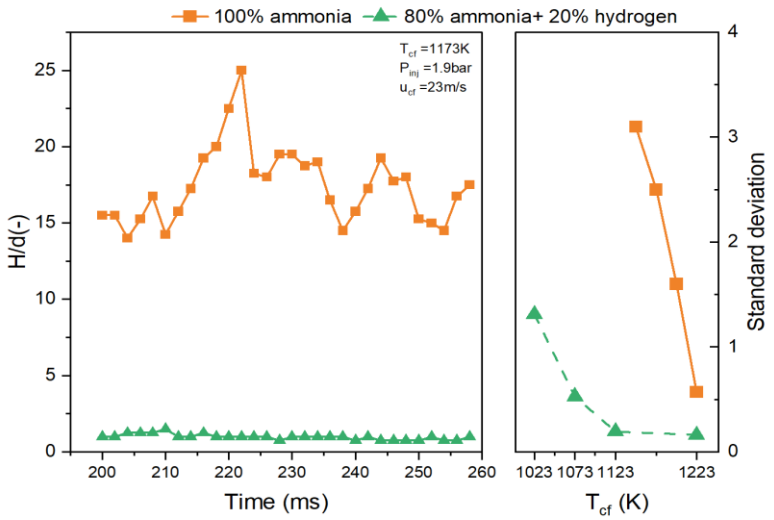

(a) H/d between ammonia and ammonia+20% hydrogen (b) The standard deviation of different fuels

Figure 4.4.3: The lifted height and standard deviation comparison between ammonia and ammonia-hydrogen blending fuels

The critical temperature is 1123 K, which divide the flame stability into different two stages. Below the critical temperature of 1123 K, combustion is controlled by the ignition delay, and it reduces with an augment of the co-flow temperature, that enhances the heat exchange between the fuel and the co-flow. Above 1123 K, a further increment of T_{cf} slightly effect on the auto-ignition. Therefore, if hydrogen ratio is fixed, the stability is almost not sensitive to further changes when the temperature beyond the T_{cf} threshold.

The standard deviation comparison between pure ammonia and ammonia-hydrogen blending fuels are reported in figure 4.4.3 at T_{cf} = 1173 K, P_{inj}= 1.9 bar and U_{cf} = 23 m/s. The standard deviation for both fuels exhibit a marked decrease as the co-flow temperature increases. Notably, the standard deviation for lifted height of pure ammonia is significantly larger than that of the ammonia-hydrogen mixture. Additionally, the pure ammonia is affected by more pronounced fluctuations, and these almost disappear with the hydrogen addition.

A blow off occurs for ammonia at P_{inj}=1.6 bar and co-flow temperature 973 K, shown in figure 4.4.4. At this boundary condition, the lifted flame exhibits a critical auto-ignition behaviour, which is defined the repetition of extinctions and re-ignitions. In fact, the burnt gas could induce local acceleration in the streamwise velocity due to the buoyancy, thus leading to blowout. Conversely, as the influence of thermal buoyancy decreases, a reduction in the streamwise velocity ensues, restoring the conditions conducive to auto-ignition. The interplay between the buoyancy-induced streamwise velocity and the flame's auto-ignition threshold is a critical determinant of flame stability.

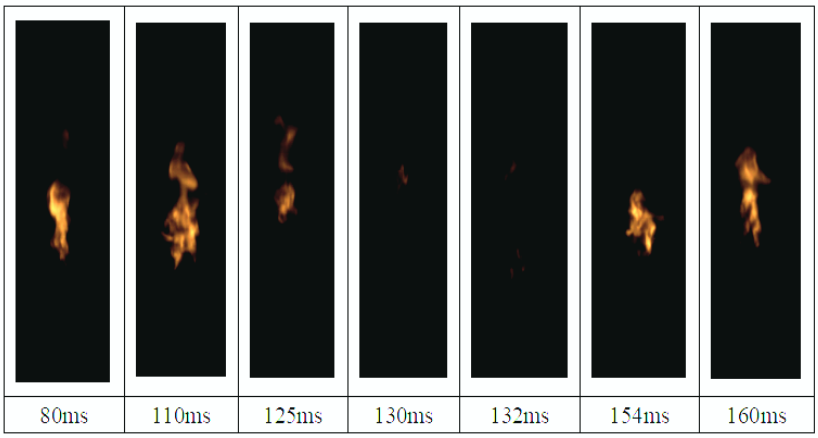

Figure 4.4.4: The extinctions and re-ignitions of ammonia/20%hydrogen blending flame with time.

4.5 The diffusion flame characteristics of blending fuel at higher hydrogen ratios

The ammonia-hydrogen flame characteristics under a lower hydrogen ratio have been instigated in above chapter. But the max hydrogen ratio in mixture is limited by experimental device and test safety. Considering the risk hydrogen experimental, the laminar diffusive flames of ammonia-hydrogen-methane have been used to investigate the ammonia effect on mixture combustion performance under hydrogen ratio excess 30% condition. The experimental injection system is same with the platform in chapter 4.4 and a constant flow pilot flame has been used to ignite the different mixture fuels under a same ignition energy condition.

Figure 4.5.1 systematically investigates the color and brightness of laminar flames for ammonia-hydrogen and ammonia-methane blending fuels. The study

reveals that beyond a 50% threshold of ammonia concentration, the flame stability for the ammonia-methane combination becomes worse, indicating a need for enhanced flame stabilization techniques at elevated ammonia percentages. Additionally, methane enrichment leads to a shift in flame coloration from an orange to a vivid yellow, a transition that reflects the flame temperature and chemical composition of the flame. The bright yellow of a methane-air flame is predominantly due to the incandescence of CN radicals and CO_2 [174]. In contrast, the orange hue in ammonia combustion is attributed to emission spectra from H_2O, OH, and NH_2 species. Corroborating studies, such as in reference [96], affirm that flames with a high ammonia content (X_{NH3}=0.80) manifest a yellow/orange tint resulting from the emissive contributions of NO, OH, NH_2, CN, and CO_2 species within the flame.

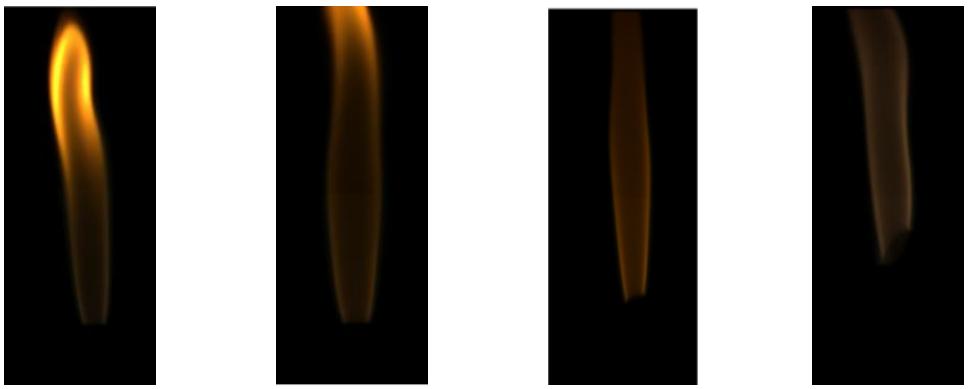

Figure 4.5.1: Ammonia-methane laminar diffusion flame.

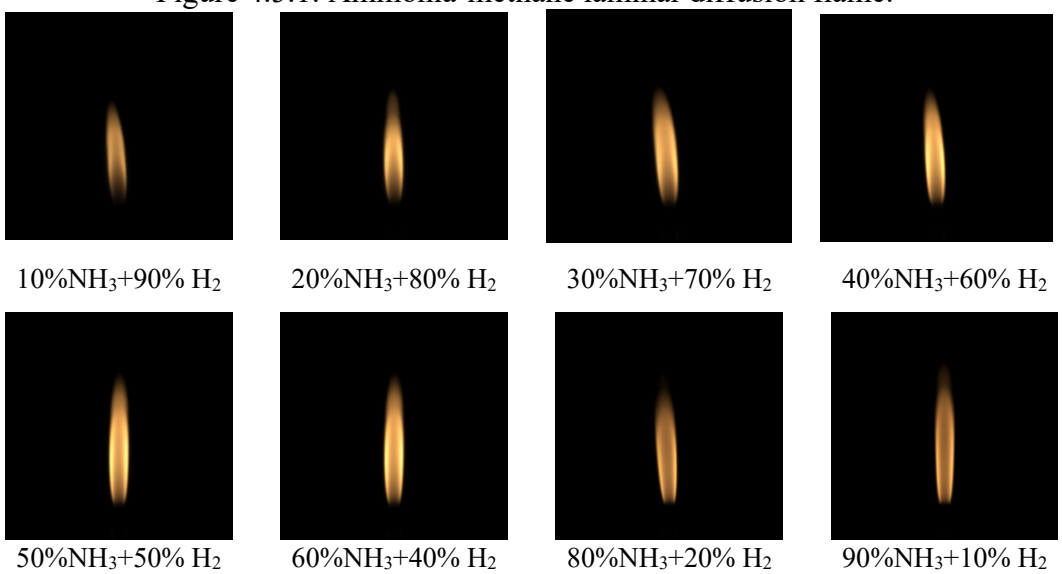

Figure 4.5.2: Ammonia-hydrogen laminar diffusion flame.

Figure 4.5.2 illustrates the ammonia-hydrogen laminar flame, exhibiting a color transformation from dark yellow to orange with increasing ammonia concentration. The gray value analysis presented in figure 4.5.3 demonstrates that a decrease in mixture flame gray value with rising ammonia proportions in the ammonia-methane blending fuels, whereas an increase in hydrogen content causes

the gray value to peak at an ammonia concentration of 50%, indicative of the maximal flame temperature at this ratio.

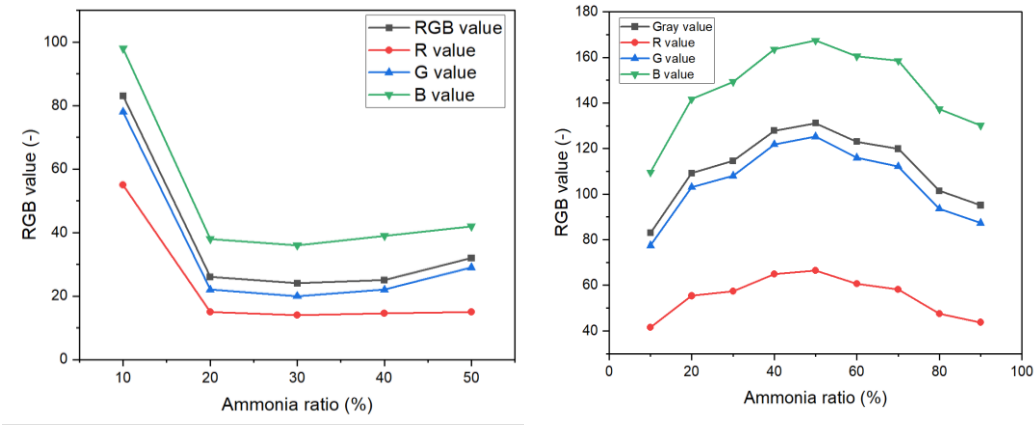

Figure 4.5.3: Ammonia-methane (left) and ammonia-hydrogen (right) diffusion laminar flame gray value

Subsequent experimental investigation of the ammonia-hydrogen-methane ternary fuel system, as reported in figure 4.5.4, reveals that methane addition increases the flame length, whereas hydrogen reduces flame length. Moreover, hydrogen enhances flame luminance, whereas methane induces a reduction in luminance. A critical observation is that the addition of a mere 6% hydrogen facilitates the stabilization of the ammonia-methane-hydrogen flame, a contrast to the 50% methane requirement for achieving a stable ammonia-methane flame. The presence of hydrogen also results in a diminution of flame lifted height, as depicted in figure 4.5.5, attributed to an increased laminar flame speed and a decreased ignition delay, consequently reducing flame height.

These experimental results are investigated for the potential utility of ammonia dissociation technology, in which NH_3 dissociated into N_2 and H_2, in optimizing combustion for both pure ammonia and ammonia-hydrogen mixtures. Nevertheless, the addition of N_2 is observed to exert a dilutive effect on the flame, as evidenced in figure 4.5.6, characterized by a noticeable diminish impact on flame color and length, which signifies a reduction in both flame velocity and chemical reaction kinetics.

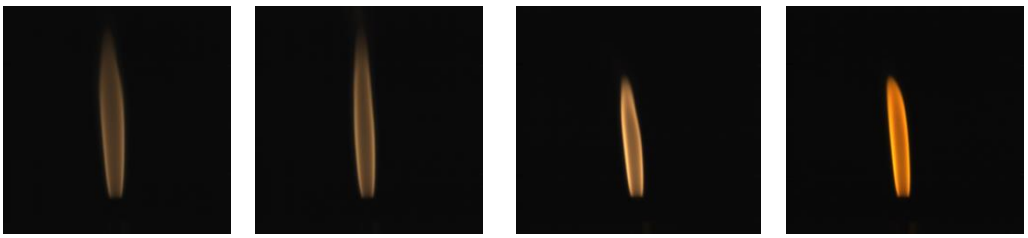

(a)6%H_2+68%CH_4 +26%NH_3 | (b)6%H_2+34%CH_4+ 60%NH_3 | (c)30%H_2+10%CH_4 +60NH_3 | (d)6%H_2+10%CH_4+ 84%NH_3

Figure 4.5.4: Ammonia-methane-hydrogen diffusion laminar flame.

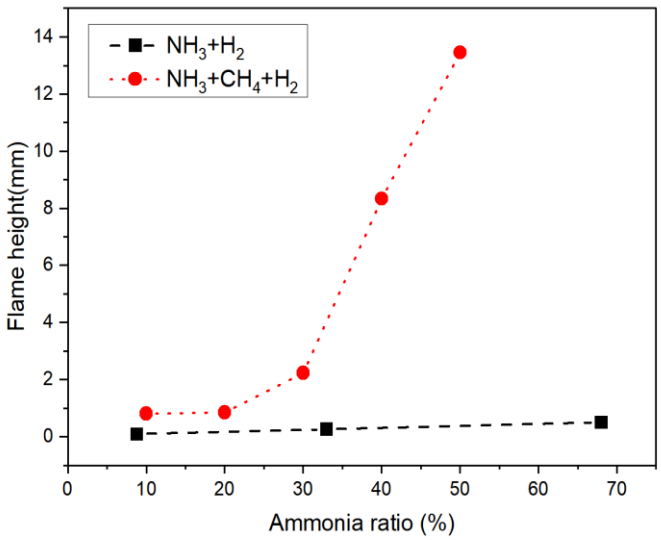

Figure 4.5.5: The flame height of ammonia-hydrogen-methane laminar diffusion flame.

(a) 50%NH_3+50%H_2 (b) 50%NH_3+25%N_2+25%H_2 (N_2:H_2=1:1) (c) 50%NH_3+20%N_2+30%H_2 (N_2:H_2=2:3)

Figure 4.5.6: Ammonia-hydrogen-nitrogen mixture diffusion laminar flames

4.6 Auto-ignition characteristics of ammonia-methane blending fuel

Ammonia-methane is one of interim methods to meet zero carbon emission and has a wildly potential to use in shipping and power industrial [92-95]. As one of popular flame enhancement technology, the ammonia-methane laminar flame characteristics have mentioned in chapter 4.5. A rigorous examination of ammonia-methane turbulent flame, which typify the predominant combustion regime in engine applications, is essential for an in-depth understanding of the combustion process and subsequent optimization of engine performance. While investigations into laminar flame provide clarity on the enhancement effects of

methane, such analyses alone are inadequate to make a guideline for ammonia engines. A new combustion method using a lower methane ratio should be investigated.

In order to evaluate the methane flame enhancement ability, the turbulent flame images of ammonia-methane at different T_{cf} have been shown in figure 4.6.1. In order to compare all the flame enhancement methods ability, the test conditions of ammonia-methane are standardized to match those of ammonia: T_{cf} ranges from 1123 K to 1223 K, the P_{inj} is 1.6 bar and the U_{cf} is 23 m/s. Considering that methane and hydrogen have different energy densities, the comparison is not based on the same volume fraction of ammonia, but the methane or hydrogen with the same calorific value. At the same time, keeping the total amount of ammonia in the premixed tank in a same content. According to discussion in chapter 4.4, the stable ammonia-hydrogen flame will be produced in 20% hydrogen ratio. So, the methane volume has a same calorific value with 20% volume fraction of hydrogen which means the hydrogen is 20% and the methane is 8% volume fraction.

Figure 4.6.1 presents the flame characteristics of ammonia-methane jet flames at different co-flow temperatures. There is a clear trend observed: as T_{cf} increases, the flames exhibit enhanced stability and brightness, and the lifted height is reduced. Elevated temperatures facilitate the auto-ignition of the ammonia-methane blending fuels, leading to improved combustion characteristics. The flame's color predominantly remains orange with regions of yellow; this is due to lower methane concentration, resulting in a coloration similar to that of a pure ammonia flame. Correspondingly, with an increase in T_{cf}, there is a decrease in flame lifted height and an expansion in both flame length and area, indicating enhanced combustion performance.

Another key observation is that the boundary of auto-ignition at higher temperatures changes. For a pure ammonia flame, stable combustion can be established at approximately 1173K under consistent injector pressure and co-flow velocity conditions. In contrast, the ammonia-methane blending fuels requires temperatures above 1100K to form a stable lift flame, while the ammonia-hydrogen mixture achieves stability at a significantly lower temperature of 973K. Adding 8% methane can decrease 3% lowest required T_{cf} to form a stable flame but adding 20% hydrogen can decrease 17%. This indicates that while both methane and hydrogen contribute to combustion enhancement, hydrogen shows a greater capability, as demonstrated by its more significant effect on lowering the auto-ignition temperature threshold. In summary, the calorific value added by methane and hydrogen is not the sole determinant of combustion enhancement; the chemical activity of the additives also plays a crucial role. Hydrogen, in particular, exhibits a superior enhancement effect on the flame, effectively reducing the combustion boundary and promoting auto-ignition at lower temperatures compared to methane.

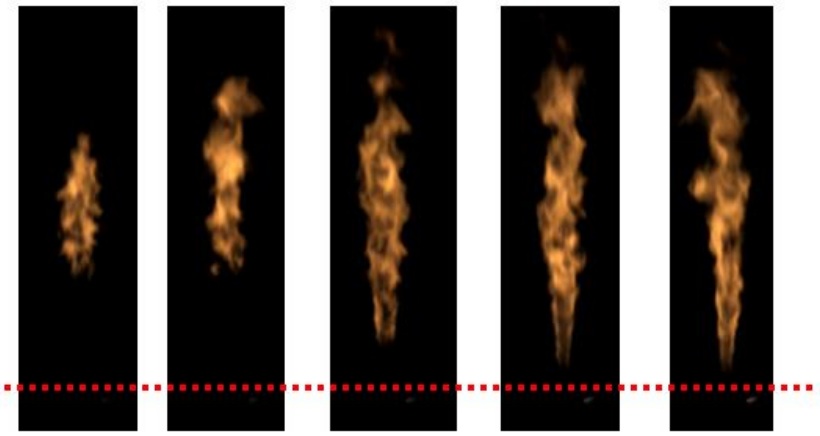

1123K 1148K 1173K 1198K 1223K

Figure 4.6.1: Ammonia-methane flame at different co-flow temperatures. (P_{inj} = 1.6 bar and U_{cf} = 23 m/s)

Figure 4.6.2 displays the variation in the flame area of an ammonia-methane mixture at different co-flow temperatures. As T_{cf} increases, there is a notable expansion in the flame area, which can be attributed to the enhanced combustion efficiency at elevated temperatures. The temperature sensitivity, indicated by the slope in figure 4.6.2, diminishes with increasing T_{cf}, showing a reduction in the incremental benefits of co-flow temperature on flame enhancement. The flame area can be defined fuel auto-ignition efficiency: when T_{cf} =1173K, the auto-ignition efficiency is much higher than that of T_{cf} <1173 K but the flame area is similar with T_{cf}>1173 K. Therefore, the T_{cf} of 1173 K is identified as the optimal temperature for the combustion of ammonia with 8% methane ratio. The flame length shows a similar tendency with flame area, shown in figure 4.6.2. It means the flame length is the main character to change flame area and match with Eq 3.2.

Figure 4.6.3 presents the temporal variation of the gray value for ammonia-methane flame at co-flow temperatures of 1148 K and 1123 K. It is observed that a higher T_{cf} correlates with both an increased gray value and reduced fluctuations, indicating greater flame stability. In comparison with the ammonia-hydrogen gray values depicted in figure 4.2.4, the ammonia-methane gray values are lower, suggesting that the flame temperature of ammonia-hydrogen is comparatively higher.

Figure 4.6.4 and 4.6.5 show the ammonia-methane flame characteristics at different injection pressures. With the injection pressure increases, the flame area initially increases and subsequently decreases, which represents an optimal combustion efficiency when injection pressure is 2.2 bar. Surpassing this pressure threshold, an excess of fuel alters the local equivalence ratio, thereby inhibiting auto-ignition. Furthermore, a higher injection pressure has a higher fuel velocity which lead to the energy exchange time decreases and unburned fuel increases. Flame length shows similar changes with flame area which means the flame longitudinal diffusion is the main diffusion direction.

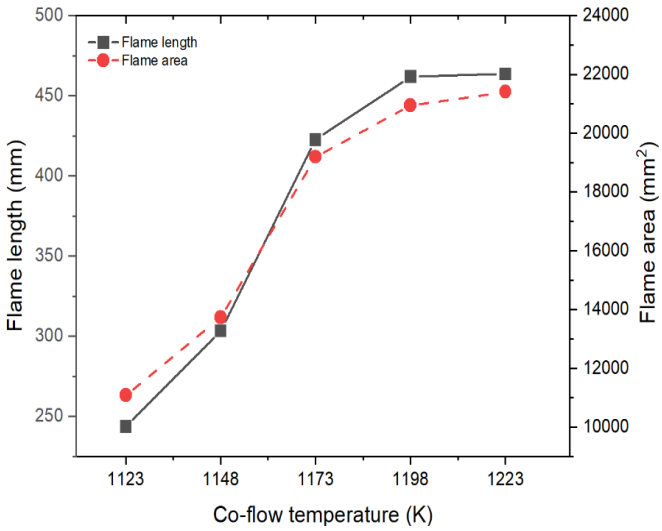

Figure 4.6.2: Ammonia-methane flame area and length at different co-flow temperatures.

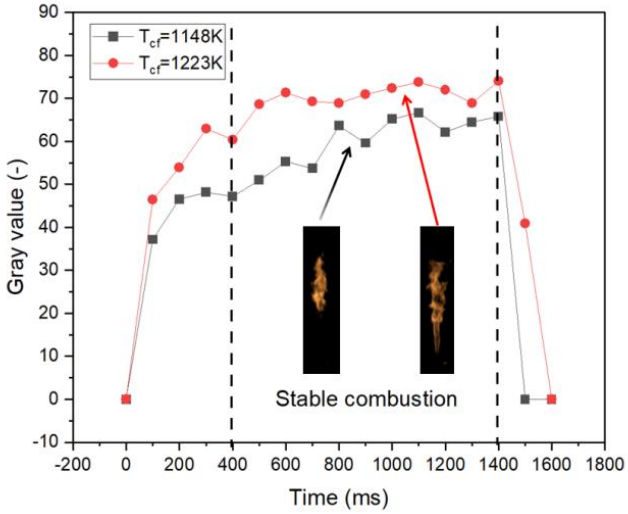

Figure 4.6.3: Ammonia-methane flame gray value with time at different co-flow temperatures.

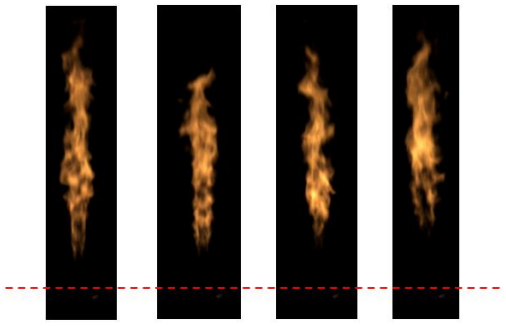

1.6 bar 1.9 bar 2.2 bar 2.5bar

Figure 4.6.4: Ammonia-methane flame at different injection pressures.

(T_{cf} =1223 K)

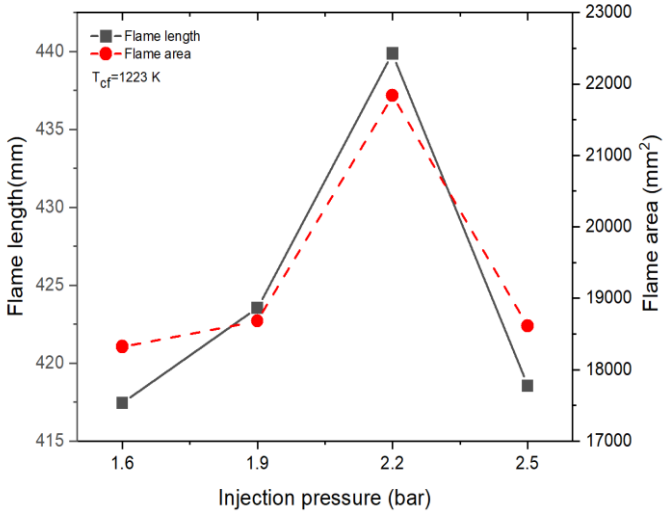

Figure 4.6.5: Ammonia-methane flame area and length at different injection pressures.

(T_{cf} =1223 K)

The combustion stability of ammonia-methane at different co-flow temperatures has been shown in figure 4.6.6. With the co-flow temperature increases, the standard deviation of H/d decreases which means fluctuation of H/d decreases. Two threshold values of co-flow temperature exist in the decline tendency of svd, which represent three different auto-ignition phases of ammonia-methane fuels. A drastic fluctuation of H/d has been shown in 1123 K, which reparents the auto-ignition boundary of ammonia-methane fuel. The shorter flame length, smaller flame area, flickered flame brightness and fluctuant lifted height are the main characters in auto-ignition boundary. When the co-flow temperature beyond 1148 K, flame move into a steady combustion phase in which all the flame morphology show a lower fluctuation. Then, once the co-flow temperature increases to 1173 K, the standard deviation shows a further decline. The reason is that the co-flow temperature sensibility on H/d decreases.

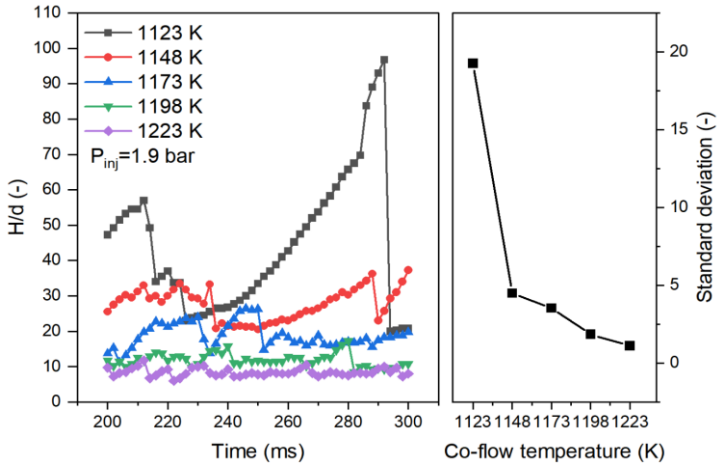

Figure 4.6.6: Ammonia-methane combustion stability at different co-flow temperatures.

The injection pressure effect on combustion stability has shown in figure 4.6.7. With the injection pressure increases, the standard deviation of H/d increases. P_{inj}= 2.2 bar is the threshold. Once the injection pressure beyond 2.2, the flame H/d has an obvious increment, which means the jet flame turn to an unstable combustion phase. On the one hand, excess ammonia changes the local equivalence ratio to hinder jet flow auto-ignition; On the other hand, the thermal exchange time decreases because of velocity increases.

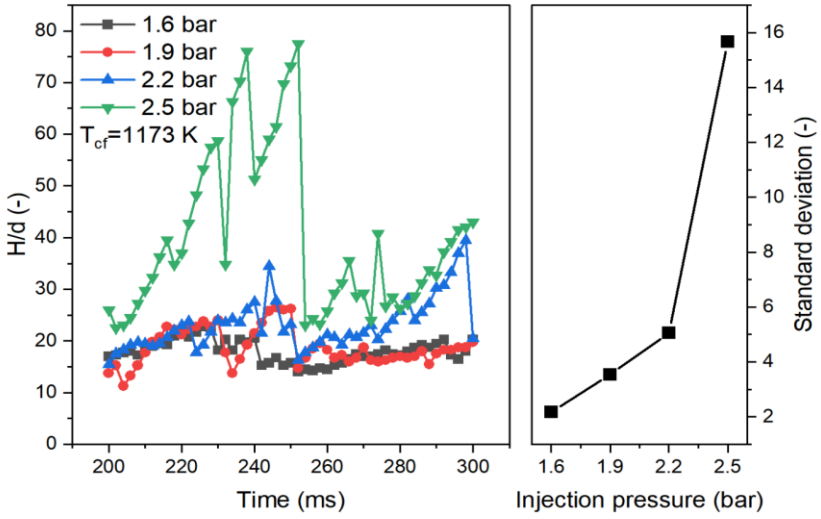

Figure 4.6.7: Ammonia-methane combustion stability at different injection pressures.

4.7 The comparison of auto-ignition characteristics between different fuels

4.7.1 The comparison between ammonia and ammonia blending fuels

Figure 4.7.1 presents the ignition delay between ammonia-hydrogen and ammonia-methane blending fuels at a range of co-flow temperatures. As the co-flow temperature increases, both blending fuels exhibit reduced ignition delay compared to pure ammonia combustion, showing that methane and hydrogen both act as combustion accelerants for ammonia. Notably, methane has a less pronounced effect on reducing the ignition delay of ammonia: at a co-flow temperature of 1173 K, the methane addition results in a 28% reduction in ignition delay relative to pure ammonia. In contrast, hydrogen presents a stronger impact, leading to a 56% reduction under the same conditions. Thus, hydrogen possesses a superior capability in reducing ignition delay compared to methane. The mechanism for this disparity is attributed to hydrogen's more significant enhancement of both the diffusivity and the availability of reactive radical species within the ammonia flame, as discussed in reference [92]. Hydrogen, being a more reactive fuel, promotes more effective diffusion and increases the concentration of radicals necessary for initiating and propagating the combustion

process, thereby resulting in shorter ignition delay than those achieved with methane.

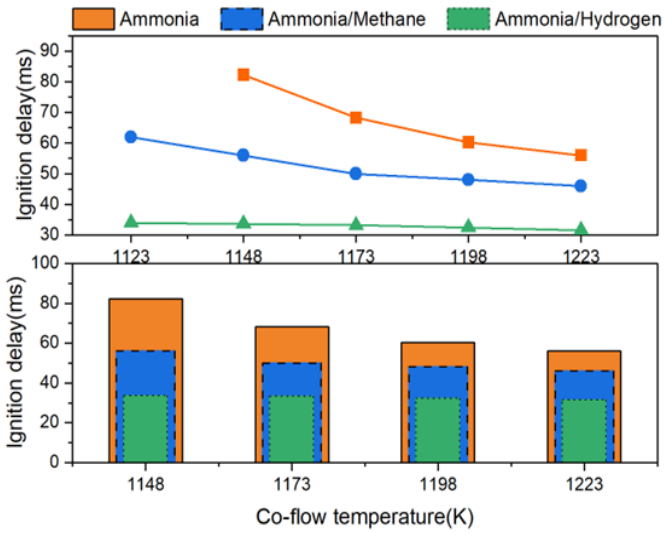

Figure 4.7.1: Ignition delay of ammonia, ammonia-methane and ammonia-hydrogen at different co-flow temperatures.

(U_{cf} = 23 m/s, P_{inj} = 1.6 bar)

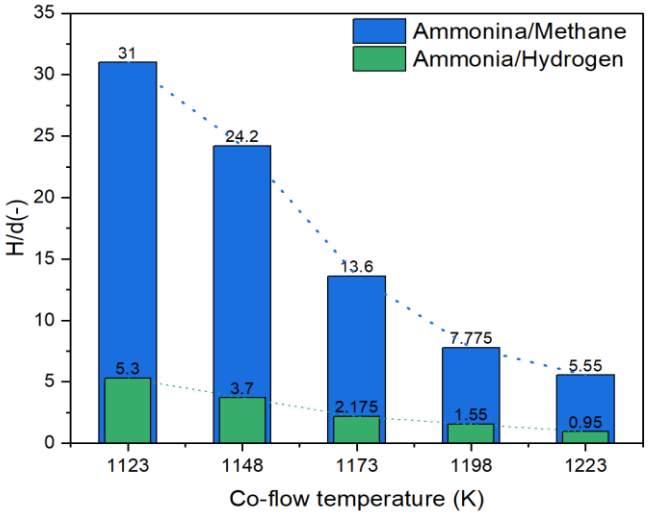

Figure 4.7.2: The lifted height of ammonia blending fuels at different co-flow temperatures.

(U_{cf} = 23 m/s, P_{inj} = 1.6 bar)

The flame lifted height of ammonia-hydrogen and ammonia-methane at different co-flow temperatures shown in figure 4.7.2. With the co-flow temperature increases, the lifted height of two blending fuels both show a decline. The lifted height of the ammonia-methane is obviously higher than that of ammonia-hydrogen, and the lifted height of ammonia-methane is more than five times that of ammonia-hydrogen. The lifted height difference is bigger in a lower T_{cf} =1123 K than a higher T_{cf} =1123 K. At 1123 K, adding 20% hydrogen results in a lifted height reduction approaching 80% compared to the addition of methane.

When the co-flow temperature exceeds 1198K, the discrepancy in lifted heights between the two mixtures diminishes. The reason is that a higher co-flow temperature can shorten the flame enhancement ability because higher temperature improves the chemical reaction speed to reduce the chemical ignition delay difference of all the fuels. A shorter ignition delay represents a lower lifted height. As the co-flow temperature increases, the difference between the two fuels gradually decreases.

Figure 4.7.3 shows the comparison of the lifted height of ammonia-hydrogen and ammonia-methane flames at different jet pressures. The lifted height increases with the jet pressure increases. At a same injection pressure, the lifted height of ammonia-methane is significantly higher than that of ammonia-hydrogen. The injection pressure, as a physical factor, has a strong effect on the auto-ignition boundary and combustion stability. Once the injection pressure excess 1.9 bar, the lifted heights of two fuels have an obvious increment, which is similar with characteristic of pure ammonia because the ammonia is the main fuel in blending gas. This phenomenon means the chemical factor from hydrogen or methane is less than physical factor form jet momentum to change the flames.

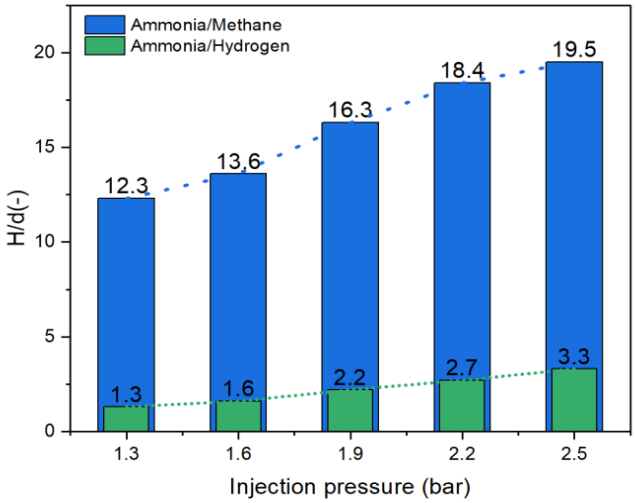

Figure 4.7.3: The lifted height at different injection pressures of ammonia blending fuels.

(U_{cf} = 23 m/s, T_{cf} = 1123 K)

4.7.2 The comparison between traditional fuels and ammonia fuels

Ammonia as an alternative carbon free fuel, has a great potential in heavy vehicle and shipping industry. How to evaluate the improvement ability of flame enhancement methods and whether the combustion performance of ammonia mixture can be improved to match with the traditional fuels (diesel, gasoline and ethyl alcohol) are indispensable questions. The lowest auto-ignition temperatures and lifted heights have been compared the combustion performance of different fuels including ammonia, ammonia/20% hydrogen, ammonia/8% methane, diesel,

n-hexane, gasoline and ethyl alcohol. All the experimental data is based on same controllable thermal atmosphere burner [167-174]. In order to an accurate comparison, the min auto-ignition temperature of liquid hexane has been added. The test conditions of co-flow in hexane test are same with ammonia fuels for an available comparison. The experimental results of min auto-ignition temperature have shown in figure 4.7.4. The lowest auto-ignition temperature represents the co-flow temperature in which a stable flame can be observed by camera. The ammonia auto-ignition temperature is 1148K which is higher than 1073K of diesel. Ammonia/20% hydrogen blending fuel has a lower auto-agitation temperature (973K) than diesel. One reason is that hydrogen addition lead to min auto-ignition temperature of overall mixture fuel decreases. The other reason is that diesel spray needs a higher temperature for liquid evaporation. Adding methane can obtain a lower auto-ignition temperature than pure ammonia. Only adding 8% methane ratio, the auto-ignition of ammonia-methane is close to diesel. A higher methane ratio has a better combustion performance, because pure methane auto-ignition is close to 900K.

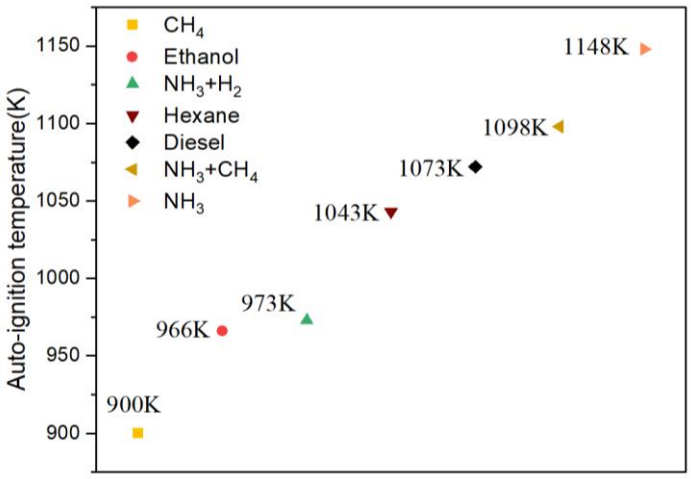

Figure 4.7.4: The lowest stable auto-ignition temperature of different fuels.

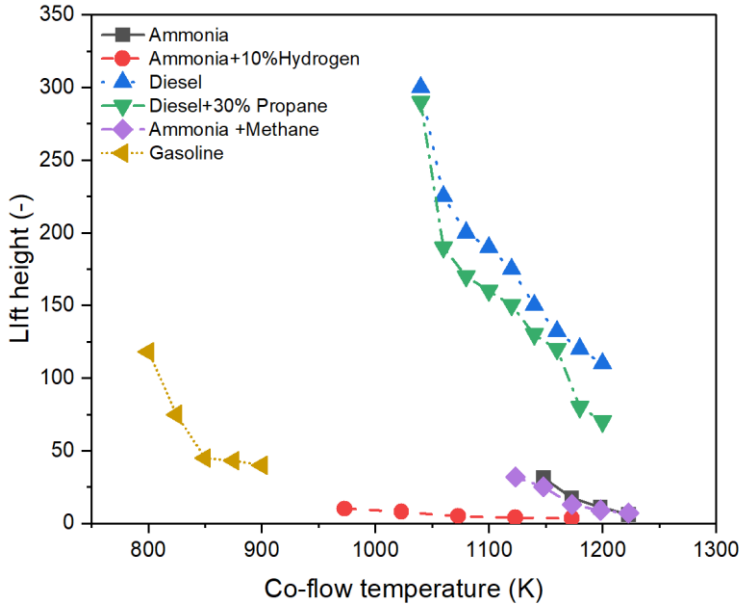

Figure 4.7.5: The lifted height of different fuels.

The lifted height comparison has shown in figure 4.7.5. With the co-flow temperature increases, lifted height of all the fuels decreases. The liquid fuel has a much higher lifted height. The reason is that the liquid fuel injection pressure is much higher than ammonia injection pressure in this work and the liquid spray need time to atomize to gas which may decrease the thermal exchanging time with co-flow. Consider the high liquefaction temperature of ammonia, the ammonia spray is close to propane. Propane addition can decrease the lifted height of diesel and propane mixture. Thus, ammonia and ammonia mixture fuel have a lower lifted height than diesel.

4.8 conclusion

In this chapter, the auto-ignition characteristics of ammonia-hydrogen and ammonia-methane blending fuels have been investigated. The main conclusions are shown as follow:

Compared to pure ammonia, ammonia-hydrogen flame has a higher flame brightness and a large flame area. Ammonia flame with a low hydrogen ratio shows an orange color, which is similar with pure ammonia. With the increasing of hydrogen ratios, the flame brightness increases. The auto-ignition of hydrogen is the reason why the beginning brightness is lower.

With the co-flow temperature increases, the lifted height gradually decreases, while the flame length, area, perimeter and brightness increase. The reason is that the more pronounced heat transfer between the hot co-flow and the fuel jet promotes the fuel auto-ignition. When the hydrogen ratio beyond 10%, the flame length growth slower, which means 10% hydrogen ratio is a most economic to enhance the ammonia flame. Hydrogen addition has a stronger effect than T_{cf} increment on combustion. The increment of jet momentum lead to flame area increase. Once the injection pressure is above 1.6 bar, the flame area augment slope reduces.

With the co-flow temperature increases, the ignition delay shows a downward trend due to the enhanced heat transfer between the jet flow and co-flow. With the hydrogen ratio increases, the ignition delay of ammonia-hydrogen mixture gradually decreases. With the increasing of hydrogen ratio, the lifted height shows a downward trend, which represents that the ignition delay decline lead to mixture fuel auto-ignition occur closer to the tube outlet. The lifted height is less sensitive to the co-flow temperature when T_{cf} excess the critical temperature (1073K). It means the heat exchange efficiency has a limitation between and co-flow and jet flow. The 20% hydrogen ratio is an optimal ratio for ammonia-hydrogen combustion stability. The standard deviation of the flame lifted height is significantly lower with hydrogen ratios increases. When the hydrogen ratio is higher than 20%, the standard deviation decline tendency decreases and the standard deviation reaches a turning point.

With co-flow temperature increases, the ignition delay and lifted height of ammonia-methane and ammonia-hydrogen blending fuels show a downward trend,

and both are lower than that of pure ammonia combustion. Hydrogen has a stronger flame enhancement ability than methane to shorten ignition delay, the lifted height of ammonia-methane is significantly higher than that of ammonia-hydrogen blending fuel.

Chapter 5

Auto-ignition characteristics and combustion stability mechanism of ammonia in oxygen-enriched

5.1 Experimental conditions of ammonia auto-ignition in oxygen-enriched

A series of ammonia combustion investigations in rich-oxygen with an obvious enhancement effect on ammonia combustion in different oxygen ratios, have been shown in table 1.2. Therefore, oxygen enrichment can be considered an effective method for intensifying the combustion process. However, excess oxygen could diluent the ammonia, adversely affecting its auto-ignition. The accurate threshold at which oxygen begins to have a dilution effect on ammonia combustion, has not been thoroughly explored. In the Chapter 5, the auto-ignition characteristics of ammonia-oxygen have been investigated, based on Controllable Active Thermo-Atmosphere burner.

The excess oxygen coefficient R_o has been used to evaluate the oxygen-enriched combustion. The R_o has defined in Eq (5.1).

$$R_o = \frac{X_o}{E_0} - 1 \quad (5.1)$$

The X_o is oxygen mole fraction in really experimental, the E_o is the stoichiometric ratio in air based on the $4NH_3+5O_2 = 6H_2O+4NO$.

The parameters of experiments have been reported in table 5.1, including co-flow velocity, co-flow temperature, jet pressure and excess oxygen coefficient. Both the co-flow velocity and the ammonia injection pressure ensure a higher Reynolds; therefore, a turbulent flow state can be considered both the injected fuel and the co-flow.

Table 5.1: Experimental conditions of ammonia-oxygen fuel

Parameters	Value
Co-flow velocity (U_{cf}) [m/s]	25
Injection pressure (P_{inj})[bar]	1.3, 1.6, 1.9, 2.2, 2.5
Co-flow temperature (T_{cf}) [K]	1073-1203
Excess oxygen coefficient (R_o)	0.2, 0.6, 0.8, 1.0, 1.2, 1.4

5.2 Morphology characteristics of ammonia auto-ignition flame in oxygen-enriched

Figure 5.2.1 shows the experimental results of ammonia-oxygen flame at T_{cf} = 1098-1198 K, P_{inj}= 1.9 bar and R_o= 0.6. The data indicate that with an increase in co-flow temperature, the brightness of the flame substantially improves, the lifted height notably decreases, and the flame area expands incrementally. Compared with the flame of ammonia in chapter 3, the brightness of the ammonia-oxygen flame is brighter than that of pure ammonia. Additionally, the central region of the ammonia-oxygen flame exhibits a higher intensity of brightness, which represents the chemical reaction of combustion is more violent. The addition of oxygen evidently modifies the combustion compared to the auto-ignition of pure ammonia.

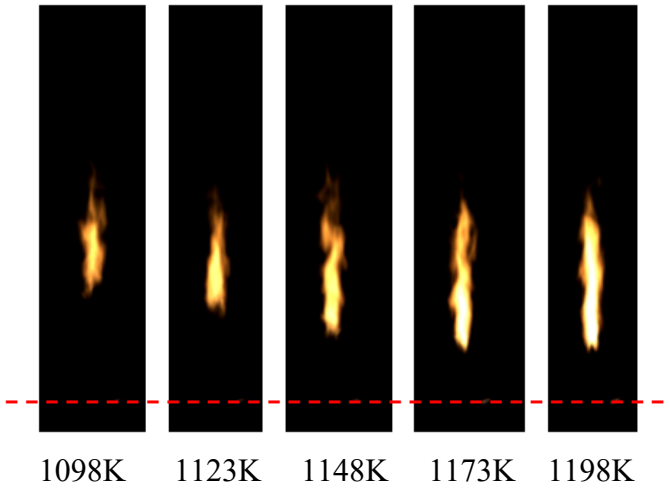

Figure 5.2.1: Ammonia-oxygen flame at different co-flow temperatures.
(R_o=0.6, P_{inj}=1.9 bar)

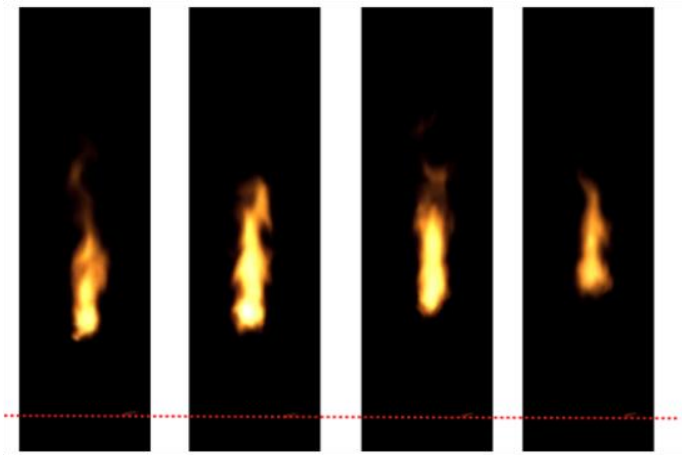

1.6bar 1.9bar 2.2bar 2.5bar

Figure 5.2.2: Ammonia-oxygen flame at different injection pressures.

(R_o=0.6, T_{cf}=1148 K)

Further experimental data depicted in figure 5.2.2 show that augmenting the injector pressures from 1.6 to 2.5 bar initially lead to a first increase than decrease in both flame area and length. The initial positive correlation between jet pressures and combustion effectiveness can be attributed to the oxygen-enriched environment, which enhances the combustion chemical kinetics. In contrast to the combustion of pure ammonia, the additional oxygen promotes ammonia combustion. An increase in jet momentum directly correlates with a higher turbulence intensity, fostering a more homogeneous mixture of ammonia with oxygen and consequently facilitating a more efficient combustion process. The increase in injector pressure contributes to a greater ammonia mass, thereby augmenting the flame brightness.

The auto-ignition boundary of ammonia-oxygen has been reported in figure 5.2.3. The ammonia cannot form a flame in every oxygen coefficient when the co-flow temperature is lower than 1078 K. A combustion boundary can be found in 1098 K, in which the ammonia-oxygen mixture can be observed a flickering unstable flame sometimes. Once the temperature beyond 1098 K, a continuous and stable flame can be formed. When the oxygen coefficient excess to 1.4, the minimum auto-ignition temperature increases to 1123 K. The reason is that the flame is difficult to propagate and form a continuous flame in a higher oxygen ratio, and a higher T_{cf} can enhance the flame speed to improve the flame propagation.

The figure 5.2.4 show the flame areas at different oxygen coefficients. The flame area shows a down trend with the oxygen coefficients increases. The flame area exists an obvious decline once the oxygen coefficient increases to 1.2. The experimental results reveal a substantial contraction in flame area, an approximate 400% reduction, when the oxygen ratio (R_o) is increased from 0.2 to 1.2. This observation suggests a dilution effect due to the addition of oxygen, which becomes obvious when R_o exceeding 1.2. This dilution phenomenon implies that beyond a certain concentration, oxygen no longer serves as an effective oxidant to

facilitate combustion but rather begins to diminish the reactive volume, thereby inhibiting the combustion process.

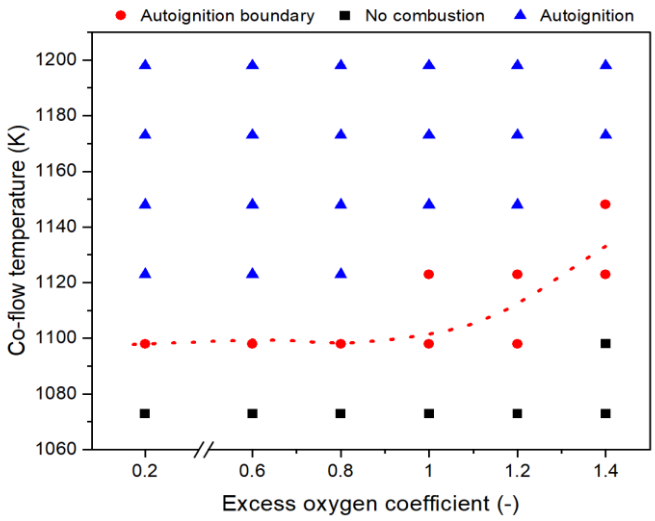

Figure 5.2.3: The ammonia-oxygen combustion boundary.

(P_{inj}=1.9 bar)

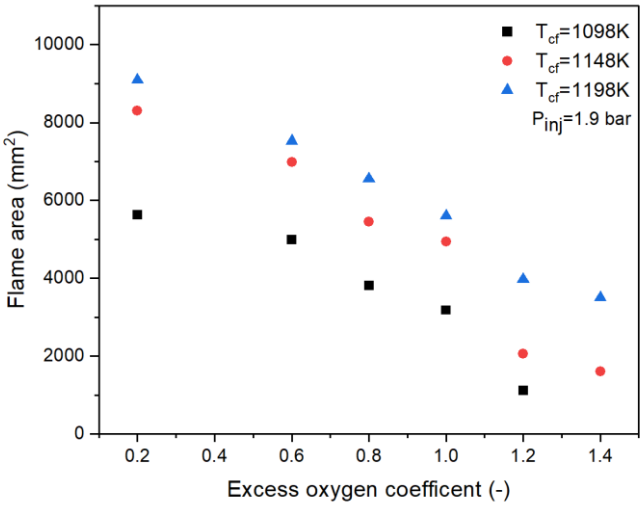

Figure 5.2.4: The flame area of ammonia-oxygen at different co-flow temperatures.

Figure 5.2.5 shows the flame length at various oxygen coefficients and co-flow temperatures. The flame length exhibits a decreasing trend as the oxygen coefficients increase, similar to the flame area. A higher co-flow temperature enhances flame diffusion and improves combustion efficiency. However, there is a critical point at an excess oxygen coefficient of 1.0, where the flame area and length show a different rate of decline. This implies that although increasing the oxygen expands the flammable boundary of ammonia when the R_o<1.0, the flame encounters difficulties in diffusion and ignition under R_o>1.0 conditions.

Figures 5.2.6 and 5.2.7 illustrate the flame area and flame length at various oxygen coefficients and injection pressures. The geometric morphology of the

flame exhibits similarities beyond an excess oxygen coefficient of 0.8. When injection pressure is below 1.9 bar, the increase in flame length and area corresponds to an increase in jet flow momentum. Although more energy is required for the autoignition of the increased jet fuel, the intensified oxygen facilitates complete combustion of ammonia, resulting in an increase in flame area and length. However, once the pressure exceeds 1.9 bar, the excessive oxygen begins to hinder the ammonia auto-ignition and the faster jet velocity reduces the thermal time with co-flow, leading to a decrease in flame area and length. Conversely, at an excess oxygen coefficient of 0.2, there is a continuous increase in flame area and length. This indicates that all the jet flow can be fully ignited, even though when the jet pressure is increased to 2.5 bar, due to the enhancement effect of oxygen on the flame combustion.

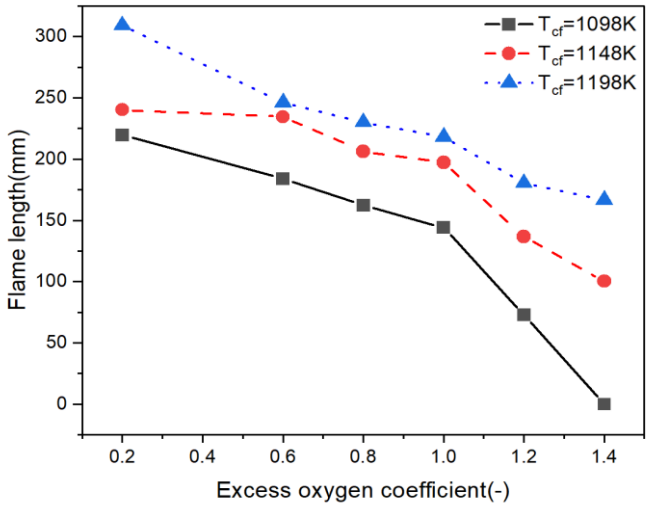

Figure 5.2.5: The flame length of ammonia-oxygen at different R_o.

(P_{inj}=1.9 bar)

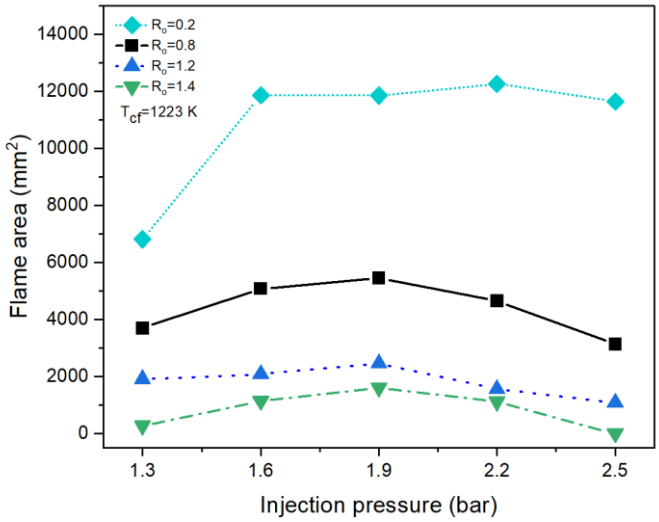

Figure 5.2.6: The flame area of ammonia-oxygen at different injection pressures.

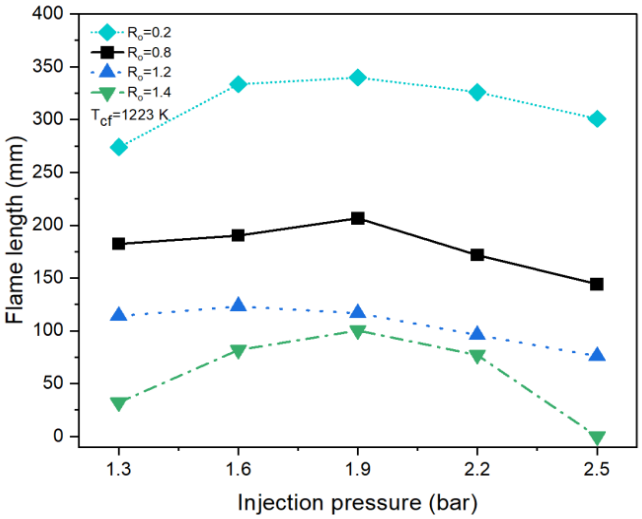

Figure 5.2.7: The flame length of ammonia-oxygen at different injection pressures.

5.3 Ignition delay and lifted height of ammonia in oxygen-enriched

R_o and T_{cf} are important factors on ammonia-oxygen flame. In this section, the ignition delay of ammonia-oxygen at T_{cf} =1098-1198 K, P_{inj}= 1.6 bar and R_o=0.2-1.4 have been investigated. Ignition delay of ammonia-oxygen mixture at different R_o and T_{cf} have shown in figure 5.3.1. With R_o increases, the ignition delay of the ammonia-oxygen flame first decreases then increases. The reason is that the increment of oxygen in the mixture is conducive to the stable combustion of ammonia due to chemical reaction acceleration. But the excessive oxygen content leads to the decrease of ammonia content in the mixture gas, leading to the flame difficult to propagated to form an ability auto-ignition. In addition, when the T_{cf} is 1198 K and R_o increases from 0.2 to 0.8, the ignition delay decreases nearly 12.6%; but when R_o increases from 0.8 to 1.4, the ignition delay increases by 22.5%. At R_o=1.0, the ignition delay is shorter than at R_o=0.6, indicating that the combustion enhancement effect at R_o=1.0 surpasses that at R_o=0.6, due to a more pronounced augmentation effect outweighing dilution effect. However, as the R_o rises to 1.2, the ignition delay exceeds that observed at R_o=0.6 or R_o=0.8, suggesting that the dilution effect begins to dominate over the enhancement effect. The dilution effect will be higher than the enhance effect on at higher R_o. These findings imply that there exists an upper limit to the efficacy of oxygen enrichment as a flame enhancement strategy. The maximum combustion enhancement capacity is reached within a R_o range of 0.8 to 1.0, after which the benefits of additional oxygen are decreased by its dilution effects. This threshold establishes a critical point for optimizing oxygen-enriched ammonia

combustion systems, highlighting the necessity for precise control of the oxygen ratio to achieve a balance between combustion enhancement and dilution.

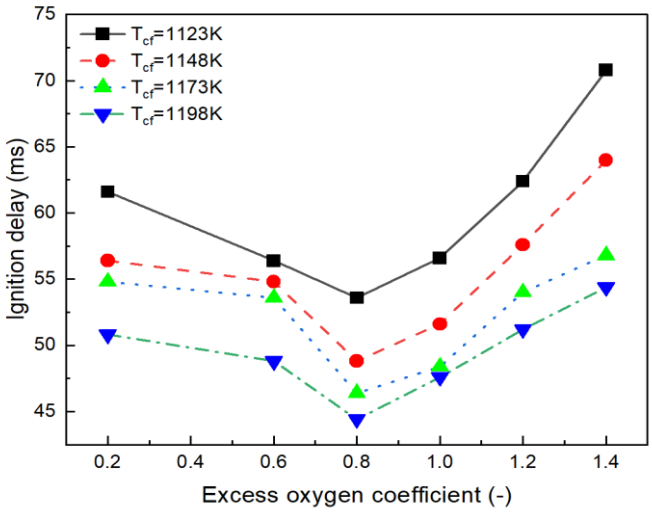

Figure 5.3.1: Ignition delay of ammonia-oxygen at different excess oxygen coefficients and co-flow temperatures.

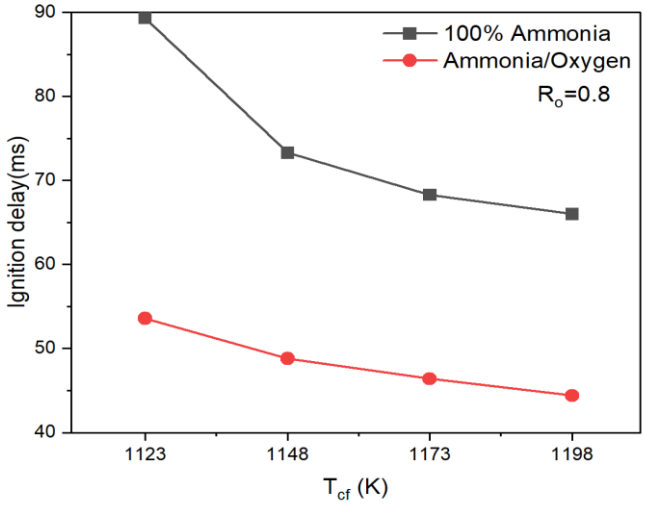

Figure 5.3.2: Ignition delay comparison of ammonia and ammonia-oxygen at different co-flow temperatures.

Figure 5.3.2 compares the pure ammonia and ammonia-oxygen ignition delay at same T_{cf}. The data indicate that ignition delay of ammonia-oxygen blending fuel is reduced by approximately 30%-39% compared to that of pure ammonia at the same T_{cf}. Notably, this reduction in ignition delay is more pronounced at lower T_{cf} values, such as $T_{cf} = 1123$ K, suggesting that oxygen enrichment has a greater impact on flame enhancement at lower temperatures. The heightened sensitivity to oxygen enrichment in lower T_{cf} implies that the chemical kinetics play a dominant role. Excess oxygen conditions bolster the combustion process even when T_{cf} is relatively low because the reaction kinetics are more strongly influenced by the availability of oxygen. The importance of oxygen

concentration in influencing the ignition characteristics, particularly in environments where co-flow conditions are not sufficient to achieve rapid ignition.

Figure 5.3.3 shows the lifted height of ammonia-oxygen jet flame at different R_o and T_{cf}. With the T_{cf} increases, the flame lifted height gradually decreases. When the T_{cf} is higher than 1173 K, the downtrend of the lifted height is obviously slow down. The turning temperature for stable auto-ignition of ammonia-oxygen flame is 1173 K. When the co-flow temperature is lower than 1173 K, the lifted height is highly sensitive to the co-flow temperature. Conversely, when the co-flow temperature exceeds turning point, the response of lifted height to a further increase in T_{cf} is less pronounced, and the combustion process tends to stabilize.

While the addition of oxygen is effective in reducing ignition delay, the data suggest that the turning temperature for stable auto-ignition remains unaffected by oxygen enrichment, as opposed to the addition of hydrogen or methane. This implies that oxygen addition, although beneficial for reducing the ignition delay, exerts a less substantial impact on extending the combustion stability boundary compared to the addition of hydrogen. High diffusivity and reactivity of hydrogen can significantly extend the flammability limits and lower the lifted height, thus enhancing the combustion boundary to a greater extent than oxygen.

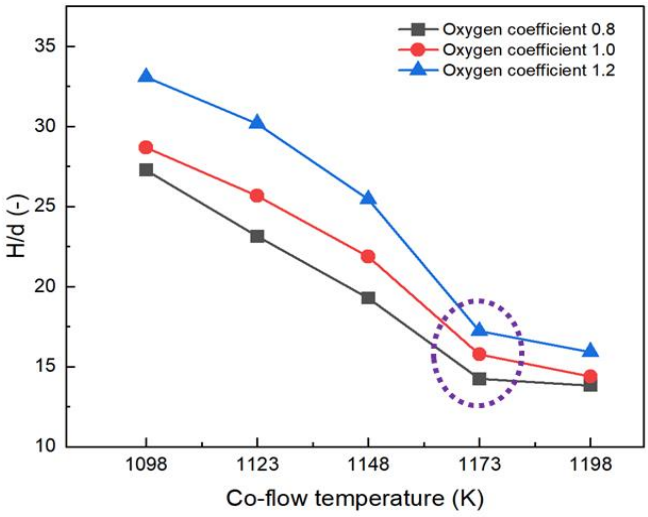

Figure 5.3.3: Lifted height of ammonia at different excess oxygen coefficients and co-flow temperatures.

Figure 5.3.4 shows the lifted height of ammonia-oxygen jet flame with jet velocity increases at R_o= 0.8-1.4, U_{cf} = 25 m/s and T_{cf} =1203 K. The lifted height gradually increases with the increase of jet pressure and jet velocity. In addition, the injection pressure increases the fluctuation of the flame lifted height lead to the combustion instability increases. A higher injection increases the concentration of ammonia in the area near to the ammonia injection tube, leading to augmented local equivalence ratios, therefore, the auto-ignition is not promoted and the ammonia flame will move further away from the injector tube outlet. The ammonia in different P_{inj} =0.4-1.0 MPa cannot occur a sharp burst of noise. But

in the previous test of $H_2/Ar/O_2$ [22], the hydrogen combustion is accompanied by a sharp sound when the jet pressure is 1.0 MPa and 1.15 MPa. It means ammonia-oxygen has a lower intense combustion a certain extent.

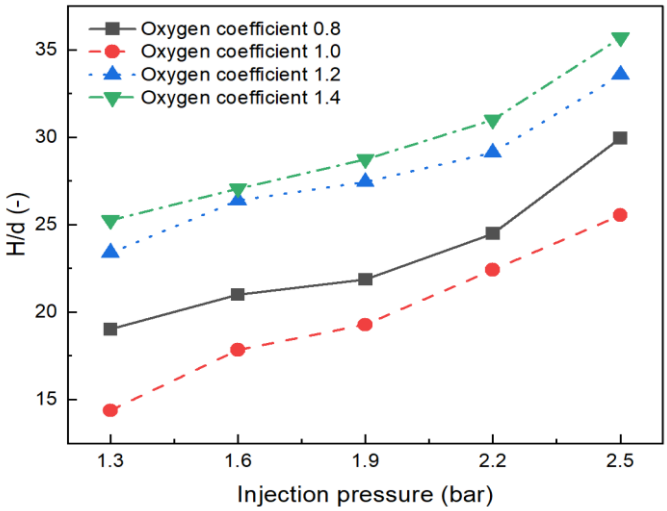

Figure 5.3.4: Lifted height with increasing jet velocity at different excess oxygen coefficients.

5.4 Combustion stability of ammonia in oxygen-enriched

The stability of ammonia-oxygen combustion is a critical parameter for practical applications, and fluctuations of lifted height can be indicative of the stability of the flame under different conditions. Figure 5.4.1 presents the time-dependent behavior of the ammonia-oxygen flame lifted height at a constant co-flow temperature of 1200 K, an oxygen ratio (R_o) ranging from 0.6 to 1.2, and an injection pressure (P_{inj}) of 1.9 bar. The data show that there is a noticeable temporal fluctuation in the flame lifted height. The observed standard deviations of the lifted height, over the time window of 200-260 ms, reach a minimum when R_o=0.8. The reduced fluctuation in flame height at R_o=0.8, indicating a more stable combustion process.

Similar with pure ammonia flames, a further insight into the combustion stability is provided by figure 5.4.2, which describes the critical auto-ignition behavior of the ammonia-oxygen mixture. The behavior is characterized by the cyclic pattern of flame extinction and re-ignition events, which typically occur near the blowout limits. During these events, the auto-ignited flame can locally accelerate the streamwise velocity due to the thermal expansion of hot gases, potentially leading to flame blowout, as observed at around 246 ms. Subsequently, as the local velocity decreases due to a reduction in buoyancy forces, the conditions may become benefit for auto-ignition to occur once again, leading to re-ignition at approximately 250 ms.

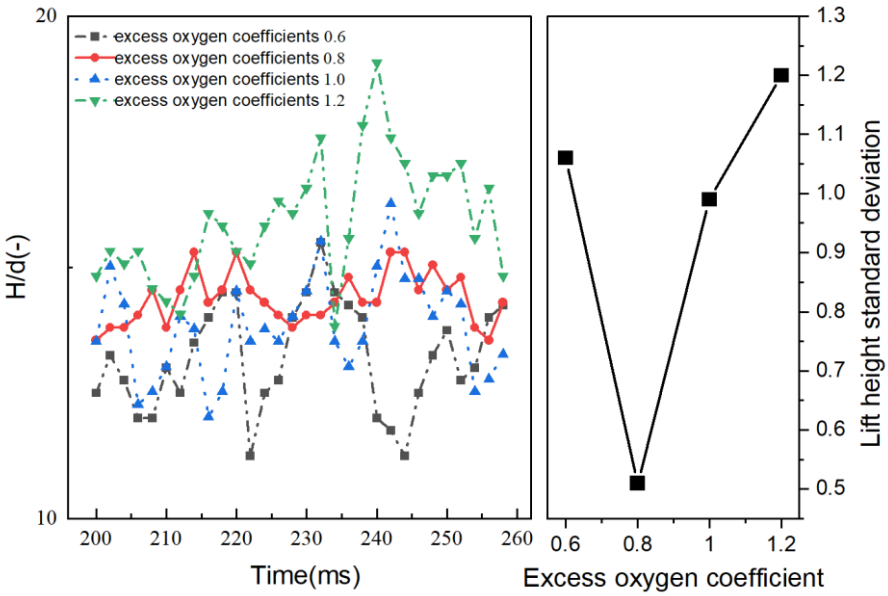

(a) The H/d of ammonai-oxygen ar differnet R_o.

(b) The lift heigt standard deviation of different R_o.

Figure 5.4.1: Flame lifted height and standard deviation with time at different excess oxygen coefficients.

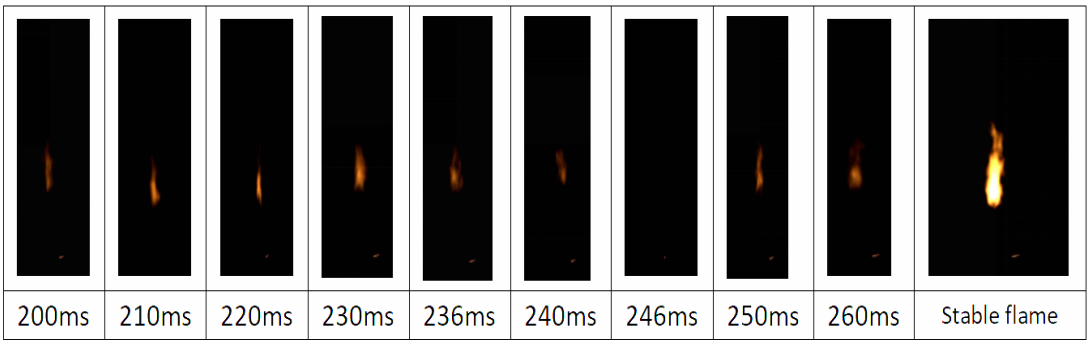

Figure 5.4.2: The lifted flame critical auto-ignition behaviour at R_o=1.2, T_{cf}=1200K, P_{inj}=1.9 bar and the stable flame at R_o=0.8, T_{cf}=1200 K, P_{inj}=1.9 bar.

Figure 5.4.3 compares the flame lifted height of ammonia-oxygen combustion in 200-260 ms (R_o=1.0, U_{cf}=25 m/s, P_{inj}=1.9 bar). With T_{cf} increases, the flame lifted height fluctuation of ammonia-oxygen combustion decreases which means the flame stability increases. The decline trend of lifted height standard deviation is not linear. A temperature turning point at T_{cf} =1173 K divide the standard deviation into two parts: standard deviation decline is very rapidly when T_{cf}< 1173 K which represent the lifted height fluctuation sensitivity to is high; Once the 1173 K, the temperature sensitivity become smaller. Compare to the pure ammonia result in chapter 3, the lifted height standard deviation of ammonia-oxygen is smaller than pure ammonia, which represent oxygen addition has an enhancement effect on combustion stability.

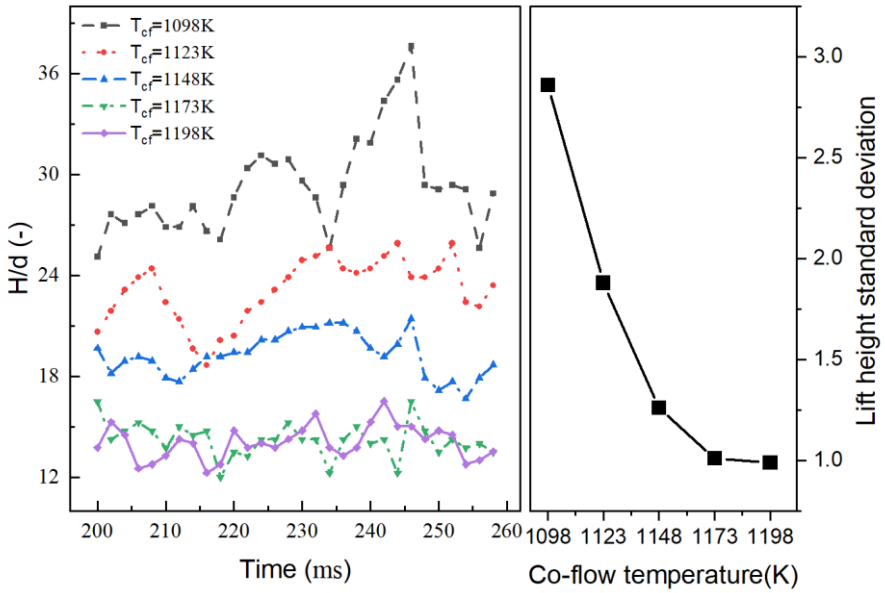

(a) The H/d of ammonai-oxygen at differnet T_{cf}.

(b) The lift heigt standard deviation of different T_{cf}.

Figure 5.4.3: Flame lifted height and standard deviation of ammonia-oxygen with time at different co-flow temperatures.

5.5 Chapter Summary

In this chapter, the turbulence jet flames of ammonia-oxygen at high temperatures, based on Controllable Active Thermo-Atmosphere burner, have been investigated. The jet flame morphology of ammonia, auto-ignition boundary, the ignition delay, combustion stability mechanism and flame fluctuation have been explored and summarized in an oxygen-enriched condition. The main conclusions are shown as follow:

With the co-flow temperature increases, the flame of ammonia combustion become brighter. The brightness of the ammonia-oxygen flame is higher than that of pure ammonia and the ammonia-oxygen flame has a brighter in the flame center, which represent the chemical reaction of combustion is more violent.

With an increment of injection pressure from 1.6 to 2.5 bar, the flame area and flame length first increase than decrease with the injection pressures increase. The turning injection pressure is 1.9 bar. With injection pressure increases, the oxygen effect first enhances the combustion than impedes. The reason is the competition between oxygen enhancement effect and dilution effect.

The ammonia cannot form a flame in every oxygen coefficient when the co-flow temperature is lower than 1073 K. Once the co-flow temperature increases to 1123 K, a continuous and stable flame can be formed. When the oxygen coefficient excess to 1.2, the min auto-ignition temperature for forming a stable flame increases to 1148 K.

With R_o increases, the ignition delay of the ammonia-oxygen flame first decreases then increases. Therefore, there exist an optimal excess oxygen coefficient to shorten the ignition delay of the ammonia. When the R_o is close to

0.8, the ignition delay of ammonia-oxygen is minimal. The ignition delay of ammonia-oxygen has a 30%-39% decline than the pure ammonia at same co-flow temperatures.

With the T_{cf} increases, the flame lifted height gradually decreases. When the T_{cf} is higher than 1173 K, the downtrend of the lifted height is obviously slow down. The temperature sensibility become lower once the T_{cf} > 1173 K. The flame lifted height of ammonia-oxygen combustion has an obvious fluctuation with time and the standard deviation of flame lifted height in 200-260 ms has shown a lowest point when the R_o is equal to 0.8.

Chapter 6

Pollutants production characteristics of ammonia and ammonia blending fuels at high temperatures and pressures

6.1 The simulation condition introduction

The combustion of ammonia fuel exhibits a higher propensity for nitrogen oxides (NOx) emissions compared to hydrocarbon fuels, which presents a significant challenge for emission control of internal combustion engines (ICEs). The thermal NOx from Zelodovich mechanism of ammonia fuel, same with hydrocarbon fuels, is the main production NOx mechanism. Besides the thermal fuel NOx, the excess N element in ammonia supply much more NOx [103]. Thus, the complexity of NOx formation from ammonia combustion is distinct from that of hydrocarbon fuels, necessitating a comprehensive examination of control strategies for NOx emissions in ICEs. Nitrous oxide (N_2O), a component of NOx, is particularly problematic due to its stability and resistance to oxidation, which complicates its reduction through conventional after-treatment systems. Considered its contributions to global warming, controlling N_2O emissions is of paramount importance under the latest emission laws [181]. N_2O has applications in automotive racing as a fuel booster and it can be dissociated at above 300 ℃. These characteristics show that combustion control strategies in cylinder could be used to control N_2O emissions effectively. Furthermore, enhancing combustion efficiency within the cylinder can reduce the presence of unburned ammonia (NH_3), which is also regulated as a pollutant. By utilizing simulation, researchers can gain a prediction for pollutant generation, enabling the development of targeted strategies for NOx emission control. It is critical for informing the design

of both in-cylinder combustion optimization and after-treatment technologies, with the goal of meeting stringent emission regulations while maintaining or improving combustion performance and efficiency.

Table 6.1: Simulation conditions

Parameters	Value
Environment Pressure (P) [MPa]	0.1-10
Temperature (T) [K]	1.3, 1.6, 1.9, 2.2, 2.5
Fuel component	NH_3, NH_3/H_2, NH_3/CH_4, NH_3/O_2
Equivalent ratio	0.7-1.2
Air component	21% O_2 + 79% N_2
Simulation model	Closed Homogeneous Batch Reactor
Gas reactant	Fuel/Air

In this chapter, the auto-ignition simulation model has been validated by auto-ignition experimental data of ammonia and ammonia blending fuels, then emission characteristics have been predicted to investigate the emission production mechanism. The simulation software is CHEMKIN, which is a package for solving complex chemical reaction problems, including a variety of chemical reactors. It can be used to simulate combustion processes, catalytic processes, chemical vapor deposition, plasma and other chemical reactions [182]. The simulation condition has shown in table 6.1.

The simulation model is closed homogeneous batch reactor which has a wildly used to calculate the auto-ignition for different fuels. For Closed Homogeneous Batch Reactor, the condition is content pressure. This condition is same with the CATA combustion condition (no volume limitation and atmospheric pressure). Moreover, the Closed Homogeneous Batch Reactor has a good performance to simulate the auto-ignition characteristics in high temperature. The auto-ignition of jet flow occurs in expermental test after a well-mixed with air in a homogeneous high temperature which is similar with Homogeneous Batch Reactor. Thus, the simulation is significative to predict the emission in a certain extent. A wide range of temperatures, environment pressures and fuel types have been chosen to investigate the ammonia and ammonia blending fuels pollutants generation mechanism.

6.2 Pure ammonia pollutants at elevated temperatures and pressures

The series of references for ammonia combustion had led to develop various chemical kinetic mechanisms, as listed in table 1.2. In this simulation analysis, four established mechanisms by Glarborg [137], CEU [144], Konnov [145], and MEI [153] have been used. These models have been compared against

experimental ignition delay data of pure ammonia fuel within the temperature range of 1153 K to 1223 K, as presented in figure 6.2.1. The study utilizes a closed-homogeneous-transient reactor model, with the specific simulation parameters detailed in table 6.1. It should be noted that the simulation assumes no heat loss, implying adiabatic conditions. Upon comparison, the simulation results show that the CEU and MEI mechanisms provide a better match with the experimental data, particularly at temperatures above 1200 K. Furthermore, the CEU mechanism has a good match with Mathieu experimental data [144]. The ignition delay within Closed Homogeneous Batch Reactor model has been defined as: the required time in which mixture gas temperature increases beyond 400K from the initially temperature. Therefore, these mechanisms have been chosen for further exploration to pollutant formation in the high-temperature combustion of pure ammonia.

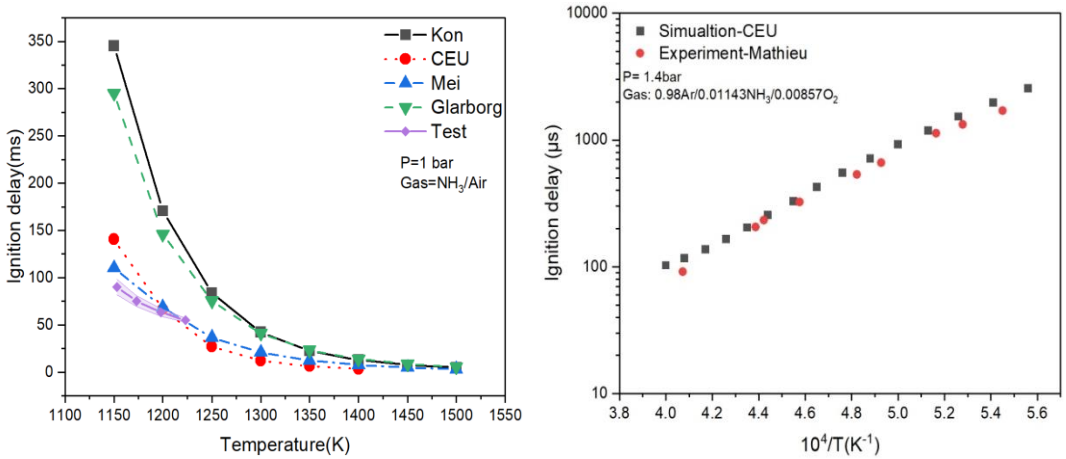

Figure 6.2.1: Comparison of ignition delay between experiments and simulations for pure ammonia combustion.

The emissions of nitrogen oxides (NOx) at different equivalence ratios ranging from 0.7 to 1.4 have been analyzed using Mei's mechanism, illustrated in figure 6.2.2. At an equivalence ratio of 1, nitric oxide (NO) is identified as the primary pollutant. With equivalence ratio increases, it indicates a declining trend in NOx emissions. This trend is attributed to the fact that the increase in NH_3 will promote the DeNOx reduction reaction which reduce the formation of NOx and transform to N_2+H_2O. However, as the NOx levels decrease, there is an obvious rise in unburned ammonia due to incomplete combustion. This excess ammonia could potentially be utilized in aftertreatment systems to further reduce pollutant. Conversely, when the equivalence ratio approaches 0.7, a surplus of oxygen leads to more complete ammonia combustion and higher flame temperatures. This condition enhances the formation of NOx, thereby resulting in an overall increase in NOx emissions.

DeNOx reduction reactions as follow Eq. (6.1) to Eq. (6.3):

$2NO+2NH_3+1/2O_2=2N_2+H_2O$ (6.1)

$NO_2+2NH_3+1/2O_2=3/2N_2+3H_2O$ (6.2)

$NO+NO_2+2NH_3=2N_2+3H_2O$ (6.3)

Figure 6.2.3 shows the influence of different environment temperatures on the products of pure ammonia flame under the conditions of 0.1 MPa and equivalent ratio 1, based on MEI's mechanism. It can be found that as the temperature increases, the NO, NO_2 and N_2O, all increase. The concentration of NO is the highest, and the mole fraction of it is as high as 3000-6000 ppm. Although NO_2 and N_2O also increase, their absolute value is not high. Therefore, NO is the main combustion pollutant under high temperature conditions.

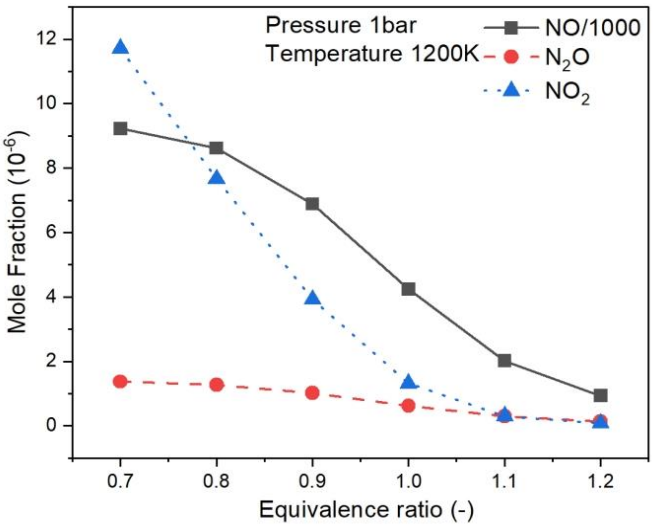

Figure 6.2.2: NOx pollutant generation at different equivalence ratios, based on Mei's mechanism.

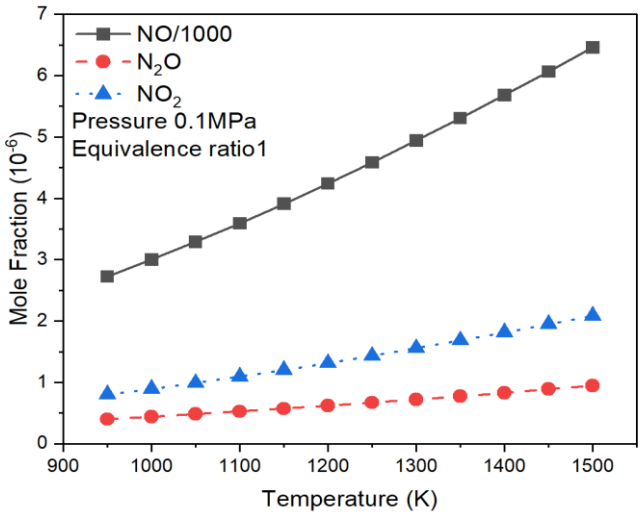

Figure 6.2.3: Emission of pure ammonia combustion flame at different initial temperatures, based on Mei's mechanism.

Figure 6.2.4 shows the pure ammonia combustion flame products at different background pressures, based on Mei's mechanism. It can be found that as the pressure increases, N_2O and NO_2 increase, while NO decreases. The findings show that as pressure increases, the amounts of N_2O and NO_2 elevate, whereas NO exhibits a decrease. Although the NO concentration decreases, it remains the main component of pollutants. The key chemical reaction is that the absolute rate

of NO production from equation NO+OH+M=>HNO+M has increased from $6.53x10^{-6}$ mol/(cm^3 • s) at 1 bar to $2.66x10^{-3}$ mol/(cm^3 • s) at 25 bar. The absolute rate of NO and OH will accelerate the consumption of NO that will be transformed into HNO. Research by Hayakawa indicates that the third-body reaction OH+ H+M=>HNO+M is highly sensitive to the formation of HNO from NOx under high-pressure conditions [77].

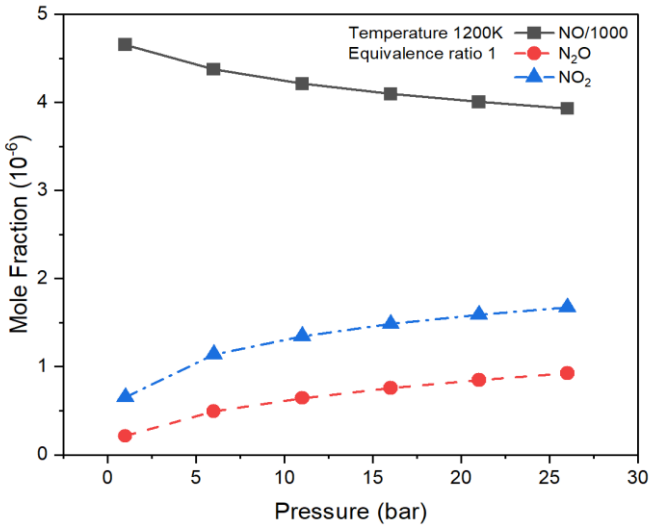

Figure 6.2.4: Emission of pure ammonia flame at different background pressures, based on Mei's mechanism.

Figures 6.2.5 and 6.2.6 present the ignition delay and combustion emission for pure ammonia under conditions of elevated temperatures and pressures. There is a notable discrepancy in the ignition delay predicted by the Mei and CEU mechanisms at 1150 K, due primarily to differences in their respective rates of ammonia conversion to NH_2. The rate of NH_2 production based on the Mei mechanism is calculated to be $7.98x10^{-3}$ mol/(cm^3 • s), whereas the CEU mechanism has a slightly lower rate of $6.74x10^{-3}$ mol/(cm^3 • s). This NH_2 generation is productid from the reaction NH_3+OH =>NH_2+H_2O; a higher rate of NH_2 production suggests a more vigorous reaction between NH_3 and OH, potentially leading to faster ignition. For example, the ignition delay according to the Mei mechanism declines from 36ms at 0.1 MPa to just 5 ms at 1 MPa.

As pressure increases, the rate of increase for NO_2 and N_2O is observed to diminish. At 1550 K, an increase in pressure from 1 MPa to 5 MPa results in N_2O concentration rising from 1ppm to 2 ppm, an increment rate of 1ppm per 4 MPa. However, a pressure increases from 5 to 9 MPa results in a smaller rise in N_2O concentration, at 0.6 ppm, equating to an increase rate of 0.15 ppm per MPa. Alongside rising ambient pressures, NO concentrations continue to decline, while levels of N_2O and NO_2 persistently ascend.

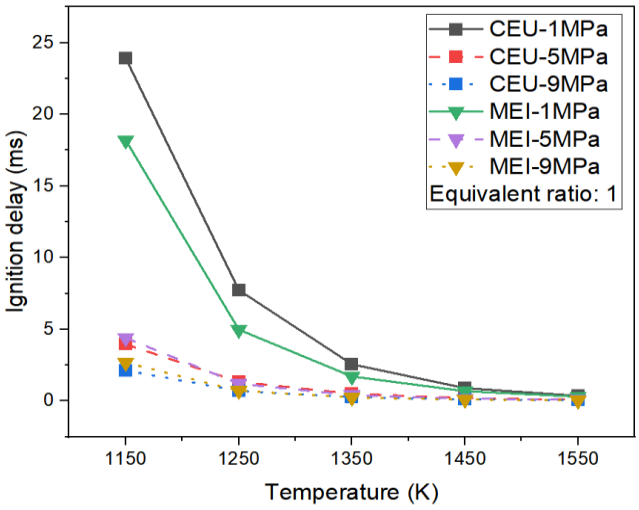

Figure 6.2.5: Ignition delay of pure ammonia fuel under high temperatures and pressures.

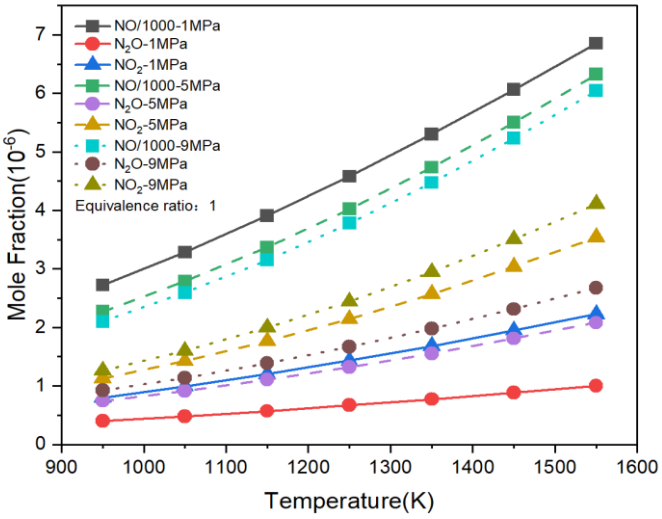

Figure 6.2.6: Combustion pollutant generation of pure ammonia fuel under high temperatures and pressures, based on Mei's mechanism.

In order to investigate the steam influence on ammonia emission reduction, the ammonia with 10% steam has been finished in figure 6.2.7. When the temperature is 1300 K, the NO decreases nearly 27% from 4580 to 3360 ppm, once 10% steam addition. The water addition not only decreases the flame temperature to reduce the NOx, but also enhances the DeNOx reactions. Adding steam can decompose and consume O radicals through reaction $H_2O+O=OH+OH$, so the reaction $NH_2+O=NO+H_2$ is inhibited and the generation of NO is reduced [122]. H_2O accelerates the consumption of O_2; therefore, NOx emissions are greatly reduced [183], further controlling the production of NOx. Steam reduces NOx emissions without compromising the stability of premixed and non-premixed combustion processes. So, water injection technology may have an impact on the emission reduction of internal combustion engines.

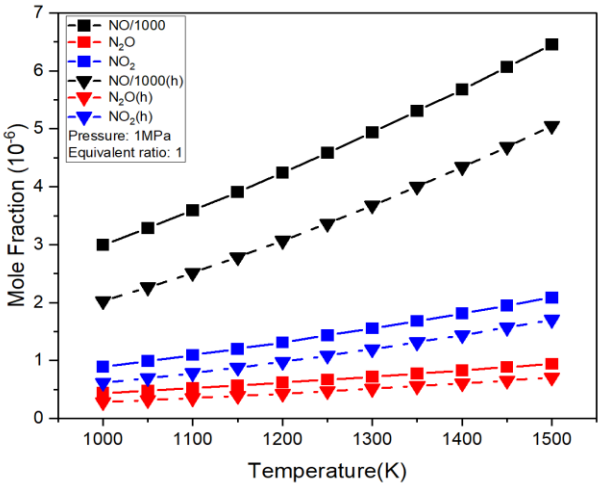

Figure 6.2.7: The emission of ammonia with 10% steam, based on Mei's mechanism: (h) means 10% water addition.

6.3 Ammonia-hydrogen blending fuel pollutants at elevated temperatures and pressures

In order to evaluate the optimal hydrogen ratios (X_H) and predict the emission, the hydrogen enhancement effect on ammonia has been investigated from 900 K to 1500 K and 1 bar to 10 bar. The figure 6.3.1 and 6.3.2 show the temperature and hydrogen ratios effect on ignition delay. With temperature and hydrogen ratios increases, the ignition delay decreases. The ignition delay has an obvious decline once the hydrogen ratio increases to 10%, which means 10% hydrogen ratio is an optimal ratio to ignite the ammonia-hydrogen mixture. Once the auto-ignition performance of ammonia-hydrogen trend to be stable until the hydrogen ratios increase to 20%, which means 20% is an optimal ratio to form a stable flame.

The temperature has an obvious impact on NOx production. With the increase of temperature, NOx increases, shown in figure 6.3.3 and 6.3.4. The figure 6.3.5 shows the NO production main chemical reactions of ammonia-hydrogen at different temperatures. The reactions absolute rate of HNO+H<=>NO+H_2, NO+H<=>NH+O and N+NO<=>N_2+O increases at a higher temperature. These absolute rates show that O and H are the main chemical groups. H_2 can transform to H easier in higher temperature. A higher temperature lead to H_2 consume increase and booster the HNO transform to NO.

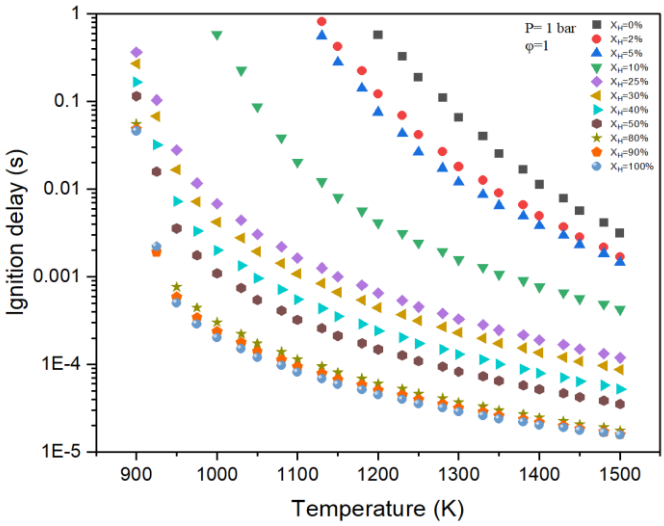

Figure 6.3.1: Ammonia-hydrogen ignition delay at different temperatures.

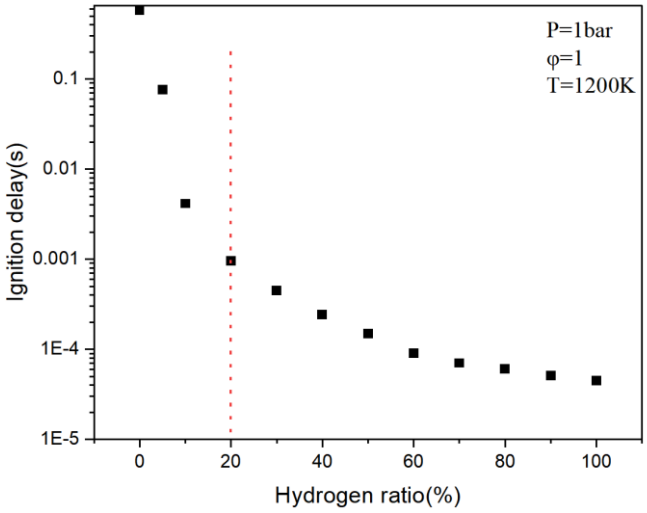

Figure 6.3.2: Ammonia-hydrogen ignition delay at different hydrogen ratios.

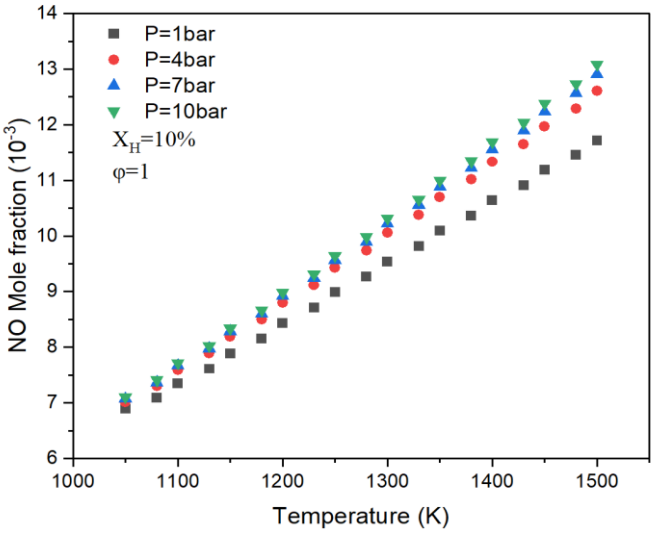

Figure 6.3.3: The NO mole fraction of ammonia-hydrogen at different environment pressures.

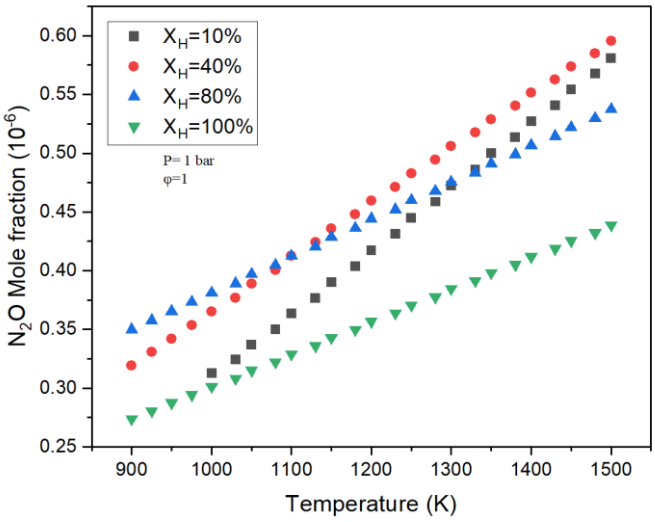

Figure 6.3.4: The N_2O mole fraction of ammonia-hydrogen at different hydrogen ratios.

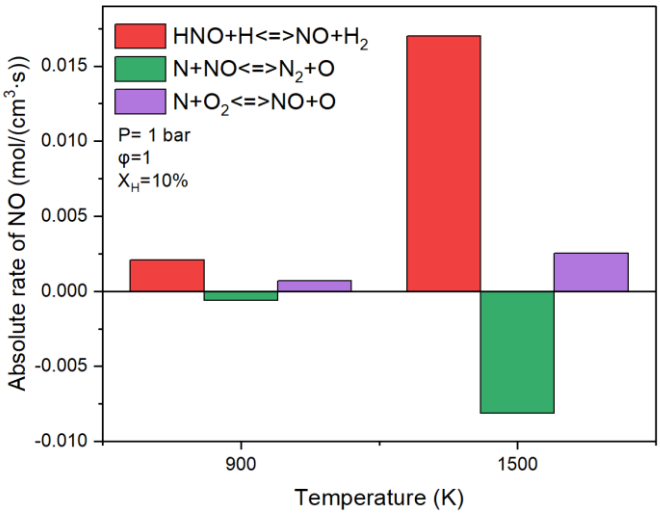

Figure 6.3.5: NO production main chemical reactions of ammonia-hydrogen at different temperatures.

The increase of NO_2 is related with NO and the main chemical reactions have shown in figure 6.3.6. The increase of NO enhances the NO oxidation absolute rate, which transform NO to NO_2. In the meanwhile, the increase of NO mole fraction accelerates the negative reaction (NO+OH=>NO_2+H) to increase the NO_2. The figure 6.3.7 shows the N_2O main chemical reactions of ammonia-hydrogen. The increase of NO mole fraction also accelerates the NH+NO<=>N_2O+H absolute rate to increase the N_2O.

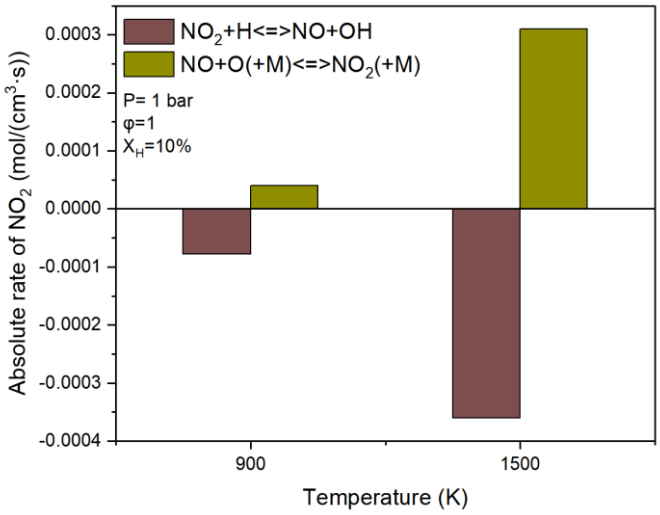

Figure 6.3.6: NO_2 production main chemical reactions of ammonia-hydrogen at different temperatures.

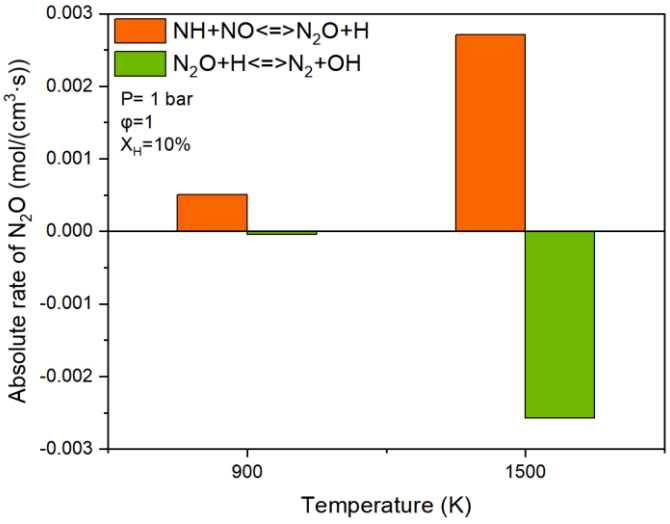

Figure 6.3.7: N_2O production main chemical reactions of ammonia-hydrogen at different temperatures.

Ammonia disassociation is one of advanced ammonia-hydrogen reform technology and has a widely patient to use in internal combustion engines. Its fundamental chemical principle is that ammonia can be disassociated into hydrogen and nitrogen close to 700℃ without catalyst [49] or with catalyst. Ammonia dissociation is introduced in Chapter 1. In this part, the disassociation simulation ratio (X_d) has been defined in Eq 6.4. For example, the X_d=0% or X_d=100% represent 100% ammonia or hydrogen/nitrogen mixture, respectively.

$$X_d = \frac{X_{disassociated}}{X_{initial}} \quad (6.4)$$

Where, $X_{disassociated}$ is the disassociated ammonia and $X_{initial}$ is initial ammonia.

The ignition delay of ammonia disassociation flame have shown in figure 6.3.8. The ignition delay overall decrease when the decomposition ratio (X_d) of ammonia surpasses 10%. And with the X_d increases, the auto-ignition temperature

boundary extends. The ignition delay of ammonia dissociation fuel increases because of the dilution effect from nitrogen, which is different with ammonia-hydrogen shown in figure 6.3.1. Once the X_d reach to 50%, the ignition delay increasing tendency decreases, which means ammonia disassociation mixture gas combustion performance trend to the hydrogen combustion.

Due to the unstable combustion characteristics of ammonia, the NOx production, close to the combustion boundary, is necessary to investigate. The auto-ignition boundary represents the lowest auto-ignition temperature at which the ignition delay can be calculated (cf. figure 6.3.9). The N_2O has an obvious increment at the auto-ignition boundary and increases with the environment temperature increases. With the X_d increases, the auto-ignition boundary temperature decreases. Compared to the pure ammonia (X_d=0%), ammonia disassociation blending fuel has a lower N_2O emission at auto-ignition boundary (cf. figure 6.3.10).

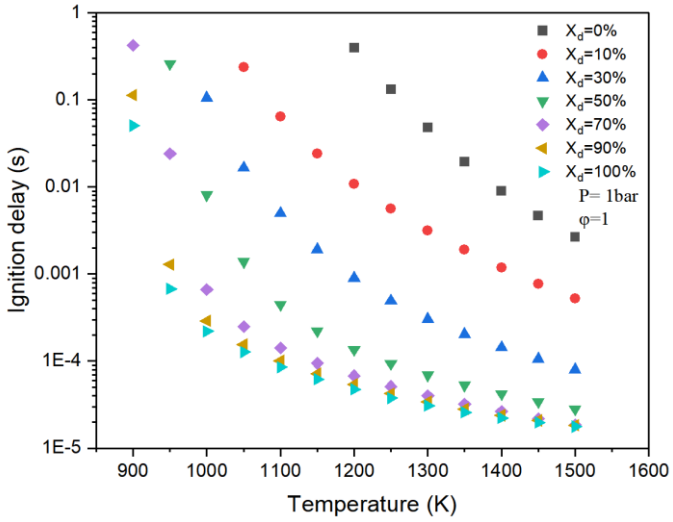

Figure 6.3.8: The ignition delay of ammonia disassociation blending fuel.

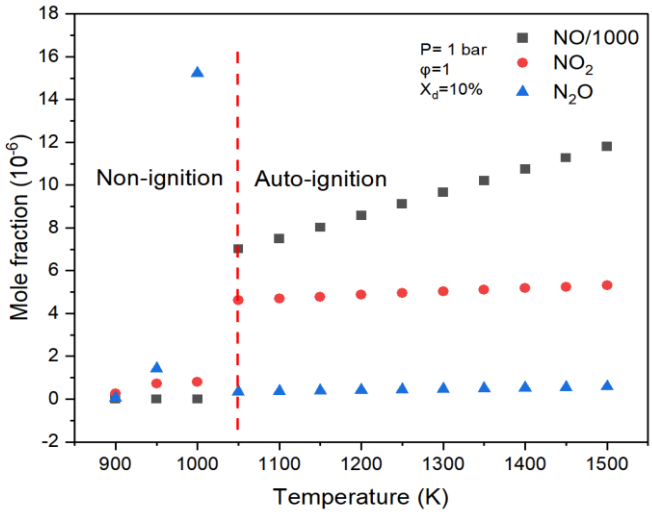

Figure 6.3.9: The main pollutants of ammonia disassociation blending fuel at different environment temperatures.

The figure 6.3.11 shows the NO and N_2O mole fraction at different X_d and environment temperatures. As the temperature rises, there is a corresponding increase in NO production. The increasing trend can be attributed to enhance absolute rate of the reaction HNO+H<=>NO+H_2, which intensifies with temperature, thereby boosting the generation of NO, as shown in figure 6.3.12. Once the X_d excess than 30%, the NO and N_2O has a lower increases slope, which means the ammonia dominant the pollutants when X_d<30% and the hydrogen dominant the pollutants when X_d>30%.

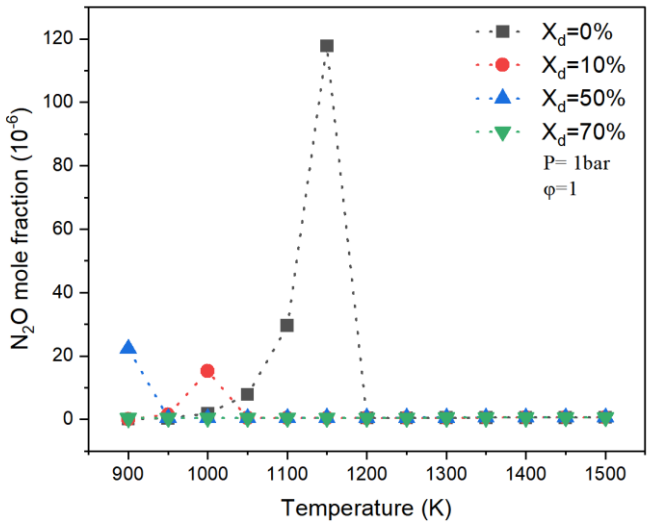

Figure 6.3.10: N_2O production of ammonia disassociation blending fuel at combustion boundary.

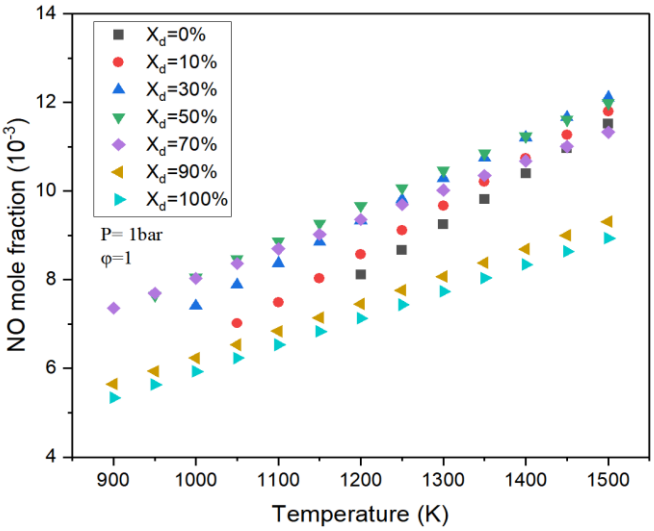

Figure 6.3.11: The NO mole fraction of ammonia disassociation blending fuel at different X_d.

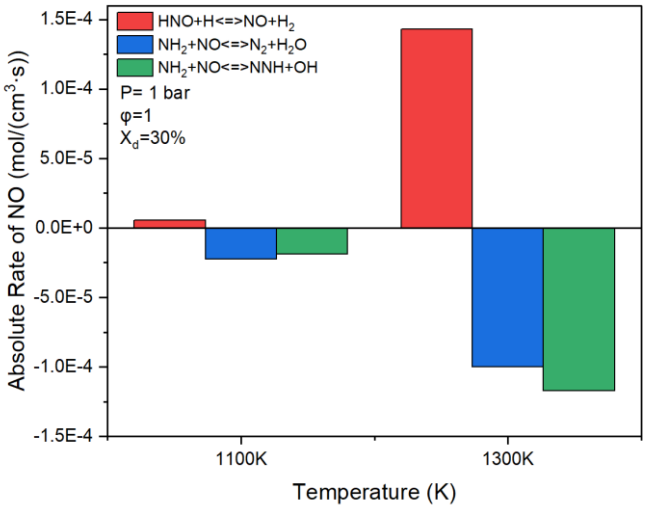

Figure 6.3.12: The main chemical reaction of NO at different temperatures.

The figure 6.3.13 shows the N_2O production at different X_d and temperatures. The N_2O show a similar result with NO. With the temperature increases, the N_2O increases due to main chemical reactions NH+NO<=>N_2O+H and N_2O+H<=>N_2+OH absolute ratio increase in figure 6.3.14. The NH+NO<=>N_2O+H and N_2O+H<=>N_2+OH have an obvious fluctuation once the X_d increases, shown in figure 6.3.15. With the X_d increases, the absolute ratio of main N_2O reaction increases. But because of ammonia ratio decline in disassociation fuel, the N_2O overall production decreases.

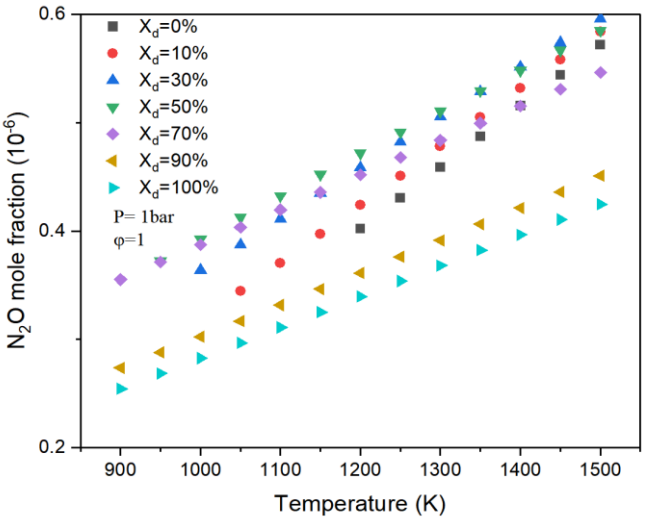

Figure 6.3.13: The N_2O production at different disassociation ratios.

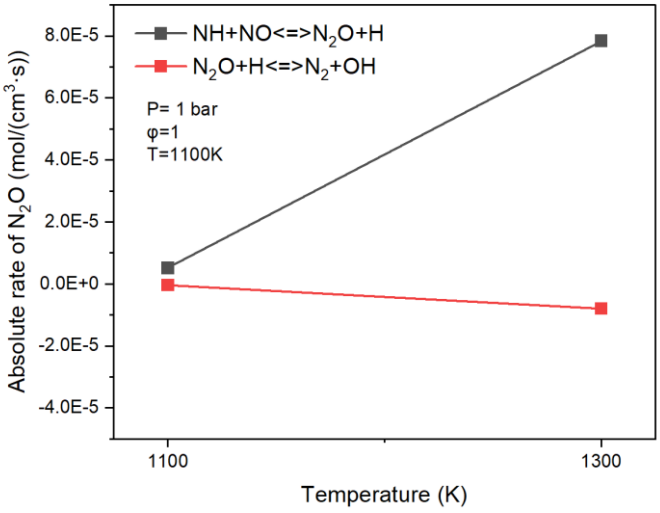

Figure 6.3.14: The N_2O main chemical reaction at different temperatures.

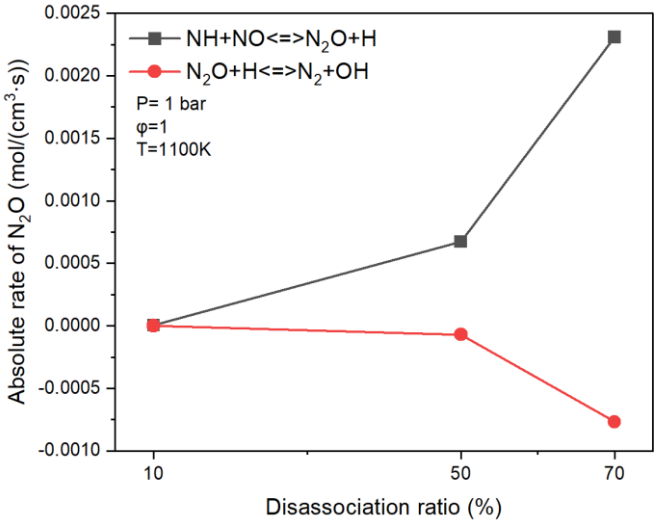

Figure 6.3.15: The N_2O main chemical reactions at different disassociation ratios.

These exist a disassociation ratio which has a highest emission when the X_d=50%, shown in figure 6.3.16 and 6.3.17. NO and N_2O first increase than decline. The N_2O has a different growth tendency at different X_d. The N_2O growth trend beyond 50% disassociation ratios is higher than that of lower 50%. The reason is that when the disassociation ratio increases to 100%, the NOx is produced by the thermal Zeldovich mechanism from hydrogen combustion. But when the hydrogen ratio is lower, the NOx is produced both by ammonia fuel and Zeldovich mechanism. With the hydrogen increases, the N_2O production from ammonia fuel decreases, which lead to hinder growth trend. Thus, 10% is an optimal disassociation with a lower ignition delay, low disassociation cost and lower NOx emission.

As indicated in figure 6.3.18, environmental pressure markedly influences the production of N_2O. Increment in both temperatures and pressures contribute to a rapid rise in N_2O levels. At higher pressures, the absolute rates of the reactions NH+NO<=>N_2O+H and NH_2+NO_2<=>N_2O+H_2O significantly increase. This

implies that these reactions pathways are enhanced by pressure, leading to a greater N_2O formation. The absolute ratio of N_2O (+M)<=>N_2+O(+M) has an obvious inversion with pressure increases, which lead to N_2O production increases, shown in figure 6.3.19. At the auto-ignition boundary, particularly at a temperature of 1000K, N_2O production is elevated, which are shown by figures 6.3.20 and 6.3.21. These figures show that the passive absolute rate of the reaction NH_2+NO_2<=>N_2O+H_2O increases. The Zeldovich mechanism, which is a dominant pathway for NOx formation at high temperatures, has a reduced impact at the gas mixture temperature of 1000 K, which is substantially lower than the typical temperature threshold for thermal NOx production (around 1800 K). Therefore, the Zeldovich mechanism is less relevant for N_2O formation at auto-ignition boundary condition.

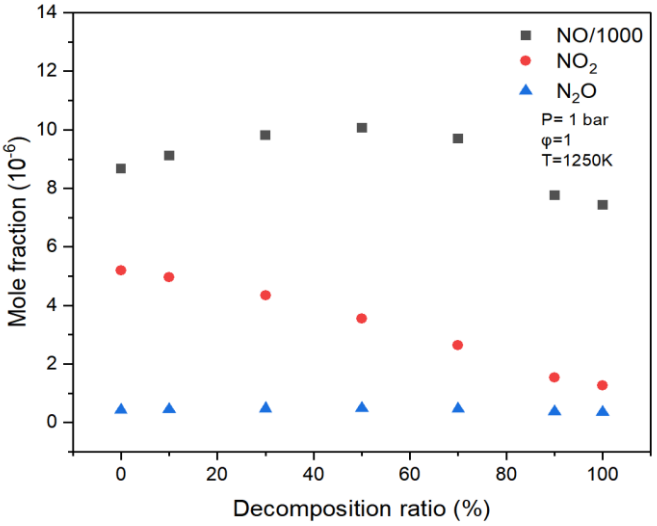

Figure 6.3.16: The NOx mole fraction at different X_d.

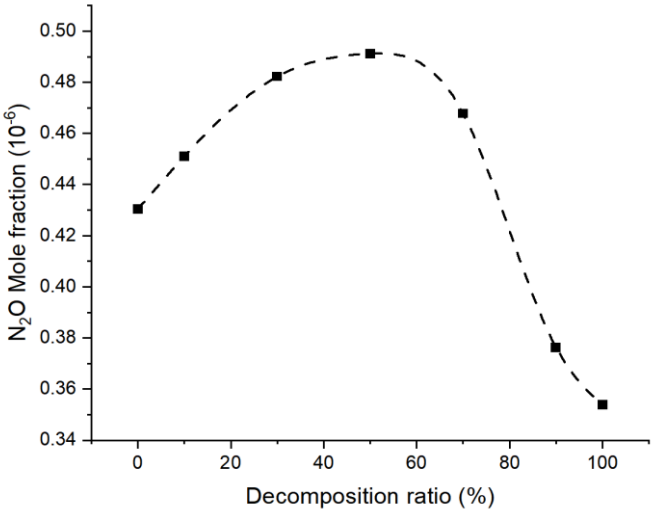

Figure 6.3.17: The N_2O mole fraction at different X_d.

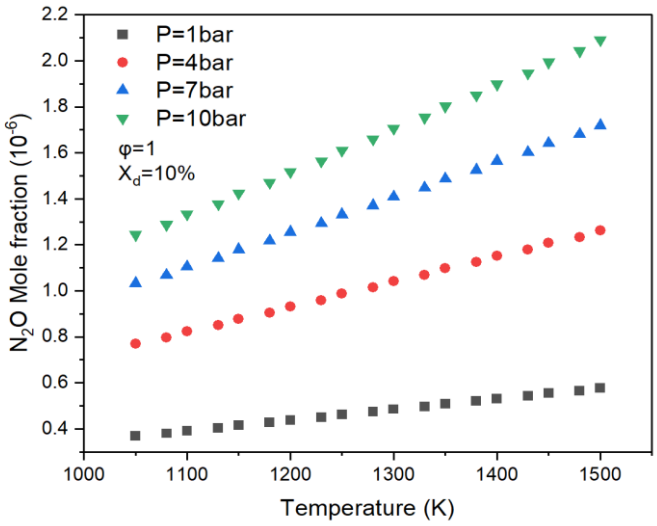

Figure 6.3.18: The N_2O mole fraction at different temperatures and environment pressures.

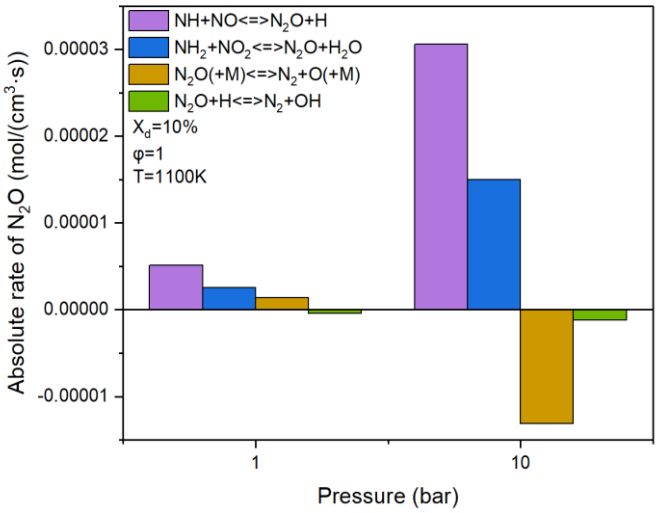

Figure 6.3.19: The main N_2O chemical reactions at different environment pressures.

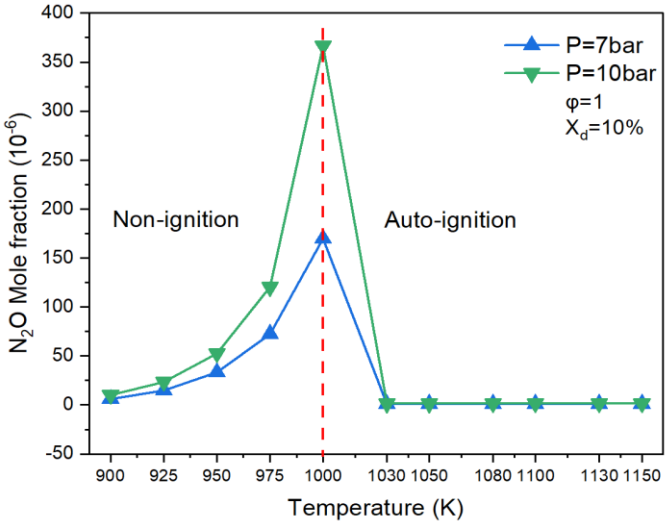

Figure 6.3.20: The N_2O production at auto-ignition boundary.

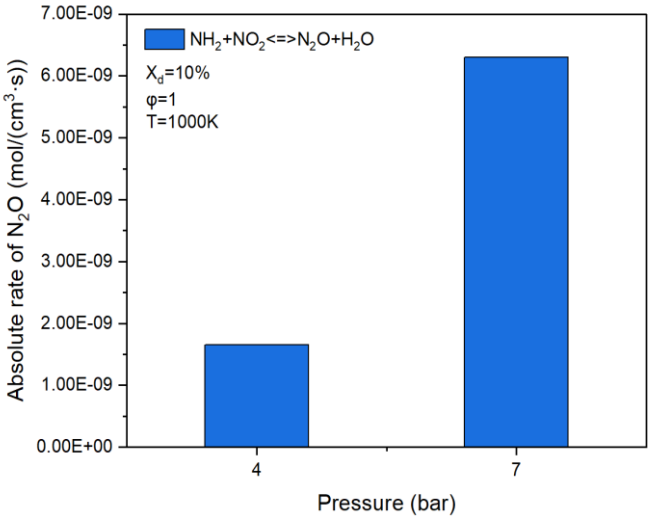

Figure 6.3.21: The N_2O main chemical reaction at different pressures.

6.4 Ammonia-methane blending fuel pollutants at elevated temperatures and pressures

The CEU mechanism [92] has been chosen to investigate the ammonia-methane ignition delay at different methane ratios, shown in figure 6.4.1. With the methane ratio and temperature increase, the ignition delay shows a decline trend. The chemical reaction sensitivity coefficients of inhibiting ignition reactions $CH_4+H=CH_3+H_2$ and $CH_3+O=CH_2O+H$ are reduced, further promoting ignition [184]. The H and OH radicals have a large impact on NH_3 flames [185,186]. With the methane ratio increases, the increasing of H and OH radical production lead to an obvious decline of ignition delay especially in lower temperatures. The temperature increment lessens the difference from methane ratio increment. The ammonia-methane ignition delay at high environment pressures have shown in figure 6.4.2. The ignition delay decline shows an obvious gap beyond 30 bar.

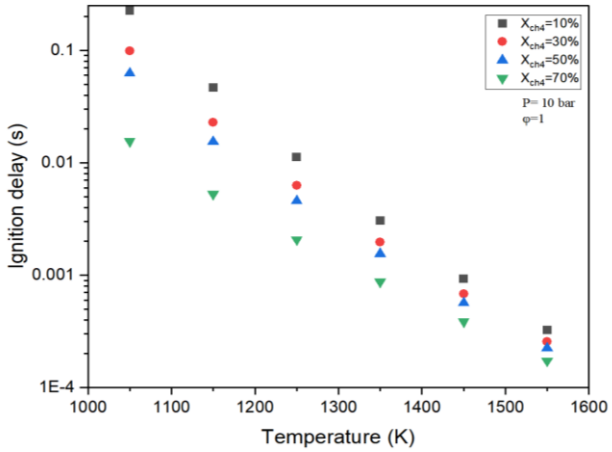

Figure 6.4.1: Ignition delay of ammonia-methane at different temperatures and different X_{CH4}.

The NO is the main pollutant of ammonia-methane mixture fuel. Due to the flame temperature increases (cf. figure 6.4.3), the NOx of ammonia/10% methane blending fuel, shown in figure 6.4.4, is higher than that of pure ammonia (cf. figure 6.2.3). In figure 6.4.5, the pollutant of ammonia-methane includes not only NO, but also CO_2. In a lower temperature, the CO_2 is the main pollutant. However, the NO and CO_2 show a competition in higher temperature. When the temperature beyond 1400K, the NO will be the main pollutant. The H-abstraction reactions between NH_2 and CH_4 becomes a major consumption pathway for CH_4[184].

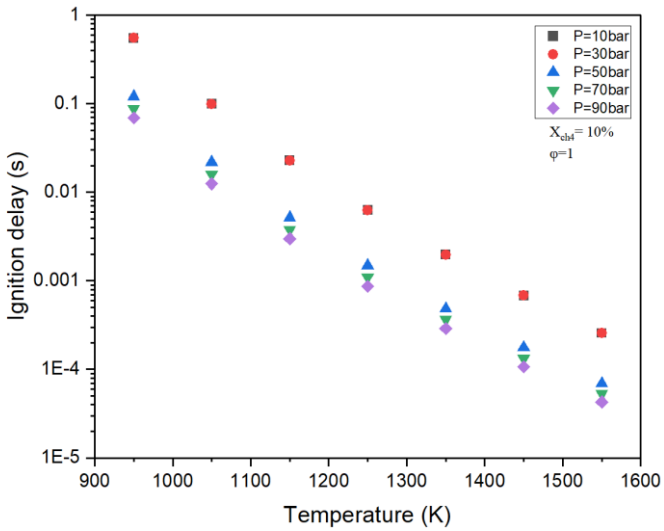

Figure 6.4.2: Ammonia-methane ignition delay at different temperatures and environment pressures.

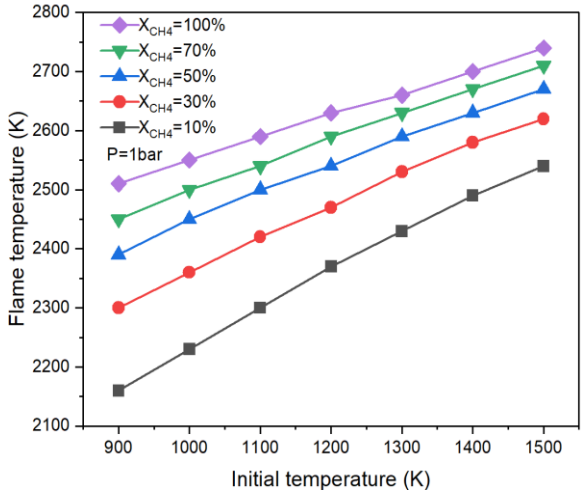

x

Figure 6.4.3:The adiabatic flame temperature of ammonia-methane at evaluated initial temperatures.

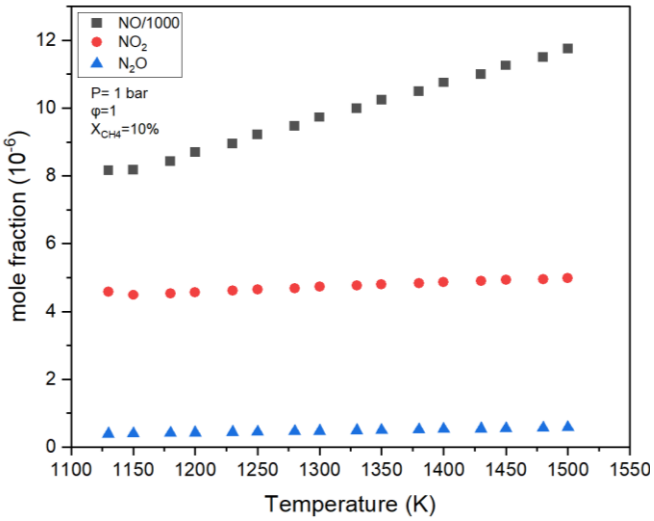

Figure 6.4.4: NOx emissions of ammonia-methane blending fuel.

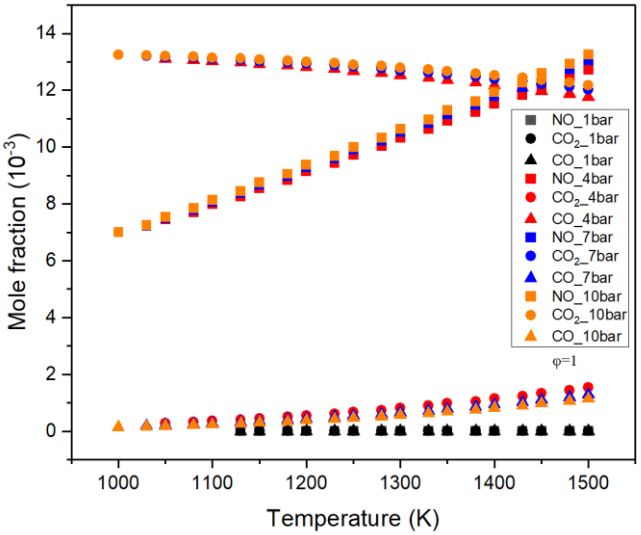

Figure 6.4.5: NO, CO and CO_2 mole fraction of ammonia-methane at different temperatures and pressures.

Unstable combustion and misfire lead to not only power lost but also increase the emission. The figure 6.4.6 and 6.4.7 report a series of pollutants from non-ignition to auto-ignition conditions. At the ignition boundary (1100 K), the CO is the main pollutant and the CO_2 and NO is lower. The reason is that CO_2 has been reduced by main chemical reaction: $NH+CO_2=HNO+CO$. It leads to CO_2 transform to CO and let CO higher than CO_2. The other reason is that the incomplete combustion and lower temperature hinder the CO transform to CO_2. When the combustion occurs, the gas temperature increases, the main chemical is $CO+OH=CO_2+H$ and the CO decreases but CO_2 increases due to CO transform, then the CO_2 will become higher than CO. The methane has a competition with ammonia. At the combustion boundary, the CO mole fraction is higher than NO. The NO is generated by NH_3 oxidation reaction. So, the methane combustion mechanism is prior than NH_3 combustion mechanism. At the ignition delay point, two main chemical reactions occur: $HCO+O_2=CO+H_2O$ and $HNO+CO=NH+CO_2$.

The intermediate product (HNO) in ammonia claim has been consumed to hinder the ammonia combustion.

NO is lower at the combustion boundary and the N_2O is main pollutant at 1100 K, shown in figure 6.4.7. The chemical reaction $NH_2+NO_2=N_2O+H_2O$ is the main reaction at the combustion boundary (1100 K), so the N_2O is higher than NO_2. The N_2O production is very low in lower temperatures (<1000 K), due to the combustion chemical will not occur in lower temperatures. The mixture gas temperature does not reach the auto-ignition temperature. But when the combustion occurs beyond 1150 K, the main chemical reaction is $N_2O+H=NH+NO$, the N_2O will transform to NO. This is the reason why the N_2O mole fraction is low and NO increases in a higher temperature.

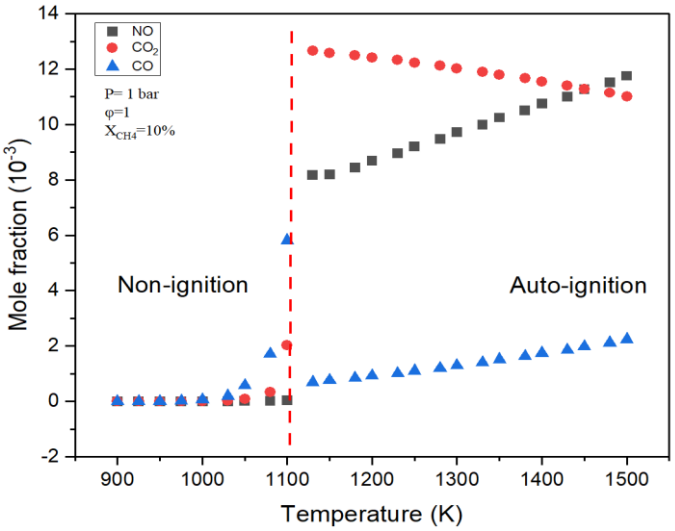

Figure 6.4.6: NO, CO and CO_2 emission between non-ignition and auto-ignition.

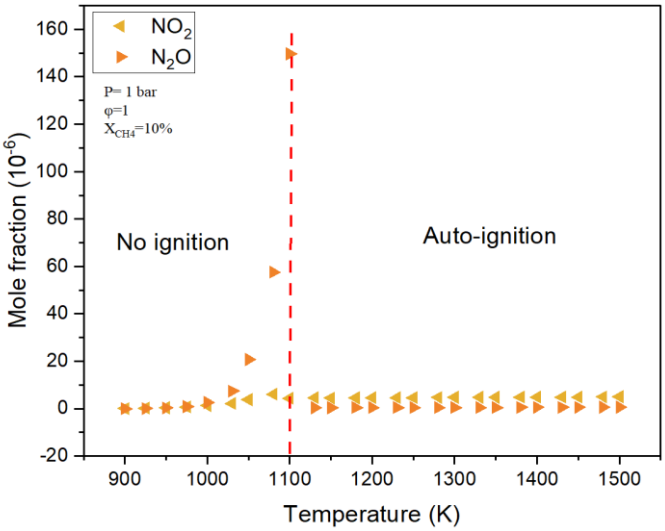

Figure 6.4.7: N_2O and NO_2 emission between non-ignition and auto-ignition.

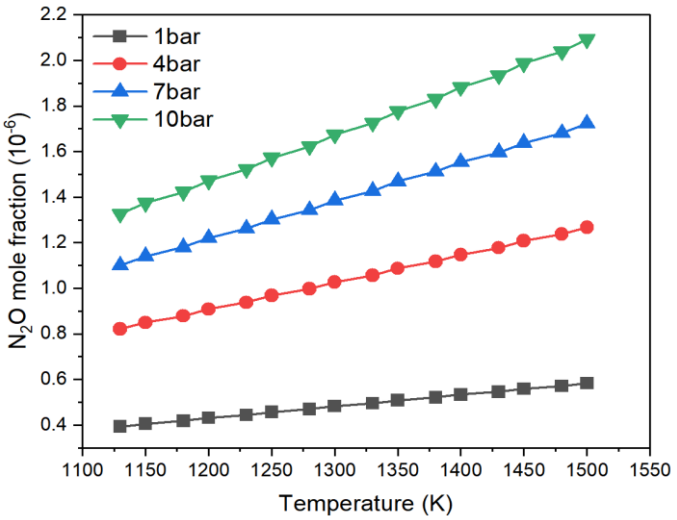

Figure 6.4.8: N_2O emission at different environment temperatures.

With the pressure increases, the chemical reactions $NO+HNO_2=NO_2+OH$ and $NH_2+NO_2=N_2O+H_2O$ absolute rate increase. So, the N_2O increases with the environment pressures increases, shown in figure 6.4.8. and 6.4.9. With the environment pressure increases, the N_2O increases at a lower auto-ignition temperature. A higher environment pressure can accelerate the auto-ignition but increases the NOx at boundary. So, the ammonia-methane combustion needs to adjust environment pressure and temperature to ensure a sufficient auto-ignition.

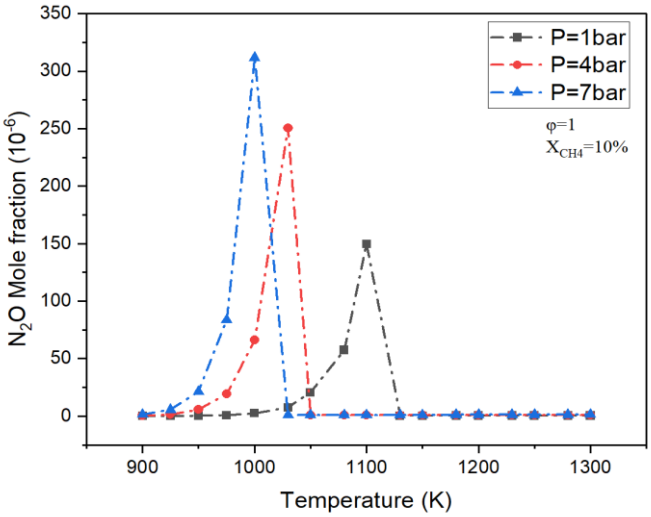

Figure 6.4.9: N_2O mole fraction of ammonia-methane blending fuel at high environment pressures.

6.5 Ammonia pollutants in oxygen-enriched condition

The MEI mechanism, as cited in reference [153], is recognized for its application in the study of ammonia combustion under oxygen-enriched and high-pressure conditions. The specific conditions referenced in [153], with oxygen ratios ranging from 25% to 45% and pressures between 1 to 5 atm, same with the

experimental conditions in Chapter 4, thus providing a relevant experimental verification for further simulation.

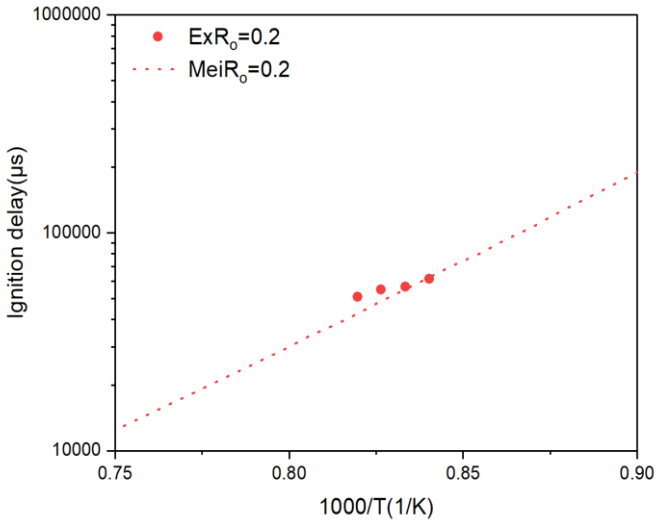

Figure 6.5.1: Comparison of experimental and simulation results.

In figure 6.5.1, the comparison of ignition delay from both experimental data (E_xR_o) and simulation results ($MeiR_o$) derived from the MEI mechanism is illustrated. E_xR_o refers to the experimental ignition delay of ammonia-oxygen blending fuel from Chapter 4, while R_o represents the excess oxygen coefficients. The experimental results exhibit longer ignition delay, due to the mixing times and gas transport times within the injection system.

Figures 6.5.2 and 6.5.3 demonstrate that the production of NO increases with increasing oxygen ratio. The primary chemical reactions contributing to NO generation are NH_2+NO<=>NNH+OH and HNO+O_2<=>NO+HO. An excess of O_2 promotes these forward reactions, leading to more NO production, while the concurrent consumption of NH_2 propels the reverse reaction.

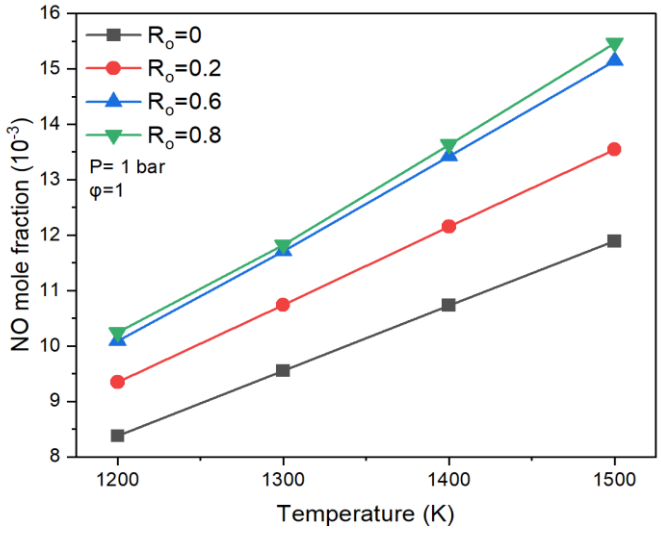

Figure 6.5.2: NO mole fraction of ammonia-oxygen at different oxygen ratios.

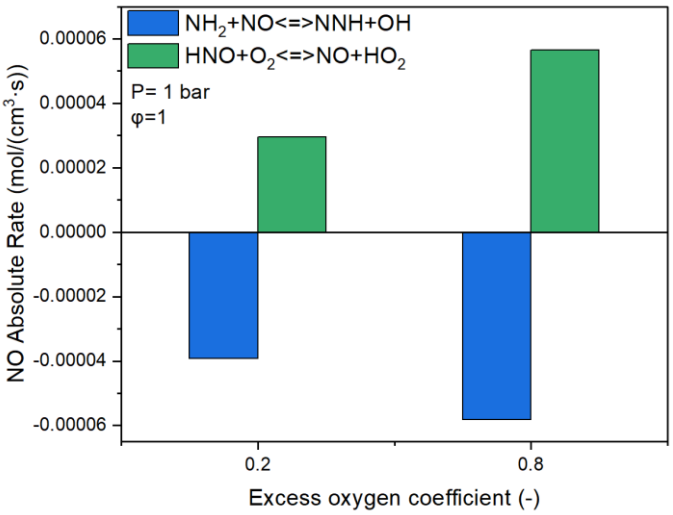

Figure 6.5.3: NO main chemical reactions of ammonia-oxygen at different oxygen ratios.

The concentration of NO_2 shows a pronounced increase with higher oxygen ratios, as shown in figures 6.5.4 and 6.5.5. The reactions driving NO_2 production include $H_2NN+O_2<=>NH_2+NO_2$, $NO+HO_2<=>NO_2+OH$, $NO_2+H<=>NO+OH$, and $NH_2+NO_2<=>H_2NO+NO$. The growth in NO and O_2 mole fractions have an influence on NO_2 increasing directly. Nitrous oxide (N_2O) trends upwards similarly to NO, with key contributing reactions being $NH+NO<=>N_2O+H$ and $NH_2+NO_2<=>N_2O+H_2O$, as evidenced by figures 6.5.6 and 6.5.7. At the auto-ignition boundary, figures 6.5.8 and 6.5.9 show that N_2O concentrations are particularly high, governed by the chemical reaction $NH_2+NO_2<=>N_2O+H_2O$.

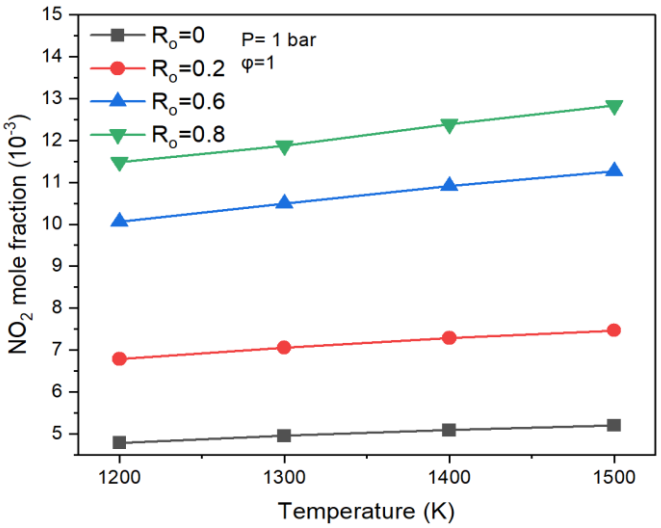

Figure 6.5.4: NO_2 mole fraction of ammonia-oxygen at different ratios.

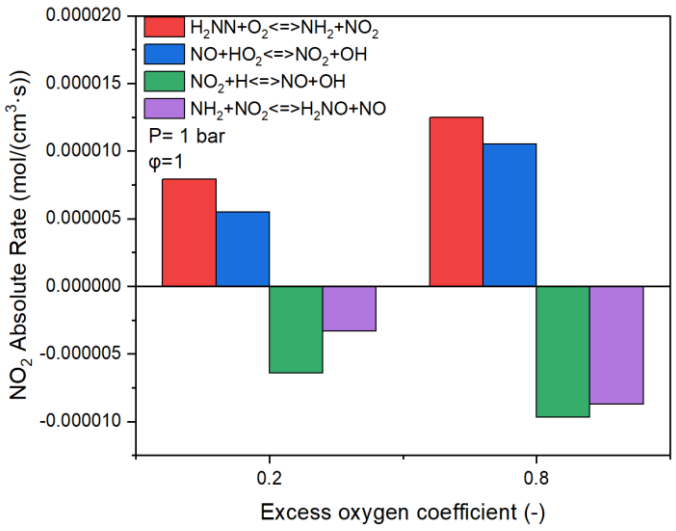

Figure 6.5.5: NO_2 main chemical reactions of ammonia-oxygen at different oxygen ratios.

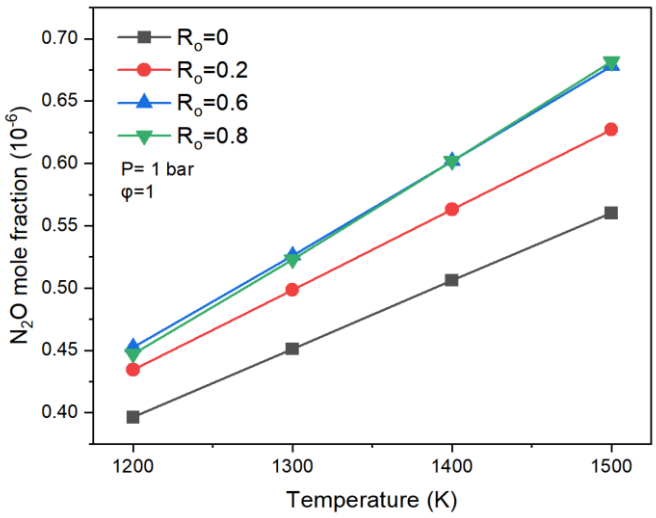

Figure 6.5.6: N_2O mole fraction of ammonia-oxygen at different oxygen ratios.

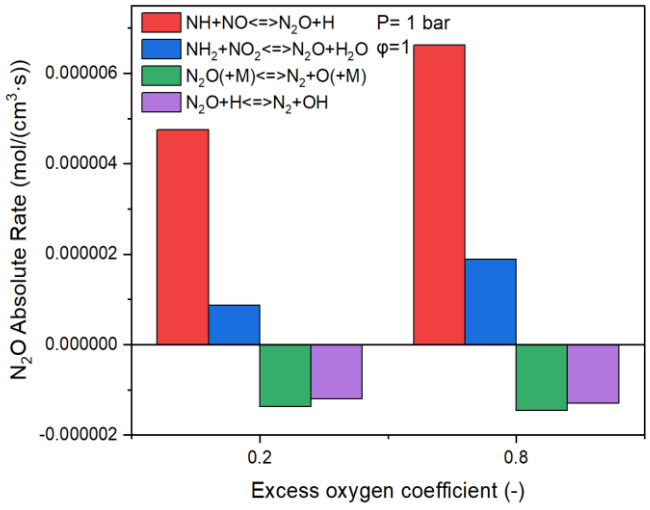

Figure 6.5.7: N_2O main chemical reactions of ammonia-oxygen at different oxygen ratios.

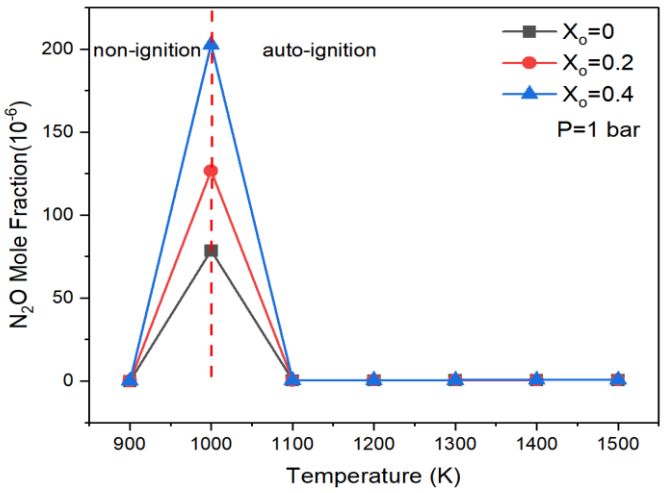

Figure 6.5.8: N_2O mole fraction of ammonia-oxygen at combustion boundary.

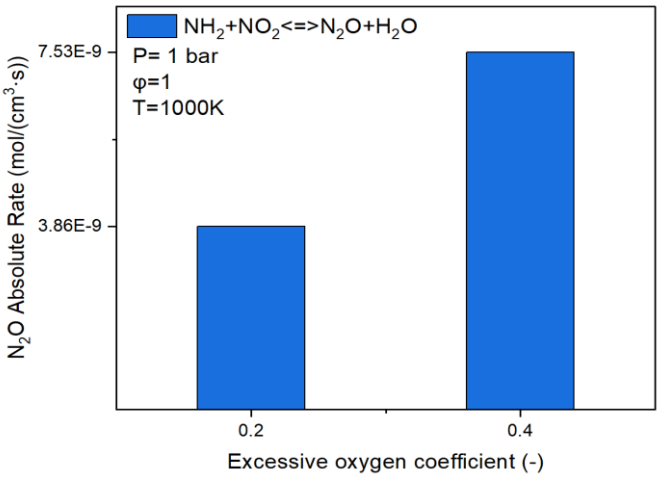

Figure 6.5.9: N_2O main chemical reaction of ammonia-oxygen at combustion boundary.

In summary, the simulation results provide an emission prediction of ammonia in oxygen-enriched and high-temperature conditions. The mechanism helps elucidate the complex interplay between various species and reactions in the production of NO, NO_2, and N_2O, with the experimental conditions serving to validate and refine the theoretical models.

6.6 Chapter Summary

In this chapter, the auto-ignition and emission characteristics of ammonia, ammonia-hydrogen, ammonia dissociation and ammonia-oxygen blending fuels have been predicted by CHEMKIN simulation. The main conclusions are shown as follow:

Four popular mechanisms have been selected to compare with experimentally measured ignition delay of pure ammonia fuel at a temperature from 1153 K to 1223 K. The experimental data show a good match when the temperature excess 1200 K, based on CEU and MEI mechanisms. As the temperature increases, the NO, NO_2 and N_2O, all increase. NO is the main combustion pollutant under high

temperature conditions. As the pressure increases, N_2O and NO_2 increase, while NO decreases. Although the NO concentration decreases, it remains the main component of pollutants. The reason is that the absolute rate of NO production from equation NO+OH+M=>HNO+M has increased. When the temperature is 1300 K, the NO decreases nearly 27% from 4580 to 3360 ppm, once 10% steam addition.

For ammonia-hydrogen mixture fuels, with the increase of temperature, NOx increases. The reactions absolute rate of HNO+H<=>NO+H_2, NO+H<=>NH+O and N+NO<=>N_2+O increase at a higher temperature. These absolute rates show that O and H are the main chemical groups. The ignition delay of ammonia dissociation fuel has an obvious decline once X_d =10%. And with the X_d increases, the auto-ignition temperature boundary extends. The N_2O has an obvious increment at the auto-ignition boundary and the NO is the main pollutant with the initial temperature increases. With the X_d increases, the auto-ignition boundary temperature decreases. Compared to the pure ammonia (X_d=0%), ammonia disassociation blending fuel has a lower N_2O emission at auto-ignition boundary. With the temperature increases, the NO increases because of HNO+H<=>NO+H_2. The ammonia dominant the pollutants when X_d<30% and the hydrogen dominant the pollutants when X_d>30%.

The NO and CO_2 are the main pollutants of ammonia-methane blending fuel. The NOx of ammonia/10%methane is higher than that of pure ammonia. In a lower temperature, the CO_2 is the main pollutant. However, the NO and CO_2 show a competition at high temperature. When the temperature beyond 1400K, the NO will be the main pollutant. The chemical reaction NH_2+NO_2=N_2O+H_2O is the main reaction at the combustion boundary (1100 K), so the N_2O is higher than NO_2.

Production of NO increases with increasing oxygen ratios. The primary chemical reactions contributing to NO generation are HNO+O_2<=>NO+HO and NH_2+NO<=>NNH+OH. An excess of O_2 promotes these forward reactions, leading to more NO production.

Chapter 7

Conclusion

7.1 Brief overview of the current work

To investigate the auto-ignition characteristics of ammonia and ammonia blending fuels, a combustion test system has been designed using a Controllable Active Thermo-Atmosphere burner. The flame enhancement methods, which include the addition of hydrogen, methane, and oxygen-enriched combustion, have been tested under various conditions. The main results show as follows:

The jet flame morphology, auto-ignition boundary, ignition delay, combustion stability mechanism and flame fluctuation have been explored and summarized. An auto-ignition boundary of pure ammonia has been reported. With the co-flow temperature increases, the flame brightness, flame length and flame area increase. A higher co-flow temperature lead to a lower ignition delay. Once the T_{cf}>1198 K, the decline trend of ignition delay decreases. At the high co-flow temperature, the physical gas mixing effect become the dominated factor on ignition delay because the temperature effect on chemical reaction has been reach to maximum. When the co-flow temperature increases to 1173 K, the flame core gradually concentrates, the fuzzy boundary disappears, the fire core is closer to the nozzle exit, flame core area increases and the core structure is close to a preliminary flame. Flame lifted height of the ammonia decreases with an augment in the co-flow temperature, and there is a critical temperature at 1198 K beyond which the effect of T_{cf} on H/d dramatically reduces. Lifted height data are satisfactorily fitted by a modified mixing-strain model, showing that the combustion is controlled by the large-scale mixing.

Compared to pure ammonia, ammonia-hydrogen flame has a higher flame brightness and a larger flame area. Ammonia flame with a low ratio of hydrogen shows an orange color, which is similar with pure ammonia. With the increasing of hydrogen percentages, the flame becomes brighter with a longer growing time. A higher combustion activity of the hydrogen is the reason why the beginning brightness is lower. With the co-flow temperature increases, the lifted height

gradually decreases, while the flame length, area, perimeter and brightness increase. The reason is that a stronger heat transfer, between the hot co-flow and the fuel jet flow, promotes the fuel auto-ignition. When the hydrogen ratio beyond 10%, the flame height growth slower, which means 10% hydrogen ratio is a most economic ratio to enhance the ammonia flame. Hydrogen addition has a stronger effect than T_{cf} increment on flame morphology. With the co-flow temperature increases, the ignition delay shows a downward trend due to the enhanced heat transfer. The lifted height is less sensitive to the co-flow temperature increment when T_{cf} excess the critical temperature (1073 K). It means the heat exchange efficiency has a limitation between co-flow and jet flow. Combustion stability analysis shows that the 20% hydrogen ratio is an optimal ratio for ammonia-hydrogen combustion stability. With co-flow temperature the increases, the ignition delay and lifted height of both ammonia-methane and ammonia-hydrogen mixture shows a downward trend, and both are lower than that of pure ammonia combustion. Hydrogen has a better ability than methane to shorten ignition delay. At a same jet pressure, the lifted height of ammonia-methane is significantly higher than that of ammonia-hydrogen, which means hydrogen has a stronger flame enhancement effect on ammonia flame.

The brightness of the ammonia-oxygen flame is brighter than that of pure ammonia, which represents the chemical reaction of combustion is more violent. With the increment of jet pressure from 1.6 to 2.5 bar, the flame area and length first increase than decreases with the jet pressures increases. The turning injection pressure is 1.9 bar. The jet pressure increments first enhance the combustion than hinder. The ammonia cannot form a flame in every oxygen coefficient when the co-flow temperature is lower than 1073 K. Once the temperature increases to 1123 K, a continuous and stable flame can be formed. When the oxygen coefficient excess to 1.2, the minimum temperature for forming a stable flame increases to 1148 K. With R_o increases, the ignition delay of the ammonia-oxygen flame first decreases then increases. When the R_o is close to 0.8, the ignition delay of ammonia-oxygen is minimal. With the T_{cf} increases, the flame lifted height gradually decreases. When the T_{cf} is higher than 1173 K, the downtrend of the lifted height is obviously slow down. The temperature sensibility become lower once the T_{cf}>1173 K. The flame lifted height of ammonia-oxygen combustion has an obvious fluctuation with time. The standard deviations of flame lifted heights in 200-260 ms have shown a lowest point when the with the R_o is equal to 0.8.

As the temperature increases, the NO, NO_2 and N_2O, all increase. NO is the main combustion pollutant under high temperature conditions. As the pressure increases, N_2O and NO_2 increase, while NO decreases. When the temperature is 1300 K, the NO decreases nearly 27% from 4580 to 3360 ppm, once 10% steam addition. The ignition delay has an obvious decline once the hydrogen ratio increases to 10%. Once the auto-ignition performance of ammonia-hydrogen tend to be stable until the hydrogen ratios increase to 20%, which means 20% is an optimal ratio to form a stable flame. For ammonia-hydrogen blending fuels, with the increase of temperature, NOx increases. The reactions absolute rate of HNO+H<=>NO+H_2, NO+H<=>NH+O and N+NO<=>N_2+O increases at a higher

temperature. These absolute rate show that O and H are the main chemical groups. H_2 can transform to H easier at higher temperature. The N_2O has an obvious increment at the auto-ignition boundary. Compared to the pure ammonia (X_d=0%), ammonia disassociation blending fuel has a lower N_2O emission at auto-ignition boundary. The ammonia dominant the pollutants when X_d<30% and the hydrogen dominant the pollutants when X_d>30%. The N_2O growth trend beyond 50% hydrogen ratios is higher than that of lower 50%. The NO and CO_2 is the main pollutant of ammonia-methane blending fuel. The NOx of ammonia/10% methane blending fuel is higher than that of pure ammonia. In a lower temperature, the CO_2 is the main pollutant. However, the NO and CO_2 show a competition at higher temperature. The chemical reaction $NH_2+NO_2=N_2O+H_2O$ is the main reaction at the combustion boundary (1100 K), so the N_2O is higher than NO_2. With the pressure increases, the chemical reactions $NO+HNO_2=NO_2+OH$ and $NH_2+NO_2=N_2O+H_2O$ are main reactions and absolute rate of two reactions increase at a higher environment pressure.

7.2 Key takeaways

As the discussion mentioned above, the application of ammonia and ammonia blending fuels is one of the important methods to decarbonize in transportation sector. Turbulent diffusion combustion and auto-ignition are main combustion modes in CI or HCCI engines which is widely used in the transportation sector. At present, research on CI engines based on ammonia fuel mainly focuses on ammonia-diesel dual fuels engine which has not yet reached the utilization of low-carbon fuels completely, like pure ammonia, ammonia-hydrogen and ammonia-natural gas. The application of zero-carbon fuels in CI engines needs further investigation.

Therefore, this work first started from pure ammonia fuel, explored the jet diffusion flame characteristics of pure ammonia fuel, defined the auto-ignition boundary of pure ammonia fuel at different temperatures and Reynolds number, and revealed the influence of different factors on the auto-ignition boundary and flame morphology of ammonia fuel; then, the combustion stability of pure ammonia fuel at different conditions were explored, and the critical temperature for stable combustion of ammonia fuel was determined.

Furthermore, the combustion efficiency of ammonia fuel was enhanced by controlling the fuel addition and oxidant increment. The auto-ignition characteristics of ammonia-hydrogen and ammonia-methane blending fuels have been studied at different mixture ratios, co-flow temperatures, and jet pressures. The results show that hydrogen and methane can extend the combustion boundary, reduce the minimum auto-ignition temperature of the mixture, improve the jet flame combustion stability, and significantly reduce the ignition delay of ammonia fuel. The combustion enhancement ability of hydrogen is greater than that of methane. Among them, 5% hydrogen can effectively improve ammonia combustion, and adding 20% hydrogen can significantly improve combustion stability. As part of the flame enhancement methods, the auto-ignition

characteristics of ammonia in oxygen-enriched condition have been investigated. The enhancement and dilution effects of oxygen on ammonia combustion have been characterized, and an optimal oxygen ratio has been suggested.

Since the addition of ammonia will significantly increase the generation of NOx, a preliminary prediction of the generation of pollutants has been made in this work. The pollutants of pure ammonia, ammonia-hydrogen, ammonia-methane and ammonia-oxygen have been predicted using CHEMKIN simulations at high environment temperatures and background pressures. The addition of hydrogen significantly increases the generation of NOx. In order to achieve more efficient and cleaner combustion of ammonia fuel, the hydrogen combustion enhancement effect and the pollutants deterioration from hydrogen addition need to make a balance by controlling the hydrogen ratio. The auto-ignition characteristics of ammonia dissociation fuel can make a guiding role for ammonia internal combustion engines. The potential of different DeNOx technologies for reducing NOx are investigated, among which the addition of water steam can effectively reduce NOx.

7.3 Recommendations and future works

In this work, the auto-ignition characteristics of ammonia and ammonia blending fuels have been investigated. The popular flame enhancement methods have been evaluated in a widely boundary conditions. Considering to the ammonia enhancement methods and emission control strategy under true automobile have not been defined. So, some further recommendations and future works have shown as follow:

The design and performance test of ammonia dissociation device.

The characteristics of ammonia-hydrogen and ammonia-oxygen coaxial flames in a high temperature co-flow condition.

3D simulation models of ammonia jet diffusion flames need to be built and validated.

The NOx reduction effect of steam on ammonia or ammonia-hydrogen blending fuels at high temperatures need to be a further investigation.

7.4 Dissemination works

List of journal publications:

Ji, M., Wu, Z., Ferrari, A., Vento, O., Shang, Q., Zhang, G., & Li, L. (2024). Experimental investigation on the turbulence flame autoignition characteristics of ammonia in a high-temperature co-flow. *Fuel*, 372, 132216.

Ji, M., Wu, Z., Ferrari, A., Fu, L., & Vento, O. (2023). Experimental investigation on gasoline-water mixture fuel impingement preparation method and spray characteristics with high injection temperatures and pressures. *Energies*, 16(16), 6026.

Wu, Z., Zhang, G., Wang, C., Jin, S., ***Ji, M.,*** Hu, C., & Shang, Q. (2024). Numerical investigation on the flame propagation process of ammonia-hydrogen

blends under engine-related conditions. *International Journal of Hydrogen Energy*, 60, 1041-1053.

Deng, J., Shang, Q., ***Ji, M.***, & Li, L. (2024). The formation process of the gaseous pollutant emissions in pure ammonia fueled engines with pre-chamber jet ignition. *International Journal of Hydrogen Energy*, 82, 544-558.

Hu, C., Wu, Z., Ferrari, A., ***Ji, M.,*** Deng, J., & Vento, O. (2024). Numerical Study on Internal Flow and Cavitation Characteristics of GDI Injectors for Different Nozzle Orifice Geometries. *Energies*, 17(16), 4114.

Experimental investigation on autoignition characteristics of ammonia-hydrogen in a high temperature co-flow. [processing]

Experimental investigation on autoignition characteristics of ammonia at oxygen-rich condition, based on a high temperature co-flow. [processing]

List of international conference

Ji, M., Wu, Z., Ferrari, A., Shang, Q., Zhang, G., Li, L., Deng, J., & Fu, L. (2023). Combustion and emission characteristics of ammonia jet flames, based on a controllable activated thermal atmosphere. *SAE Technical Paper*. No. 2023-01-1645.

Ji, M., Wu, Z., Ferrari, A.(2022). Study on real time gasoline-water mixture fuel preparation and spray characteristics based on impingement method. *22nd Annual Conference of Institute for Liquid Atomization and Spray Systems-Asia*.

Shang, Q., ***Ji, M.,*** Li, L., & Huang, Y. (2023). NOx emission characteristics of active pre-chamber jet ignition engine with ammonia hydrogen blending fuel. *SAE Technical Paper*. No. 2023-01-1629.

Shang, Q., ***Ji, M.,*** Li, L., & Deng, J. (2023). Numerical investigations on formation process of N_2O in ammonia-hydrogen fueled pre-chamber jet ignition engine. *SAE Technical Paper.* No. 2023-01-7023.

Conference Poster: ***Ji, M.,*** Wu, Z., Ferrari, A., Li, L., Deng, J. (2024). The autoignition characteristics of ammonia and ammonia mixture fuels at a high temperature co-flow. *CI'S 40th International Symposium.*

List of patents:

Chinese patents: A high efficiency combustion and near zero emission system for ammonia fuel engine based on internal combustion Rankin cycle and its application. [**Authorized**]

Chinese patents: A pollutant discharge and treatment system based on ammonia hydrogen fuel power system. [under-review]

Chinese patents: A ammonia dissociation device based on an ammonia hydrogen fuel engine. [under-review]

Chinese patents: A combustion and discharge system control method for an ammonia-hydrogen fuel internal combustion engine. [under-review]

References

[1] Zhou, M., & Hu, T. (2021, July). Analysis of carbon emission status under the carbon neutral target in China for Earth's atmospheric balance. IOP conference series: earth and environmental science, Vol. 804, No. 4, p. 042082.

[2] Li, Y., Wei, Y., & Dong, Z. (2020). Will China achieve its ambitious goal-Forecasting the CO_2 emission intensity of China towards 2030. *Energies*, 13(11), 2924.

[3] Zhang, Z. (2022). China's carbon market: development, evaluation, coordination of local and national carbon markets, and common prosperity. *Journal of Climate Finance*, 1, 100001.

[4] Luna, D.; Estevez, R. Optimization of Biodiesel and Biofuel Process. *Energies* 2022, 15, 5917.

[5] Ovaere, M., & Proost, S. (2022). Cost-effective reduction of fossil energy use in the European transport sector: An assessment of the Fit for 55 Package. *Energy Policy*, 168, 113085.

[6] Cifuentes-Faura, J. (2022). European Union policies and their role in combating climate change over the years. Air Quality, *Atmosphere & Health*, 15(8), 1333-1340.

[7] Axsen, J., Bhardwaj, C., & Crawford, C. (2022). Comparing policy pathways to achieve 100% zero-emissions vehicle sales by 2035. *Transportation Research Part D: Transport and Environment*, 112, 103488.

[8] Zhou, W., Hagos, D. A., Stikbakke, S., Huang, L., Cheng, X., & Onstein, E. (2022). Assessment of the impacts of different policy instruments on achieving the deep decarbonization targets of island energy systems in Norway–The case of Hinnøya. *Energy*, 246, 123249.

[9] Kosai, S., Hanqing, L., Zhang, Z., Matsubae, K., & Yamasue, E. (2022). Multi-regional land disturbances induced by mineral use in a product-based approach: A case study of gasoline, hybrid, battery electric and fuel cell vehicle production in Japan. *Resources, Conservation and Recycling*, 178, 106093.

[10] Tanç, B.; Arat, H.T.; Conker, Ç.; Baltacioglu, E.; Aydin, K. (2020). Energy distribution analyses of an additional traction battery on hydrogen fuel cell hybrid electric vehicle. *Int J Hydrogen Energy*, 45, 26344-26356.

[11] Samsun, R. C., Rex, M., Stolten, D., & Antoni, L. (2021). *Deployment status of fuel cells in road transport: 2021 update*, No. FZJ-2021-03033.

[12] Dias, V., Pochet, M., Contino, F., & Jeanmart, H. (2020). Energy and economic costs of chemical storage. *Frontiers in mechanical engineering*, 6, 21.

[13] Wang, K., Smith, D., & Zheng, Y. (2018). Electron-driven heterogeneous catalytic synthesis of ammonia: Current states and perspective. *Carbon Resources Conversion*, 1(1), 2-31.

[14] Saygin, D., Blanco, H., Boshell, F., Cordonnier, J., Rouwenhorst, K., Lathwal, P., & Gielen, D. (2023). Ammonia Production from Clean Hydrogen and the Implications for Global Natural Gas Demand. *Sustainability*, 15(2), 1623.

[15] Chehade, G., & Dincer, I. (2021). Progress in green ammonia production as potential carbon-free fuel. *Fuel*, 299, 120845.

[16] Hiroaki Tanigawa., & Chugoku Electric Test Results of the Ammonia Mixed Combustion at Mizushima Power Station Unit No.2 and Related Patent Applications. (2018). *NH_3 Fuel Conference 2018*.

[17] Ito, S., Uchida, M., Suda, T., & Fujimori, T. (2022). Demonstration Tests of Ammonia/Natural Gas Co-firing Power Generation with a 2-MW-Class Gas Turbine. *CO_2 Free Ammonia as an Energy Carrier: Japan's Insights*, 515-522, Singapore.

[18] Nose, M., Araki, H., Senba, N., Furuichi, H., & Tanimura, S. (2022). Development of ammonia utilization technology for large gas turbines for power generation. *CO_2 Free Ammonia as an Energy Carrier: Japan's Insights*, 523-535, Singapore.

[19] Iki, N. (2022). Demonstration of ammonia fuel with small gas turbines. *CO_2 Free Ammonia as an Energy Carrier: Japan's Insights*, pp. 487-499, Singapore.

[20] Guidelines for Ships Using Ammonia as Fuels. https://www.crclass.org/wp-content/uploads/2023/02/GD-AFS-202302.pdf.

[21] The AmVeh: an ammonia fueled car from South Korea. https://nh3fuelassociation.org/2013/06/20/the-amveh-an-ammonia-fueled-car-from-south-korea.

[22] Khaksar, S. A. N., Rahimpour, H. R., & Rahimpour, M. R. (2024). Ammonia storage and transportation. Progresses in Ammonia: Science, *Technology and Membranes*, 251-270.

[23] Gong W, Willi M L. Power system having an ammonia fueled engine: U.S. Patent Application 12/219,418. 2010-1-28.

[24] Kane, S. P., Zarling, D., & Northrop, W. F. (2019, October). Thermochemical and sensible energy recuperation using thermally-integrated reactor and diesel-ammonia dual fueling strategy. *Internal Combustion Engine Division Fall Technical Conference*, Vol. 59346, p. V001T02A011.

[25] Solutions, M. E. (2019). Engineering the Future Future in the: Two-Stroke Green-Ammonia Engine. *MAN Energy Solutions: Augsburg*, Germany.

[26] Dimitriou, P., & Javaid, R. (2020). A review of ammonia as a compression ignition engine fuel. *International Journal of Hydrogen Energy*, 45(11), 7098-7118.

[27] The hydrogen market boosted by ammonia: feed, standards & balancing https://www.ammoniaenergy.org/paper/the-hydrogen-market-boosted-by-ammonia-feed-standards-balancing

[28] Joung, T. H., Kang, S. G., Lee, J. K., & Ahn, J. (2020). The IMO initial strategy for reducing Greenhouse Gas (GHG) emissions, and its follow-up actions towards 2050. *Journal of International Maritime Safety, Environmental Affairs, and Shipping*, 4(1), 1-7.

[29] https://fortescue.com/news-and-media/news/2022/10/04/fortescue-future-industries-and-deutsche-bahn-partner-on-green-fuel-to-power-carbon-free-internal-combustion-engine

[30] MacFarlane, D. R., Cherepanov, P. V., Choi, J., Suryanto, B. H., Hodgetts, R. Y., Bakker, J. M., & Simonov, A. N. (2020). A roadmap to the ammonia economy. *Joule*, 4(6), 1186-1205.

[31] Henry, W. (1809). XXVI. Experiments on ammonia, and an account of a new method of analyzing it, by combustion with oxygen and other gases; in a letter to Humphry Davy, Esq. Sec. RS &c. from William Henry, MD, FRSVP of the Lit and Phil Society, and physician to the infirmary, at Manchester. *Philosophical Transactions of the Royal Society of London*, (99), 430-449.

[32] Koch, E. (1945). Ammonia–a fuel for motor buses. *J. Inst. Pet*, 31, 213.

[33] Valera-Medina, A., Xiao, H., Owen-Jones, M., David, W. I., & Bowen, P. J. (2018). Ammonia for power. *Progress in Energy and combustion science*, 69, 63-102.

[34] Liu, S., Lin, Z., Zhang, H., Lei, N., Qi, Y., & Wang, Z. (2023). Impact of ammonia addition on knock resistance and combustion performance in a gasoline engine with high compression ratio. *Energy*, 262, 125458.

[35] Zhou, L., Zhong, L., Liu, Z., & Wei, H. (2023). Toward highly-efficient combustion of ammonia-hydrogen engine: Prechamber turbulent jet ignition. *Fuel*, 352, 129009.

[36] Starkman, E. S., James, G. E., & Newhall, H. K. (1968). Ammonia as a diesel engine fuel: theory and application. *SAE Transactions*, 3193-3212.

[37] Lhuillier C, Brequigny P, Contino F, Mounaïm-Rousselle C. (2020). Experimental study on ammonia-hydrogen/air combustion in spark ignition engine conditions. *Fuel*, 269:117448.

[38] Mounaïm-Rousselle, C., Mercier, A., Brequigny, P., Dumand, C., Bouriot, J., & Houillé, S. (2022). Performance of ammonia fuel in a spark assisted compression Ignition engine. *International Journal of Engine Research*, 23(5), 781-792.

[39] Frigo, S., & Gentili, R. (2013). Analysis of the behaviour of a 4-stroke Si engine fuelled with ammonia and hydrogen. *International Journal of Hydrogen Energy*, 38(3), 1607-1615.

[40] Mørch, C. S., Bjerre, A., Gøttrup, M. P., Sorenson, S. C., & Schramm, J. (2011). Ammonia-hydrogen mixtures in an SI-engine: Engine performance and analysis of a proposed fuel system. *Fuel*, 90(2), 854-864.

[41] Mounaïm-Rousselle, C., Bréquigny, P., Dumand, C., & Houillé, S. (2021). Operating limits for ammonia fuel spark-ignition engine. *Energies*, 14(14), 4141.

[42] Dinesh, M. H., Pandey, J. K., & Kumar, G. N. (2022). Study of performance, combustion, and NOx emission behavior of an SI engine fuelled with ammonia-hydrogen blends at various compression ratio. *International Journal of Hydrogen Energy*, 47(60), 25391-25403.

[43] Mei, B., Zhang, J., Shi, X., Xi, Z., & Li, Y. (2021). Enhancement of ammonia combustion with partial fuel cracking strategy: Laminar flame propagation and kinetic modeling investigation of $NH_3/H_2/N_2$/air mixtures up to 10 atm. *Combustion and flame*, 231, 111472.

[44] Gill, S. S., Chatha, G. S., Tsolakis, A., Golunski, S. E., & York, A. P. E. (2012). Assessing the effects of partially decarbonising a diesel engine by co-fuelling with dissociated ammonia. *International journal of hydrogen energy*, 37(7), 6074-6083.

[45] Comotti, M., & Frigo, S. (2015). Hydrogen generation system for ammonia–hydrogen fuelled internal combustion engines. *International Journal of Hydrogen Energy*, 40(33), 10673-10686.

[46] Ryu, K., Zacharakis-Jutz, G. E., & Kong, S. C. (2014). Performance enhancement of ammonia-fueled engine by using dissociation catalyst for hydrogen generation. *International journal of hydrogen energy*, 39(5), 2390-2398.

[47] Swift, E., Kane, S., & Northrop, W. F. (2022, October). Operating range and emissions from ammonia-hydrogen mixtures in spark-ignited engines. *Internal Combustion Engine Division Fall Technical Conference*, Vol. 86540, p. V001T02A013.

[48] Mercier, A., Mounaïm-Rousselle, C., Brequigny, P., Bouriot, J., & Dumand, C. (2022). Improvement of SI engine combustion with ammonia as fuel: Effect of ammonia dissociation prior to combustion. *Fuel Communications*, 11, 100058.

[49] Benés, M., Pozo, G., Abián, M., Millera, A., Bilbao, R., & Alzueta, M. U. (2021). Experimental study of the pyrolysis of NH_3 under flow reactor conditions. *Energy & fuels*, 35(9), 7193-7200.

[50] Zhou, L., Zhong, L., Liu, Z., & Wei, H. (2023). Toward highly-efficient combustion of ammonia-hydrogen engine: Prechamber turbulent jet ignition. *Fuel*, 352, 129009.

[51] Li, T., Zhou, X., Wang, N., Wang, X., Chen, R., Li, S., & Yi, P. (2022). A comparison between low-and high-pressure injection dual-fuel modes of diesel-pilot-ignition ammonia combustion engines. *Journal of the Energy Institute*, 102, 362-373.

[52] Reiter, A. J., & Kong, S. C. (2008). Demonstration of compression-ignition engine combustion using ammonia in reducing greenhouse gas emissions. *Energy & Fuels*, 22(5), 2963-2971.

[53] Şahin, Z., Akcanca, İ. Z., & Durgun, O. (2018). Experimental investigation of the effects of ammonia solution (NH_3OH) on engine performance and exhaust emissions of a small diesel engine. *Fuel*, 214, 330-341.

[54] Nadimi, E., Przybyła, G., Lewandowski, M. T., & Adamczyk, W. (2023). Effects of ammonia on combustion, emissions, and performance of the

ammonia/diesel dual-fuel compression ignition engine. *Journal of the Energy Institute*, 107, 101158.

[55] Li, M., He, X., Hashemi, H., Glarborg, P., Lowe, V. M., Marshall, P., & Shu, B. (2022). An experimental and modeling study on auto-ignition kinetics of ammonia/methanol mixtures at intermediate temperature and high pressure. *Combustion and Flame*, 242, 112160.

[56] Li, X., Ma, Z., Jin, Y., Wang, X., Xi, Z., Hu, S., & Chu, X. (2023). Effect of methanol blending on the high-temperature auto-ignition of ammonia: An experimental and modeling study. *Fuel*, 339, 126911.

[57] Lu, M., Dong, D., Wei, F., Long, W., Wang, Y., Cong, L., & Wang, P. (2023). Chemical mechanism of ammonia-methanol combustion and chemical reaction kinetics analysis for different methanol blends. *Fuel*, 341, 127697.

[58] Xu, H., Wang, J., Zhang, C., Dai, L., He, Z., & Wang, Q. (2022). Numerical study on laminar burning velocity of ammonia flame with methanol addition. *International Journal of Hydrogen Energy*, 47(65), 28152-28164.

[59] Li, M., Zhu, D., He, X., Moshammer, K., Fernandes, R., & Shu, B. (2023). Experimental and kinetic modeling study on auto-ignition properties of ammonia/ethanol blends at intermediate temperatures and high pressures. *Proceedings of the Combustion Institute*, 39(1), 511-519.

[60] Gross, C. W., & Kong, S. C. (2013). Performance characteristics of a compression-ignition engine using direct-injection ammonia-DME mixtures. *Fuel*, 103, 1069-1079.

[61] He, X., Shu, B., Nascimento, D., Moshammer, K., Costa, M., & Fernandes, R. X. (2019). Auto-ignition kinetics of ammonia and ammonia-hydrogen mixtures at intermediate temperatures and high pressures. *Combustion and Flame*, 206, 189-200.

[62] Shu, B., He, X., Ramos, C. F., Fernandes, R. X., & Costa, M. (2021). Experimental and modeling study on the auto-ignition properties of Ammonia-methane mixtures at elevated pressures. *Proceedings of the Combustion Institute*, 38(1), 261-268.

[63] Shu, B., Vallabhuni, S. K., He, X., Issayev, G., Moshammer, K., Farooq, A., & Fernandes, R. X. (2019). A shock tube and modeling study on the autoignition properties of ammonia at intermediate temperatures. *Proceedings of the Combustion Institute*, 37(1), 205-211.

[64] Pochet, M., Dias, V., Moreau, B., Foucher, F., Jeanmart, H., & Contino, F. (2019). Experimental and numerical study, under LTC conditions, of ammonia ignition delay with and without hydrogen addition. *Proceedings of the Combustion Institute*, 37(1), 621-629.

[65] Dai, L., Gersen, S., Glarborg, P., Levinsky, H., & Mokhov, A. (2020). Experimental and numerical analysis of the autoignition behavior of NH_3 and NH_3/H_2 mixtures at high pressure. *Combustion and flame*, 215, 134-144.

[66] Liao, W., Chu, Z., Wang, Y., Li, S., & Yang, B. (2023). An experimental and modeling study on auto-ignition of ammonia in an RCM with N_2O and H_2 addition. *Proceedings of the Combustion Institute*, 39(4), 4377-4385.

[67] Liao, W., Wang, Y., Chu, Z., Tao, C., & Yang, B. (2023). Chemical insights into the two-stage ignition behavior of NH_3/H_2 mixtures in an RCM. *Combustion and Flame*, 256, 112985.

[68] Drummond, L. J. (1972). High temperature oxidation of ammonia. *Combustion Science and Technology*, 5(1), 175-182.

[69] Fujii, N., Miyama, H., Koshi, M., & Asaba, T. (1981, January). Kinetics of ammonia oxidation in shock waves. *Symposium (International) on Combustion*, Vol. 18, No. 1, pp. 873-883.

[70] Salimian, S., Hanson, R. K., & Kruger, C. H. (1984). Ammonia oxidation in shock-heated NH_3/N_2O/Ar mixtures. *Combustion and flame*, 56(1), 83-95.

[71] Soloukhin, R. I. (1971, January). High-temperature oxidation of ammonia, carbon monoxide, and methane by nitrous oxide in shock waves. *Symposium (International) on Combustion*, Vol. 13, No. 1, pp. 121-128.

[72] Chen, J., Jiang, X., Qin, X., & Huang, Z. (2021). Effect of hydrogen blending on the high temperature auto-ignition of ammonia at elevated pressure. *Fuel*, 287, 119563.

[73] Alturaifi, S. A., Mathieu, O., & Petersen, E. L. (2023). A shock-tube study of NH_3 and NH_3/H_2 oxidation using laser absorption of NH_3 and H_2O. *Proceedings of the Combustion Institute*, 39(1), 233-241.

[74] Shu, B., Vallabhuni, S. K., He, X., Issayev, G., Moshammer, K., Farooq, A., & Fernandes, R. X. (2019). A shock tube and modeling study on the autoignition properties of ammonia at intermediate temperatures. *Proceedings of the Combustion Institute*, 37(1), 205-211.

[75] Mathieu, O., & Petersen, E. L. (2015). Experimental and modeling study on the high-temperature oxidation of Ammonia and related NOx chemistry. *Combustion and flame*, 162(3), 554-570.

[76] Hayakawa, A., Goto, T., Mimoto, R., Arakawa, Y., Kudo, T., & Kobayashi, H. (2015). Laminar burning velocity and Markstein length of ammonia/air premixed flames at various pressures. *Fuel*, 159, 98-106.

[77] Hayakawa, A., Goto, T., Mimoto, R., Kudo, T., & Kobayashi, H. (2015). NO formation/reduction mechanisms of ammonia/air premixed flames at various equivalence ratios and pressures. *Mechanical Engineering Journal*, 2(1), 14-00402.

[78] The identification of molecular spectra. *International Journal of Mass Spectrometry and Ion Processes*, 24(4), 472.

[79] Lhuillier, C., Brequigny, P., Lamoureux, N., Contino, F., & Mounaïm-Rousselle, C. (2020). Experimental investigation on laminar burning velocities of ammonia-hydrogen/air mixtures at elevated temperatures. *Fuel*, 263, 116653.

[80] Kumar, P., & Meyer, T. R. (2013). Experimental and modeling study of chemical-kinetics mechanisms for H_2-NH_3-air mixtures in laminar premixed jet flames. *Fuel*, 108, 166-176.

[81] Rocha, R. C., Costa, M., & Bai, X. S. (2019). Chemical kinetic modelling of ammonia-hydrogen/air ignition, premixed flame propagation and NO emission. *Fuel*, 246, 24-33.

[82] Long, Y., Li, G., Zhang, Z., Wei, W., & Liang, J. (2022). Hydrogen-rich gas generation via the exhaust gas-fuel reformer for the marine LNG engine. *International Journal of Hydrogen Energy*, 47(32), 14674-14686.

[83] Yao, S., Li, C., & Wei, Y. (2023). Design and optimization of a zero carbon emission system integrated with the utilization of marine engine waste heat and LNG cold energy for LNG-powered ships. *Applied Thermal Engineering*, 231, 120976.

[84] Kochunni, S. K., & Chowdhury, K. (2022). Concept and evaluation of energy-efficient boil-off gas reliquefiers in LNG carrier ships propelled by dual-fuel engines. *Cryogenics*, 123, 103453.

[85] Tang, Q., Fu, J., Liu, J., Zhou, F., Yuan, Z., & Xu, Z. (2016). Performance improvement of liquefied natural gas (LNG) engine through intake air supply. *Applied Thermal Engineering*, 103, 1351-1361.

[86] Zeng, K., Huang, Z., Liu, B., Liu, L., Jiang, D., Ren, Y., & Wang, J. (2006). Combustion characteristics of a direct-injection natural gas engine under various fuel injection timings. *Applied thermal engineering*, 26(8-9), 806-813.

[87] Olsen, D. B., & Lisowski, J. M. (2009). Prechamber NOx formation in low BMEP 2-stroke cycle natural gas engines. *Applied Thermal Engineering*, 29(4), 687-694.

[88] Jahirul, M. I., Masjuki, H. H., Saidur, R., Kalam, M. A., Jayed, M. H., & Wazed, M. A. (2010). Comparative engine performance and emission analysis of CNG and gasoline in a retrofitted car engine. *Applied Thermal Engineering*, 30(14-15), 2219-2226.

[89] Graham, L. A., Rideout, G., Rosenblatt, D., & Hendren, J. (2008). Greenhouse gas emissions from heavy-duty vehicles. *Atmospheric Environment*, 42(19), 4665-4681.

[90] GAS, U. (2012). NATURAL GAS FOR VEHICLES (NGV).

[91] Kumar, S., Kwon, H. T., Choi, K. H., Lim, W., Cho, J. H., Tak, K., & Moon, I. (2011). LNG: An eco-friendly cryogenic fuel for sustainable developme nt. *Applied energy*, 88(12), 4264-4273.

[92] Wang, S., Wang, Z., & Roberts, W. L. (2024). Measurements and simulation on effects of elevated pressure and strain rate on NOx emissions in laminar premixed NH_3/CH_4/air and NH_3/H_2/air flames. *Fuel*, 357, 130036.

[93] Shu, T., Xue, Y., Zhou, Z., & Ren, Z. (2021). An experimental study of laminar Ammonia-methane/air premixed flames using expanding spherical flames. *Fuel*, 290, 120003.

[94] Xiao, H., Lai, S., Valera-Medina, A., Li, J., Liu, J., & Fu, H. (2020). Study on counterflow premixed flames using high concentration ammonia mixed with methane. *Fuel*, 275, 117902.

[95] Xiao, H., Valera-Medina, A., & Bowen, P. J. (2017). Study on premixed combustion characteristics of co-firing Ammonia-methane fuels. *Energy*, 140, 125-135.

[96] Zhu, X., Khateeb, A. A., Roberts, W. L., & Guiberti, T. F. (2021). Chemiluminescence signature of premixed ammonia-methane-air flames. *Combustion and Flame*, 231, 111508.

[97] Dai, L., Gersen, S., Glarborg, P., Mokhov, A., & Levinsky, H. (2020). Autoignition studies of NH_3/CH_4 mixtures at high pressure. *Combustion and Flame*, 218, 19-26.

[98] Kurata, O., Iki, N., Matsunuma, T., Inoue, T., Tsujimura, T., Furutani, H., & Hayakawa, A. (2017). Performances and emission characteristics of NH_3-air and NH_3CH_4-air combustion gas-turbine power generations. *Proceedings of the Combustion Institute*, 36(3), 3351-3359.

[99] Valera-Medina, A., & Bowen, P. J. (2017). Study on premixed combustion characteristics of co-firing Ammonia-methane fuels. *Energy*, 140, 125-135.

[100] Vinod, K. N., & Fang, T. (2023). Experimental characterization of spark ignited ammonia combustion under elevated oxygen concentrations. *Proceedings of the Combustion Institute*, 39(4), 4319-4326.

[101] Chen, Y., Zhang, B., Su, Y., Sui, C., & Zhang, J. (2022). Effect and mechanism of combustion enhancement and emission reduction for non-premixed pure ammonia combustion based on fuel preheating. *Fuel*, 308, 122017.

[102] Zeldovich, Y. A., Frank-Kamenetskii, D., & Sadovnikov, P. (1947). *Oxidati on of nitrogen in combustion*. Publishing House of the Acad of Sciences of USSR.

[103] Kobayashi, H., Hayakawa, A., Somarathne, K. K. A., & Okafor, E. C. (2019). Science and technology of ammonia combustion. *Proceedings of the combustion institute*, 37(1), 109-133.

[104] Miller, J. A., Smooke, M. D., Green, R. M., & Kee, R. J. (1983). Kinetic modeling of the oxidation of ammonia in flames. *Combustion Science and Technology*, 34(1-6), 149-176.

[105] Dean, A. M., Chou, M. S., & Stern, D. (1984). Kinetics of rich ammonia flames. *International journal of chemical kinetics*, 16(6), 633-653.

[106] Salimian, S., Hanson, R. K., & Kruger, C. H. (1984). High temperature study of the reactions of O and OH with NH_3. *International journal of chemical kinetics*, 16(6), 725-739.

[107] Cheng, X., Li, Y., Xu, Y., Liu, Y., & Wang, B. (2022). Study of effects of ammonia addition on soot formation characteristics in n-heptane co-flow laminar diffusion flames. *Combustion and Flame*, 235, 111683.

[108] Somarathne, K. D. K. A., Hatakeyama, S., Hayakawa, A., & Kobayashi, H. (2017). Numerical study of a low emission gas turbine like combustor for turbulent ammonia/air premixed swirl flames with a secondary air injection at high pressure. *International Journal of Hydrogen Energy*, 42(44), 27388-27399.

[109] García-Ruiz, P., Uruén, M., Abián, M., & Alzueta, M. U. (2023). High pressure ammonia oxidation in a flow reactor. *Fuel*, 348, 128302.

[110] Liu, L., Tan, F., Wu, Z., & Wang, Y. (2024). Combining genetic algorithm and deep learning to optimize a chemical kinetic mechanism of ammonia under high pressure. *Fuel*, 360, 130508.

[111] Alvarez, L. F., Shaffer, J., Dumitrescu, C. E., & Askari, O. (2024). Laminar burning velocity of ammonia/air mixtures at high pressures. *Fuel*, 363, 130986.

[112] Peng, Y., Ranjan, D., & Sun, W. (2023). A shock tube study of fuel concentration effect on high-pressure autoignition delay of ammonia. *Applications in Energy and Combustion Science*, 16, 100202.

[113] Scharl, V., Lackovic, T., & Sattelmayer, T. (2023). Characterization of ammonia spray combustion and mixture formation under high-pressure, direct injection conditions. *Fuel*, 333, 126454.

[114] Wang, S., Zhu, G., Niu, Y., & Ding, Y. (2021). Experimental and kinetic studies on NO emission during pulverized coal preheating combustion process with high preheating temperature. *Journal of the Energy Institute*, 97, 180-186.

[115] Glarborg, P., Jensen, A. D., & Johnsson, J. E. (2003). Fuel nitrogen conversion in solid fuel fired systems. *Progress in energy and combustion science*, 29(2), 89-113.

[116] Ouyang, Z., Song, W., Liu, J., Zhu, J., Man, C., Zhu, S., & Ding, H. (2021). Experimental study on NOx emissions of pulverized coal combustion preheated by a 2MW novel self-sustained preheating combustor. *Fuel*, 294, 120538.

[117] Chen, Y., Zhang, B., Su, Y., Sui, C., & Zhang, J. (2022). Effect and mechanism of combustion enhancement and emission reduction for non-premixed pure ammonia combustion based on fuel preheating. *Fuel*, 308, 122017.

[118] Pugh, D., Valera-Medina, A., Bowen, P., Giles, A., Goktepe, B., Runyon, J., & Marsh, R. (2021). Emissions performance of staged premixed and diffusion combustor concepts for an NH_3/air flame with and without reactant humidification. *Journal of Engineering for Gas Turbines and Power*, 143(5), 051012.

[119] Božo, M. G., Vigueras-Zuniga, M. O., Buffi, M., Seljak, T., & Valera-Medina, A. (2019). Fuel rich ammonia-hydrogen injection for humidified gas turbines. *Applied energy*, 251, 113334.

[120] Mashruk, S., Xiao, H., & Valera-Medina, A. (2021). Rich-Quench-Lean model comparison for the clean use of humidified ammonia-hydrogen combustion systems. *International Journal of Hydrogen Energy*, 46(5), 4472-4484.

[121] Maheshwari, M., & Singh, O. (2019). Comparative evaluation of different combined cycle configurations having simple gas turbine, steam turbine and ammonia water turbine. *Energy*, 168, 1217-1236.

[122] Ariemma, G. B., Sabia, P., Sorrentino, G., Bozza, P., De Joannon, M., & Ragucci, R. (2021). Influence of water addition on MILD ammonia combustion performances and emissions. *Proceedings of the combustion Institute*, 38(4), 5147-5154.

[123] Javed, M. T., Irfan, N., & Gibbs, B. M. (2007). Control of combustion-generated nitrogen oxides by selective non-catalytic reduction. *Journal of environmental management*, 83(3), 251-289.

[124] Choe, J., Sun, W., Ombrello, T., & Carter, C. (2021). Plasma assisted ammonia combustion: Simultaneous NOx reduction and flame enhancement. *Combustion and flame*, 228, 430-432.

[125] Lin, Q., Jiang, Y., Liu, C., Chen, L., Zhang, W., Ding, J., & Li, J. (2022). Controllable NO emission and high flame performance of ammonia combustion assisted by non-equilibrium plasma. *Fuel*, 319, 123818.

[126] Shioyoke, A., Hayashi, J., Murai, R., Nakatsuka, N., & Akamatsu, F. (2018). Numerical investigation on effects of nonequilibrium plasma on laminar burning velocity of ammonia flame. *Energy & fuels*, 32(3), 3824-3832.

[127] Chen, J., Feng, G., Fan, W., & Guo, H. (2023). Stabilization of air coflowed ammonia jet flame at elevated ambient temperatures. *International Journal of Hydrogen Energy*, 48(62), 24127-24138.

[128] Colson, S., Kuhni, M., Galizzi, C., Escudie, D., & Kobayashi, H. (2022). Study of the combined effect of ammonia addition and air coflow velocity on a non-premixed methane jet flame stabilization. *Combustion Science and Technology*, 194(9), 1747-1767.

[129] Li, S., Qian, W., Liu, H., Liu, G., & Zhu, M. (2021). Autoignition and flame lift-off behavior of a fuel jet mixing with turbulent hot air coflow. *Proceedings of the Combustion Institute*, 38(4), 6385-6392.

[130] Liu, G., & Li, S. (2022). Lift-off height of autoignited jet flame in hot air coflow with different O_2 contents. *Combustion and Flame*, 242, 112144.

[131] Kolb, M., Ahrens, D., Hirsch, C., & Sattelmayer, T. (2016). A model for predicting the lift-off height of premixed jets in vitiated cross flow. *Journal of Engineering for Gas Turbines and Power*, 138(8), 081901.

[132] Liu, G., & Wu, Y. (2024). Lift-off height model of hydrogen autoignited flame in turbulent hot air coflow. *International Journal of Hydrogen Energy*, 49, 401-412.

[133] Liu, G., Li, S., & Wu, Y. (2024). Effects of coflow velocity on the lift-off characteristics of autoignited jet flame in hot air coflow. *Combustion and Flame*, 259, 113124.

[134] Førby, N., Thomsen, T. B., Cordtz, R. F., Bræstrup, F., & Schramm, J. (2023). Ignition and combustion study of premixed ammonia using GDI pilot injection in CI engine. *Fuel*, 331, 125768.

[135] Dimitriou, P., & Javaid, R. (2020). A review of ammonia as a compression ignition engine fuel. *International Journal of Hydrogen Energy*, 45(11), 7098-7118.

[136] Xia, Y., Hashimoto, G., Hadi, K., Hashimoto, N., Hayakawa, A., Kobayashi, H., & Fujita, O. (2020). Turbulent burning velocity of Ammonia-oxygen/nitrogen premixed flame in O_2-enriched air condition. *Fuel*, 268, 117383.

[137] Glarborg, P., Miller, J. A., Ruscic, B., & Klippenstein, S. J. (2018). Modeling nitrogen chemistry in combustion. *Progress in energy and combustion science*, 67, 31-68.

[138] Mendiara, T., & Glarborg, P. (2009). Ammonia chemistry in oxy-fuel combustion of methane. *Combustion and Flame*, 156(10), 1937-1949.

[139] Glarborg, P., Hashemi, H., Cheskis, S., & Jasper, A. W. (2021). On the rate constant for NH_2+ HO_2 and third-body collision efficiencies for NH_2+ H (+M) and NH_2+ NH_2 (+ M). *The Journal of Physical Chemistry A*, 125(7), 1505-1516.

[140] Stagni, A., Cavallotti, C., Arunthanayothin, S., Song, Y., Herbinet, O., Battin-Leclerc, F., & Faravelli, T. (2020). An experimental, theoretical and kinetic-modeling study of the gas-phase oxidation of ammonia. *Reaction Chemistry & Engineering*, 5(4), 696-711.

[141] Arunthanayothin, S., Stagni, A., Song, Y., Herbinet, O., Faravelli, T., & Battin-Leclerc, F. (2021). Ammonia–methane interaction in jet-stirred and flow reactors: An experimental and kinetic modeling study. *Proceedings of the Combustion Institute*, 38(1), 345-353.

[142] Shu, B., Vallabhuni, S. K., He, X., Issayev, G., Moshammer, K., Farooq, A., & Fernandes, R. X. (2019). A shock tube and modeling study on the autoignition properties of ammonia at intermediate temperatures. *Proceedings of the Combustion Institute*, 37(1), 205-211.

[143] Wang, Z., Han, X., He, Y., Zhu, R., Zhu, Y., Zhou, Z., & Cen, K. (2021). Experimental and kinetic study on the laminar burning velocities of NH_3 mixing with CH_3OH and C_2H_5OH in premixed flames. *Combustion and Flame*, 229, 111392.

[144] Wang, S., Wang, Z., Chen, C., Elbaz, A. M., Sun, Z., & Roberts, W. L. (2022). Applying heat flux method to laminar burning velocity measurements of NH_3/CH_4/air at elevated pressures and kinetic modeling study. *Combustion and Flame*, 236, 111788.

[145] Han, X., Wang, Z., He, Y., Zhu, Y., & Cen, K. (2020). Experimental and kinetic modeling study of laminar burning velocities of NH_3/syngas/air premixed flames. *Combustion and Flame*, 213, 1-13.

[146] Vandooren, J., Bian, J., & Van Tiggelen, P. J. (1994). Comparison of experimental and calculated structures of an ammonia nitric oxide flame. Importance of the NH_2+NO reaction. Combustion and flame, 98(4), 402-410.

[147] Jiang, Y., Gruber, A., Seshadri, K., & Williams, F. (2020). An updated short chemical-kinetic nitrogen mechanism for carbon-free combustion applications. *International Journal of Energy Research*, 44(2), 795-810.

[148] Okafor, E. C., Naito, Y., Colson, S., Ichikawa, A., Kudo, T., Hayakawa, A., & Kobayashi, H. (2018). Experimental and numerical study of the laminar burning velocity of CH_4-NH_3-air premixed flames. *Combustion and flame*, 187, 185-198.

[149] Okafor, E. C., Naito, Y., Colson, S., Ichikawa, A., Kudo, T., Hayakawa, A., & Kobayashi, H. (2019). Measurement and modelling of the laminar

burning velocity of methane-ammonia-air flames at high pressures using a reduced reaction mechanism. *Combustion and Flame*, 204, 162-175.

[150] Dagaut, P., Glarborg, P., & Alzueta, M. U. (2008). The oxidation of hydrogen cyanide and related chemistry. *Progress in Energy and Combustion Science*, 34(1), 1-46.

[151] Otomo, J., Koshi, M., Mitsumori, T., Iwasaki, H., & Yamada, K. (2018). Chemical kinetic modeling of ammonia oxidation with improved reaction mechanism for ammonia/air and ammonia-hydrogen/air combustion. *International Journal of Hydrogen Energy*, 43(5), 3004-3014.

[152] Song, Y., Hashemi, H., Christensen, J. M., Zou, C., Marshall, P., & Glarborg, P. (2016). Ammonia oxidation at high pressure and intermediate temperatures. *Fuel*, 181, 358-365.

[153] Mei, B., Zhang, X., Ma, S., Cui, M., Guo, H., Cao, Z., & Li, Y. (2019). Experimental and kinetic modeling investigation on the laminar flame propagation of ammonia under oxygen enrichment and elevated pressure conditions. *Combustion and Flame*, 210, 236-246.

[154] Mei, B., Zhang, J., Shi, X., Xi, Z., & Li, Y. (2021). Enhancement of ammonia combustion with partial fuel cracking strategy: Laminar flame propagation and kinetic modeling investigation of $NH_3/H_2/N_2$/air mixtures up to 10 atm. *Combustion and flame*, 231, 111472.

[155] Cabra, R., Myhrvold, T., Chen, J. Y., Dibble, R. W., Karpetis, A. N., & Barlow, R. S. (2002). Simultaneous laser Raman-Rayleigh-LIF measurements and numerical modeling results of a lifted turbulent H_2/N_2 jet flame in a vitiated coflow. *Proceedings of the Combustion Institute*, 29(2), 1881-1888.

[156] Myhrvold, T., ErtesvÅG, I. S., Gran, I. R., Cabra, R., & Chen, J. Y. (2006). A numerical investigation of a lifted H_2/N_2 turbulent jet flame in a vitiated coflow. *Combustion science and technology*, 178(6), 1001-1030.

[157] Cabra, R., Chen, J. Y., Dibble, R. W., Karpetis, A. N., & Barlow, R. S. (2005). Lifted methane-air jet flames in a vitiated coflow. *Combustion and Flame*, 143(4), 491-506.

[158] Gordon, R. L., Starner, S. H., Masri, A. R., & Bilger, R. W. (2005, July). Further characterisation of lifted hydrogen and methane flames issuing into a vitiated coflow. In *Proceedings of the 5th Asia-Pacific conference on combustion* (pp. 333-336).

[159] Wu, Z., Starner, S. H., & Bilger, R. W. (2003, December). Lift-off heights of turbulent H_2/N_2 jet flames in a vitiated co-flow. In *Proceedings of the 2003 Australian Symposium on Combustion and the 8th Australian Flame Days, Monash University, Australia*.

[160] Wu, Z., Masri, A. R., & Bilger, R. W. (2006). An experimental investigation of the turbulence structure of a lifted H_2/N_2 jet flame in a vitiated co-flow. *Flow, turbulence and combustion*, 76, 61-81.

[161] Gordon, R. L., Masri, A. R., & Mastorakos, E. (2008). Simultaneous Rayleigh temperature, OH-and CH_2O-LIF imaging of methane jets in a vitiated coflow. *Combustion and flame*, 155(1-2), 181-195.

[162] Gordon, R. L., Masri, A. R., & Mastorakos, E. (2009). Heat release rate as represented by [OH]×[CH_2O] and its role in autoignition. *Combustion Theory and Modelling*, 13(4), 645-670.

[163] Oldenhof, E., Tummers, M. J., Van Veen, E. H., & Roekaerts, D. J. E. M. (2010). Ignition kernel formation and lift-off behaviour of jet-in-hot-coflow flames. *Combustion and Flame*, 157(6), 1167-1178.

[164] Oldenhof, E., Tummers, M. J., Van Veen, E. H., & Roekaerts, D. J. E. M. (2011). Role of entrainment in the stabilisation of jet-in-hot-coflow flames. *Combustion and Flame*, 158(8), 1553-1563.

[165] Oldenhof, E., Tummers, M. J., van Veen, E. H., & Roekaerts, D. J. (2013). Conditional flow field statistics of jet-in-hot-coflow flames. *Combustion and flame*, 160(8), 1428-1440.

[166] Mendez, L. A., Tummers, M. J., Van Veen, E. H., & Roekaerts, D. J. E. M. (2015). Effect of hydrogen addition on the structure of natural-gas jet-in-hot-coflow flames. *Proceedings of the Combustion Institute*, 35(3), 3557-3564.

[167] Wu, Z., Bao, T., Zhang, Q., Yan, S., & Deng, J. (2014). Experimental study on spray combustion characteristics of gasoline-diesel blended fuel in a controllable active thermo-atmosphere. *Fuel*, 135, 374-379.

[168] Wu Z, Zhang Q, Li L. Auto-ignition and stabilization of diesel-propane lifted flames issuing into a hot vitiated co-flow. T*he 36th International Symposium on Combustion*, 2016, Seoul, Korea.

[169] Wu, Z., Zhang, Q., Li, L., Deng, J., Hu, Z., & Dibble, R. W. (2016). Autoignition and stabilization of diesel-propane lifted flames issuing into a hot vitiated co-flow. *Energy & Fuels*, 30(11), 9730-9736.

[170] Wu, Z., Zhang, Q., Bao, T., Li, L., Deng, J., & Hu, Z. (2016). Experimental and numerical study on ethanol and dimethyl ether lifted flames in a hot vitiated co-flow. *Fuel*, 184, 620-628.

[171] Zhang, E., Gong, Y., Deng, J., Hu, Z. et al., Cyclic Variations of Argon Power Cycle Engine with Fuel of Hydrogen. *SAE Technical Paper.* 2017-01-2409, 2017.

[172] Wu, Z., Xie, W., Zhang, E., Yu, Y., Qin, Q., Deng, J., & Li, L. (2019). Investigation of flame characteristics of hydrogen jet issuing into a hot vitiated nitrogen/argon/carbon dioxide coflow. *International Journal of Hydrogen Energy*, 44(52), 28357-28370.

[173] Wu, Z., Yu, Y., Xie, W., Liu, Z., Li, L., & Deng, J. (2021). Optimization of the flame characteristics of H_2-O_2 coaxial injection applied to hydrogen-fueled argon cycle engines. *International Journal of Hydrogen Energy*, 46(27), 14780-14789.

[174] Qin, Q., Wu, Z., & Ferrari, A. (2022). Study on lifted flame stabilization under different background pressures. *Journal of Thermal Science and Engineering Applications*, 14(2), 021006.

[175] Zhang, J., Sui, C., Zhang, B., & Li, J. (2023). Effects of swirl intensity on flame stability and NO emission in swirl-stabilized Ammonia-methane combustion. *Applications in Energy and Combustion Science*, 14, 100138.

[176] Liang, B., Gao, W., Zhang, K., & Li, Y. (2023). Ammonia-air combustion and explosion characteristics at elevated temperature and elevated pressure. *International Journal of Hydrogen Energy*, 48(53), 20225-20237.

[177] Delichatsios, M. A. (1993). Transition from momentum to buoyancy-controlled turbulent jet diffusion flames and flame height relationships. *Combustion and Flame*, 92(4), 349-364.

[178] Choi, B. C., Kim, K. N., & Chung, S. H. (2009). Autoignited laminar lifted flames of propane in coflow jets with tribrachial edge and mild combustion. *Combustion and Flame*, 156(2), 396-404.

[179] Turns, S. R., & Bandaru, R. V. (1992). *Oxides of nitrogen emissions from turbulent hydrocarbon/air jet diffusion flames. Final report, phase 2, January 1990-August 1992* (No. PB-93-152478/XAB; PSU-ME-R-90/91-0005). University Park.

[180] Choi, B. C., Chung, S. H. (2010). Autoignited laminar lifted flames of methane, ethylene, ethane, and n-butane jets in coflow air with elevated temperature. *Combustion and flame*, 157(12), 2348-2356.

[181] Hoekman, S. K. (2020). Review of nitrous oxide (N_2O) emissions from motor vehicles. *SAE International Journal of Fuels and Lubricants*, 13(1), 79-98.

[182] Reaction Design. CHEMKIN-PRO. San Diego: Reaction Design, 2008.

[183] Zhang, Q., Zhou, Z., Shan, S., Cai, X., & Yang, W. (2022). Chemical effect of water addition on the ammonia combustion reaction. *Thermal Science and Engineering Progress*, 32, 101318.

[184] Chu, X., Li, X., Gao, P., Ma, Z., Xiao, H., Xie, C., & Wang, X. (2024). High-temperature auto-ignition characteristics of NH_3-H_2-CH_4. *Fuel*, 365, 131228.

[185] Okafor, E. C., Naito, Y., Colson, S., Ichikawa, A., Kudo, T., Hayakawa, A., & Kobayashi, H. (2018). Experimental and numerical study of the laminar burning velocity of CH_4-NH_3-air premixed flames. *Combustion and flame*, 187, 185-198.

[186] Han, X., Wang, Z., Costa, M., Sun, Z., He, Y., & Cen, K. (2019). Experimental and kinetic modeling study of laminar burning velocities of NH_3/air, NH_3/H_2/air, NH_3/CO/air and NH_3/CH_4/air premixed flames. *Combustion and Flame*, 206, 214-226.